Institutional Repository - Research Portal
Dépôt Institutionnel - Portail de la Recherche
researchportal.unamur.be
University of Namur

THESIS / THÈSE

MASTER IN CHEMISTRY RESEARCH FOCUS

Synthesis and computational investigation of new metal-centered molecular gears

DANLOY, Esteban

Award date:
2022

Awarding institution:
University of Namur

Link to publication

General rights
Copyright and moral rights for the publications made accessible in the public portal are retained by the authors and/or other copyright owners and it is a condition of accessing publications that users recognise and abide by the legal requirements associated with these rights.

- Users may download and print one copy of any publication from the public portal for the purpose of private study or research.
- You may not further distribute the material or use it for any profit-making activity or commercial gain
- You may freely distribute the URL identifying the publication in the public portal ?

Take down policy
If you believe that this document breaches copyright please contact us providing details, and we will remove access to the work immediately and investigate your claim.

Download date: 05. May. 2024

Université de Namur
Faculté des Sciences

Synthesis and computational investigation of new metal-centered molecular gears

Mémoire présenté pour l'obtention

du grade académique de Master Chimie « Chimie du Vivant et des Nanomatériaux » : Finalité Approfondie

Esteban DANLOY

Janvier 2022

UNIVERSITE DE NAMUR
Faculté des Sciences

Secrétariat du Département de Chimie
Rue de Bruxelles 61 – 5000 NAMUR
Téléphone : +32(0)81 72.54.44 – Téléfax : +32(0)81 72.54.40
E-mail : enseignement.chimie@unamur.be - www.unamur.be/sciences

Synthèse et étude computationnelle de nouvelle machines moléculaires à centre métallique

DANLOY Esteban

Résumé

Durant les dernières décennies, l'intérêt grandissant pour les assemblages supramoléculaires présents dans les systèmes complexes inspira les chimistes pour le développement de nouvelles machines moléculaires artificielles (MMAs), faisant de cela un des objectifs contemporains des nanosciences. Certaines des premières et des plus iconiques structures de MMAs sont les engrenages moléculaires basés sur la structure du triptycène. Ces moteurs à échelle moléculaire peuvent convertir la lumière ou l'énergie chimique en mouvement rotatoire directionnel pour corréler le mouvement d'éléments mobiles d'une manière contrôlée.

Pour cela, la synthèse de nouveaux types de MMAs basées sur la structure du 9-phosphatriptycène présente un grand intérêt. Ils consistent en une structure rigide, symétrique avec beaucoup de positions fonctionalisables et leurs propriétés stériques et électroniques singulières font d'eux des candidats prometteurs pour le développement de MMAs à centre métallique. En effet, de récents travaux ont proposé la synthèse de 9-phosphatriptycènes *ortho*-substitués (Figure 1), ce qui augmente son encombrement stérique dans le complexe et permet ainsi de modifier ses propriétés dynamiques.

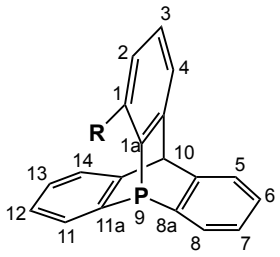

Figure 1 : Représentation d'un phosphatriptycène ortho-substitué.

Dans ce mémoire, la nouvelle synthèse a été suivie pour préparer plusieurs dérivés *ortho*-substitués du 9-phosphatriptycène (R = H, Cl, Me), adaptés pour la formation de nouvelles MMAs à centre métallique. De plus, des calculs de chimie quantique fournissent une vue générale de leurs propriétés structurelles et thermodynamiques, donnant un premier aperçu des effets de l'encombrement stérique sur le mouvement rotatoire autour de la liaison P-M (M = métal).

Mémoire de Master en sciences chimiques à finalité approfondie
Janvier 2022
Promoteurs : Pr. Guillaume BERIONNI et Pr. Benoît CHAMPAGNE

UNIVERSITY OF NAMUR

Faculté des Sciences

Secrétariat du Département de Chimie
Rue de Bruxelles 61 – 5000 NAMUR
Phone number : +32(0)81 72.54.44 – Fax number : +32(0)81 72.54.40
E-mail : enseignement.chimie@unamur.be - www.unamur.be/sciences

Synthesis and computational investigation of new metal-centered molecular gears

DANLOY Esteban

Abstract

During the last decades, the increasing interest for supramolecular assemblies in complex systems inspired chemists to develop new artificial molecular machines (AMMs), making it one of the contemporary goals of nanoscience. Some of the earliest and most iconic structures of AMMs are molecular gears based on the triptycene scaffold. These molecular scale motors can convert light or chemical energy into directional rotatory motion to correlate movable elements in a controllable manner.

For this purpose, the synthesis of new kind of AMMs based on 9-phosphatriptycene building blocks is of great interest. They consist in symmetric, rigid structure with many functionalizable positions and singular steric and electronic properties making them promising candidates for the development of metal-centered AMMs. Indeed, recent research works proposed the synthesis of *ortho*-substituted 9-phosphatriptycene (Figure 1), which increases its steric hindrance in the complexes and allow to tune their dynamic properties.

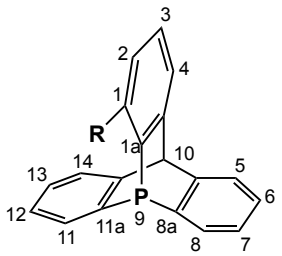

Figure 1: Representation of an ortho-substituted 9-phosphatriptycene.

In this Master thesis, the novel synthesis was followed to prepare several *ortho*-substituted 9-phosphatriptycene derivatives (R = H, Cl, Me) adapted for the subsequent formation of new metal-centered AMMs. In addition, quantum chemical calculations provided an overview of their structural and thermodynamic properties, giving a first look on the effects of steric hindrance on the rotary motion around the P-M (M = metal) bond.

Master thesis in chemistry, research focus
Janvier 2022
Promotors: Prof. Guillaume BERIONNI and Prof. Benoît CHAMPAGNE

Remerciements

Je tiens tout d'abord à remercier mes deux promoteurs, les professeurs Guillaume Berionni et Benoît Champagne pour m'avoir accueilli dans leurs laboratoires et pour m'avoir suivi tout au long de ce mémoire. Je les remercie pour leur écoute, leur disponibilité et l'expérience que j'ai pu acquérir grâce à eux. Merci également pour le temps qu'ils ont consacré aux relectures et corrections de me différents documents.

Je remercie également tous les membres des laboratoires RCO et LCT pour la bonne ambiance et les discussions productives que l'on a pu avoir. Plus particulièrement, je remercie mon encadrant Damien Mahaut pour son suivi tout au long de l'année dans les deux domaines de mon mémoire, la chimie organique et la chimie théorique.

Dédicace également aux autres mémorants du labo, Antoine, Dorothée, Jennifer et Lou pour ces bons moments passés avec vous. C'était une super année !

Ce mémoire n'aurait pas pu être possible sans le support technique des platefomres technologiques du département de chimie, et je remercie plus particulièrement Nikolay Tumanov et Luca Fusaro pour leur expertise en radiocristallographie et RMN respectivement.

Enfin je remercie profondément ma famille qui m'a toujours soutenu pendant toutes mes études. Merci aussi à Florine pour sa présence et son soutien au quotidien.

Table of content

PART I – Introduction

1. General introduction

In the field of chemistry, chemical bonds have been considered for a very long time as strong primary bonds between atoms. Far from this classical view, the supramolecular chemistry is centered on the creation of new molecular entities defined by non-covalent interactions. This introduced a controversial new kind of bonding, the mechanical bond, as strong as the weakest participating chemical bond.[1] These bonds can be defined as an entanglement in space between component parts such that they cannot be separated without breaking or distorting the chemical bonds between atoms (Figure 2).

This kind of assemblies constitute an important part of biological systems defining secondary and tertiary structures of large biomolecules and consequently, the entire behaviors of the living. Such an essential role of non-covalent interactions in complex systems inspired chemists to the development of sophisticated artificial molecular machines (AMM), making remarkable progress in the synthesis of molecular assemblies, which led to the distinction of three researchers in 2016, winning the Nobel prize in chemistry for their work on the subject. Despite some examples known for their ingenuity, artificial molecular machines are still too primitive to compete with their biological counterparts and the aim of performing useful work has not yet been achieved beyond the molecular scale.[2] However, a more fundamental understanding of these molecules would inevitably lead to a better control of the spatial ordering of assemblies allowing to use them for significant works. It began with the development of AMMs capable of performing tasks at their own scale such as molecular transport, molecules able to manipulate other nanostructures or entities that facilitate chemical transformations by lowering transition states energies, mimicking enzymes.[3]

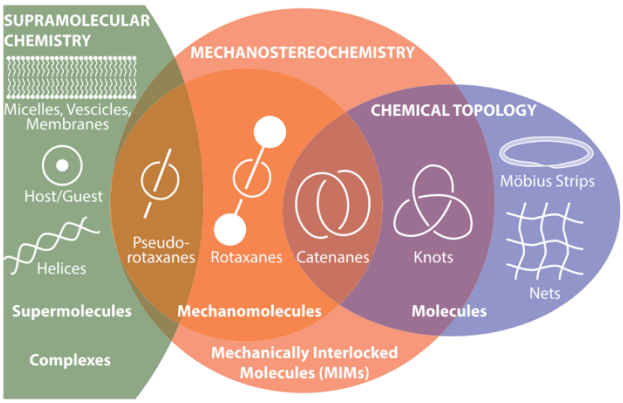

Figure 2: Venn diagram illustrating different types of molecular species intersecting in the fields of supramolecular chemistry, mechanostereochemistry, and chemical topology.[1]

2. Supramolecular chemistry

Supramolecular chemistry refers to the study of selective interactions occurring in chemical systems composed of a discrete number of molecules. Just as the field of molecular chemistry is based on covalent bonds, the supramolecular chemistry concentrates on molecular assemblies and the forces responsible for their spatial organization. The strength of these forces ranges from the weaker and reversible non-covalent interactions to strong covalent bonding, including van der Waals forces, hydrophobic effects, electrostatic interactions and metal coordination. As a result, supramolecular chemistry is a highly interdisciplinary field of science covering chemical, physical, and biological features of complex chemical species, that are held together and organized by the latter binding interactions. Its roots extend into organic chemistry for receptor construction, coordination chemistry and metal ion-ligand complexes, and biochemistry with biological processes starting with substrate binding and recognition.[4]

The existence of intermolecular forces was first postulated by Johannes Diderik van der Waals in 1873 which, associated with the works of Hermann Emil Fischer,[5] constituted the philosophical roots of supramolecular chemistry. In 1894, Fischer suggested the enzyme-substrate interaction as a "lock and key" process (Figure 3), bringing the fundamental principles of molecular recognition and host-guest chemistry. In the next century, non-covalent bonds were gradually discovered, leading to a better understanding of protein structures and other biological processes such as DNA replication, where the double strands of nucleotides are connected through reversible hydrogen bonds. Eventually, in the 1960s, chemists were able to take these concepts and apply them to synthetic systems, with the selective binding of alkali metal cations by macro(poly)cyclic ligands, the crown ethers and cryptands.

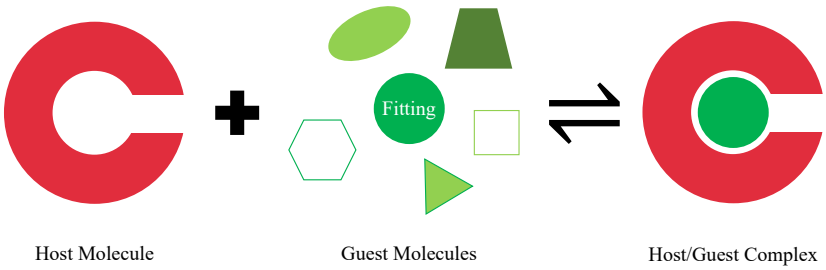

Figure 3: Representation of a reversible "lock and key" process for the selective molecular recognition of a guest molecule.

This led to the emergence of molecular recognition as a new domain of chemical research that grows with the development of synthetic receptors for the strong and selective binding of ionic and neutral substrates of different natures by means of various interactions.[6] In the next

decades, these new concepts such as molecular folding, molecular recognition and host-guest chemistry allow the 1987 Nobel prize to be awarded to Donald J. Cram, Jean-Marie Lehn and Charles J. Pederson in recognition for their contribution on the subject (Figure 4).[7]

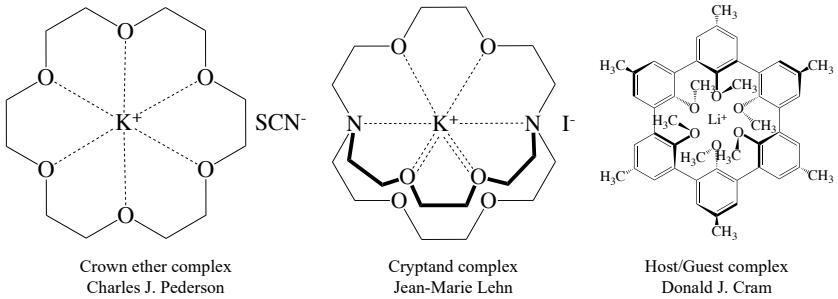

Figure 4: Representation of selective binding systems as designed by the 1987 Nobel prize winners. Image reproduced from reference [8].

A further major development to the host/guest chemistry is the design of molecular species with the ability to self-replicate without the guidance of an outside source.[9] While a supramolecular assembly can be composed of two, or a stoichiometric number of interacting molecules, it is more often composed of an indefinite number of self-assembling parts. It begins with the design of components capable of spontaneously forming well-defined superstructures through non-covalent interactions. This process, directed by molecular recognition, allows the designed generation of desired supramolecular entities in a given set of conditions. It provides a powerful tool for the construction of large structures such as micelles, membranes, vesicles and surfaces layers for instance.[4] Supramolecular chemistry is also used in crystal engineering and solid-state chemistry with the development of liquid crystals and Molecular Organic Frameworks (MOFs) (Figure 5), among others. The latter self-assembly is used for molecular recognition in order to organize a system to facilitate a chemical reaction, also known as supramolecular catalysis. In these, non-covalent interactions between the template and the reactants organize their structure and position them to facilitate the desired chemistry and minimize the side reactions.

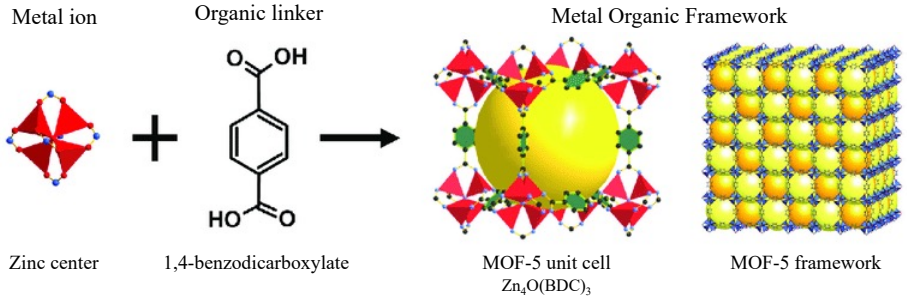

Figure 5: Synthesis of a Metal Organic Framework 5 (MOF-5) from a Zn metal cluster. Image adapted from reference [10].

Through the 1980s, researches in supramolecular chemistry allowed new emerging concepts such as Mechanically Interlocked Molecules (MIMs). It consists of molecules linked only as a consequence of their topology. In these self-assembled architectures, interactions between the different components are involved in the template-directed construction of the system (Figure 6). The study of these interactions is crucial in supramolecular chemistry to get a control of the processes requiring great precision. Indeed, non-covalent bonds are very reactive with respect to external factors such as the molecular environment and the temperature since such conditions can impact chemical equilibrium and the formation rate of highly labile bonds. Moreover, some supramolecular processes required external energy to reach thermodynamically disfavored conformations. This dynamic nature is used in some interlocked molecules such as pseudo-rotaxanes during the slipping motion required for their synthesis.

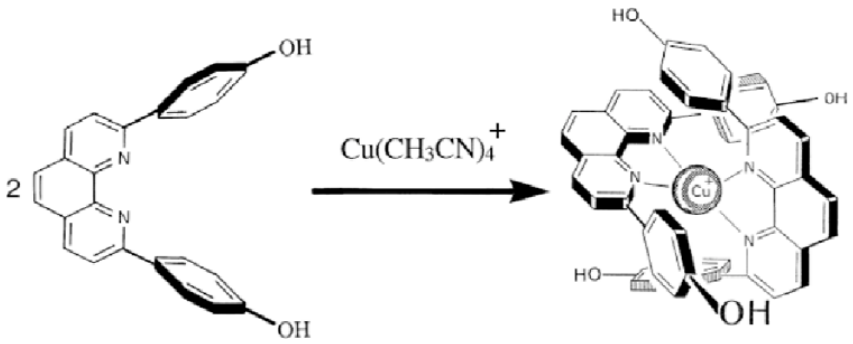

Figure 6: Example of the first template-directed catenane.[11]a

In addition, supramolecular chemistry became more sophisticated with the emergence of interlocked structure capable to perform functions such as linear or rotational movement, switching or entrapment thanks to the dynamical nature of non-covalent bonds. This molecular machinery represents the boundary between supramolecular chemistry and nanotechnology and growth with emerging new concepts including catenanes, rotaxanes or molecular gears. Multiple prototypes of highly complex self-assembled structures were developed, allowing Jean-Pierre Sauvage, Sir J. Fraser Stoddart and Bernard L. Feringa to share the 2016 Nobel Prize in chemistry for "the design and synthesis of molecular machines".[11] Along these synthetical approaches of molecular machinery, many artificial supramolecular systems were designed to copy functions of biological systems. These biological structures have attracted long-term attention for their unique capacity to employ the concepts of supramolecular chemistry. Since their discovery, these biological machines have been a source of inspiration for supramolecular researches and a complete understanding of their working mechanism was the starting point to synthetize biomimetic structures capable of performing significant task.

3. Biological molecular machines

In cellular biology, molecular machines are associated to proteins performing tasks essential for life, in response to a complex chain of biological events. These proteins are programmed to carry out motions related with the activity of cells and realize specific functions through their stimuli-responsive mechanical motions. As a result, the most complex macromolecular machines are found within cells, often in the form of multiprotein complexes with various examples of functions including energy production, cellular motion or gene expression. All these machines and their nanoscale dynamics are far more complex than any molecular machines that have yet been artificially constructed.[12]

One of the most studied and sophisticated biological molecular machines is the ATP synthase, an enzyme that catalyze the formation of the energy storage molecule, the adenosine triphosphate (ATP), using adenosine diphosphate (ADP) and inorganic phosphate (P_i). The formation of ATP from the latter molecules is energetically unfavorable and would not happen in normal conditions. In order to drive this reaction forward, ATP synthase promotes ATP synthesis during cellular respiration where the energy from protons gradients across membranes is harnessed to drive a turbine-like rotary motion used to synthetize the energy currency of cells (Figure 7).[13] Like other enzymes, the activity of the ATP synthase is reversible and if large quantities of ATP are supplied, it generates a rotary motion creating a transmembrane proton gradient used by some fermenting bacteria to drive flagella and transport nutrients into the cell. This kind of protein is ubiquitous in the livings and generate a torque motion with nearly 100% of efficiency, making the application of ATP synthase to artificial devices a promising subject.

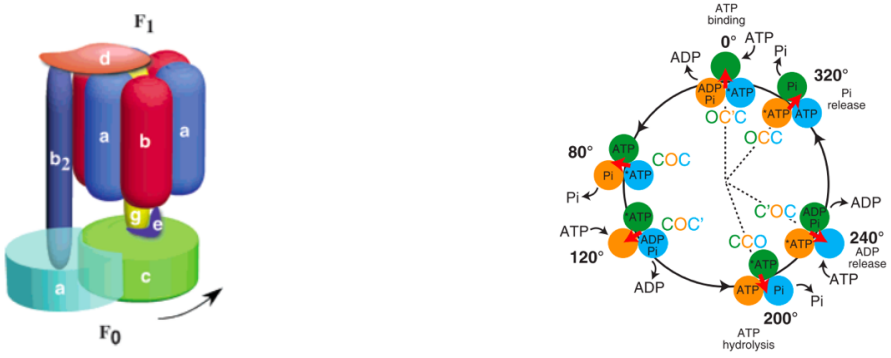

Figure 7: Schematic structure of ATP synthase (left) composed of F_1 (α-ε) and F_o (a-c) and the corresponding alternating catalytic model (right). This model states that the nucleotide binding mode of β-subunits catalytic sites depends on the angular position of γ-subunit (red arrow) and its open (O), half-closed (C') and closed (C) form. [12, 13]

One example of biological machines is constituted by a set of so-called “molecular motors”, responsible of cells motility. Due to their central role in cellular activity, these are the most extensively studied molecular machines.[14] They consist in supramolecular conjugates known to switch back and forth along linear tracks by converting chemical potential into mechanical work. These motors are capable to transport variety of cargo, power cell locomotion, drive cell division and, combined in large ensemble, allow performing diverse biological function.

Among others, motor proteins include some representative family such as myosins, which are responsible of activities like muscles contraction, vesicle transport or signal transduction, and kinesins, which move cargos inside cells away from the nucleus for functions like transport of organelles, mRNAs and chromosomal movement during mitosis and meiosis.[15] Typically, these motor proteins have three functional domains: 1) a force producing domain, the motor domain, containing an active site for ATP hydrolysis and a binding site for the cytoskeletal filament, 2) a neck domain connecting the head (motor domain) to the tail and which operate as a lever arm and 3) a cargo-binding tail domain showing high diversity to perform a wide variety of cellular functions. In these families of proteins, the most representative are myosin V and kinesin-1, where the motor produces a move in a hand-over-hand fashion from chemical reactions at the expense of ATP as fuel. Indeed, as represented in Figure 8, ATPase cycle is required to cause change of strength of binding to their polymeric track followed by small conformational changes in the motor domain that is amplified and translated into movements along the track. Once the conformational change occurred, the protein can rebind to a forward binding site by going back to a strong binding state.

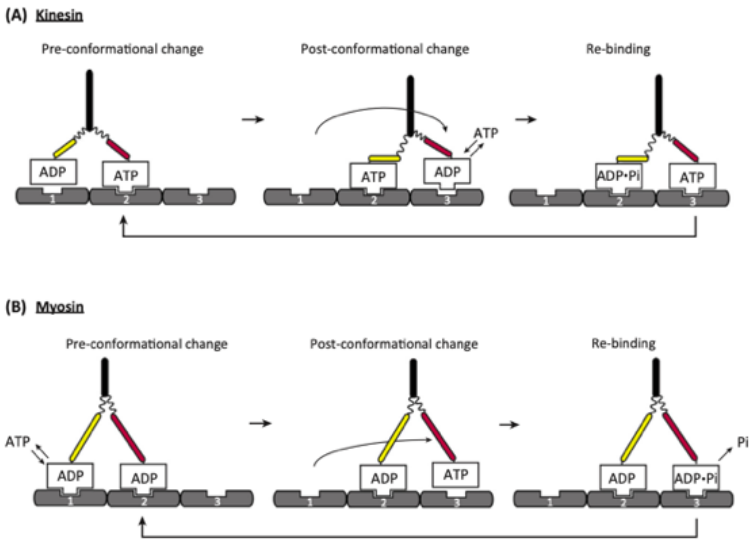

Figure 8: Schematic representation of the ATPase cycle of kinesin-1(A) and myosin V (B) moving along a filament.[14]b

As shown above, the most complex macromolecular machines are found within the livings in the form of multi-protein complexes. Despite their complexity, some of the here-described ones inspired chemists to create useful working nanomachines such cargo-carrying molecular shuttles inspired from myosins (Figure 9) or even ATP synthase-based rotary motors. However, other machines as the ones responsible for gene expression, including DNA and RNA polymerases or ribosomes are still too complex to be artificially constructed. Although not currently attainable, the construction of more complex molecular machines is an active area of experimental and theoretical research. In this context, the latter can be extremely useful to overcome the lack of methods to construct and study the features of these molecules. A certain number of molecules have been designed, and quantum chemistry-based modeling can help to characterize their properties. It can also enable to realize even more complicated machinery with some potential applications in transport at the molecular level, manipulation of structures and chemical systems or realize machines for the areas of nanotechnology. These biological systems are inspiring chemist to create machines for applications in nanomedicine. For instance, they could be used to identify and destroy cancer cells. Even more impressive would be the realization of versatile and effective molecular machines capable to perform autonomous operation such as reorder matter at a molecular or atomic scale. These molecular assemblers would open a new field in nanomedicine with the potential use of nanorobots that can be introduced in the body to repair and detect damages and infections. The proposed innovation is far beyond current capabilities in nanotechnology and a fundamental investigation of their working conditions and stability is still needed.

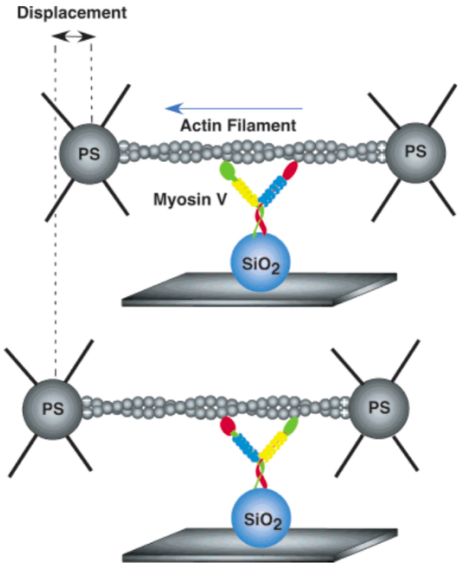

Figure 9: Representation of a cargo-carrying molecular shuttles inspired from myosins V. This molecular machine allows the directed motion of actin filament on myosin V immobilized on polystyrene beads.[12]

4. *Artificial molecular machines*

The notion of Artificial Molecular Machines (AMMs) comes from the will of chemists to associate well-known concepts of supramolecular chemistry (reversible non-covalent bonds, molecular recognition, self-assembly, …) with the unique capacity of biological systems to perform functions triggered by specific stimulus. Although biological machines remain at a level of complexity unattainable by the current AMMs, the study of less elaborate artificial systems gives rise to a better understanding of the sophisticated biological ones that inspired them. As a result, remarkable progresses were made to build artificial structures that can exploit molecular motion and the way in which nature has taken advantage of molecular machines is still inspiring chemists.[16]

Whereas biological systems harness chemical energy from favorable bond breaking/forming (e.g., ATP hydrolysis) or concentration gradient, artificial ones need an energy source compatible with the environment they are operating in. The first step toward a motion-inducing source for the utilization of artificial molecular machines was taken in 1827, when Robert Brown observed the hazardous motion of small particles, later defined as the Brownian motion.[17] At such a small scale, the forces with the greatest influence on dynamics differ significantly from those at the macroscopic level, and the significance and consequences of random thermal motion become substantial. Unfortunately, this also provides the biggest constraint for the design of synthetic molecular machines. Indeed, from the random thermal motions arises the principle of "detailed balance",[16] which states that, at equilibrium, each transition has an equal probability and rate of occurring, meaning that no directionality can exist in such motions. As a result, the only way to perform a task using Brownian motions is by the application of an unbiased driving force to the component (Figure 10), which breaks the balance and displaces the equilibrium.

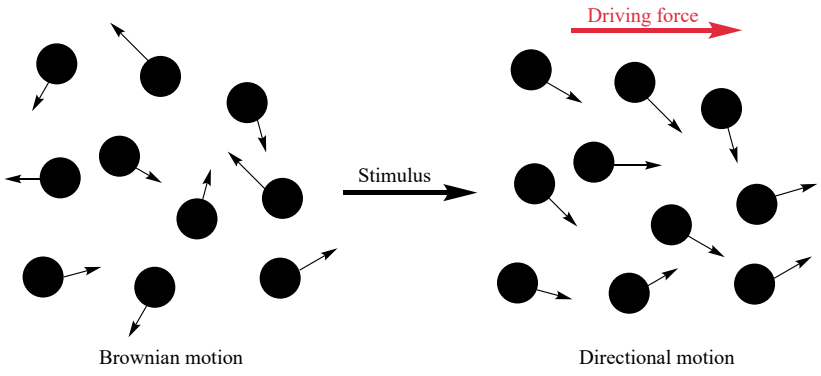

Figure 10: Illustration of the random thermal motion and the application of a stimulus-induced driving force.

The comprehension of this concept is important for the design of synthetic molecular machines abled to conduct directional motion. Once again, great inspiration comes from biological machines. These exploit Brownian motions to ensure the mobility of components evolutionary constructed to reduce their available degrees of freedom and achieve directed motion. It is the case of the previously described kinesins and myosins, which inspired chemists to construct stimuli-responsive mechanically interlocked systems capable to make directed sliding motion (Figure 11). It began in the 1980s, with the development of catenanes and rotaxanes by Jean-Pierre Sauvage and Sir J. Fraser Stoddart, respectively, which led to numerous ingenious derivatives.[18]

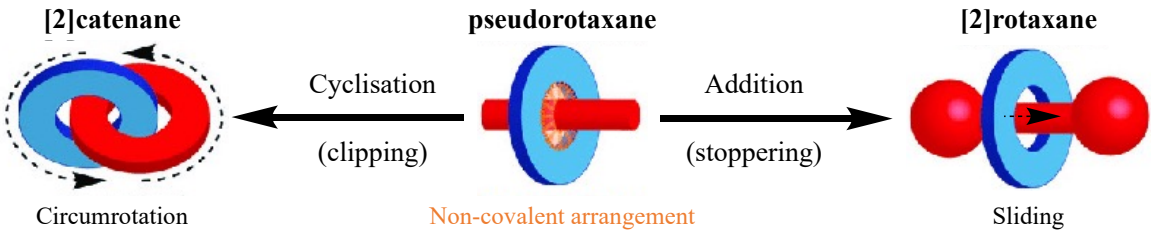

Figure 11: Formation of rotaxanes and catenanes by the passive template synthesis.[19]

In MIMs, as in biological systems, degrees of freedom are limited by mechanical bonds, limiting the number of possible random Brownian motions. The random motion of the components is the key factor in the switching process since it allows them to move along the track. As the templating methods typically used to form interlocked structures involve recognition motifs, these can be used as driving force to control motions and break the detailed balance. Indeed, these residual interactions sites are generally used as "stations" for the shuttle. This method was used by Sir J. Fraser Stoddart for the synthesis of the first two-station stimuli-responsive rotaxane.[11]b Many subsequent rotaxanes and catenanes were based on similar processes, where the movement of the shuttle between binding sites involves partial rupture of stabilizing bonds. However, in this simplified case the shuttle is statically present in the same proportions in the two stations due to their degenerate energy (Figure 12).

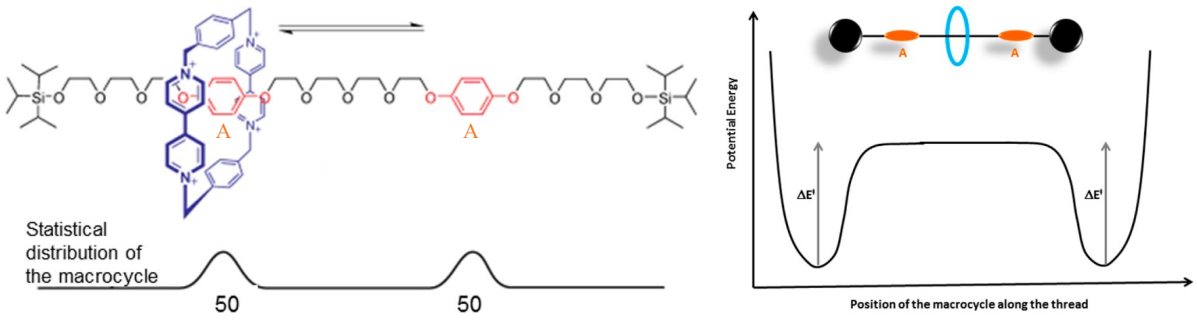

Figure 12: The first degenerate two-station molecular shuttle and its statistical distribution along the thread (left) and the corresponding potential energy surface (right).[16]

This problem can be solved by independently controlling the strength of each shuttle-station interaction. Thus, molecular motion in mechanically interlocked systems is controlled using multiple binding sites with different affinities for the macrocycle that can vary under the conditions (Figure 13). These stimuli-responsive molecular shuttles have the advantage to always have one favored station along the track. This is achieved by weakening the existing interaction or increasing the affinity for a competing binding site, inducing a new equilibrium in the system. This break of the detailed balance can be achieved by various stimulus including electrochemical redox processes, environmental changes (temperature, solvent, …), pH variations, or photochemical processes among other innovation. For a reverse or further translational motion takes place, a new stimulus is required to perturb the equilibrium, causing a new movement of the shuttle driven by thermal motion.

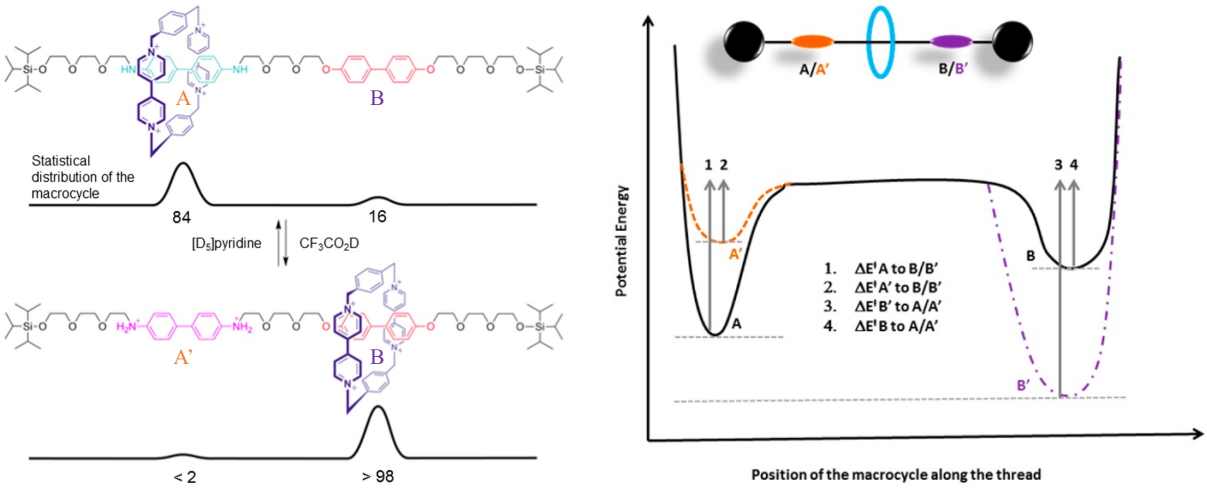

Figure 13: A pH-driven two-station molecular shuttle and its statistical distribution along the thread depending on protonation state of A (left) and the corresponding potential energy surface (right).[16]

Attempts to fabricate mechanical devices inspired from biological molecular motors rapidly led chemists to analogues of ATP synthase, harnessing chemical energy to drive a controlled rotational motion. Once again, the Brownian motions induce rapid fluctuation in organic compounds that can generate various perturbation in the structure such as lengthening/shortening or rotation of covalent bonds. Early pioneering works conducted to restricted rotation about sterically hindered single bonds of a triptycene component. These molecules showed very high rotational barriers and introduced the concept of dynamic gearing. An early example of controlled random rotary motion about a single bond was provided by Kelly et al.,[20] who utilized interactions with the neighboring substituents to impede the rotational motion, a so-called "molecular brake" (Figure 14). Diverse methods of brake follow this idea to impede or halt the free rotation of the triptycene moiety, but none of these structures showed a unidirectional rotation.

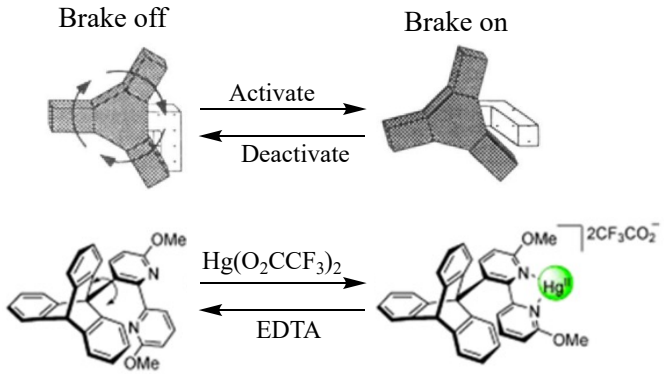

Figure 14: Reversible molecular brake operated by Hg^{2+} complexation/decomplexation. Image reproduced from reference [20].

Actually, despite the considerable efforts in the domain, the controlled conversion of thermal energy into a unidirectional motion is still difficult to achieve. Indeed, the random thermal motion of components remains a strong motion-inducing source but difficult to control due to equal rates of rotation in both directions. As previously, the key factor required to break the detailed balance and to allow directional motion of the triptycene cog is an energy input to drive the system away from equilibrium. Kelly et al. proposed a modified structure of their molecular brake, where a chemical reaction drives the system between the different intermediates (Figure 15).[21] These intermediates correspond to energy minima where the helicene pawl is situated between the rotator cogs. In order to induce a reorganization of the 9-triptycyl group, a chemical transformation is made to destabilize the current structure. As a result, the system has enough energy to pass the smaller energy barrier of rotation with random thermal motion, allowing it to perform a 120° rotation. The same process is made two more times to complete a full rotation of the gear and "resetting" the system. This machine is a landmark achievement in the realization of chemically-fueled directional rotation in molecular machines and it demonstrates the basic features of a directional motor.

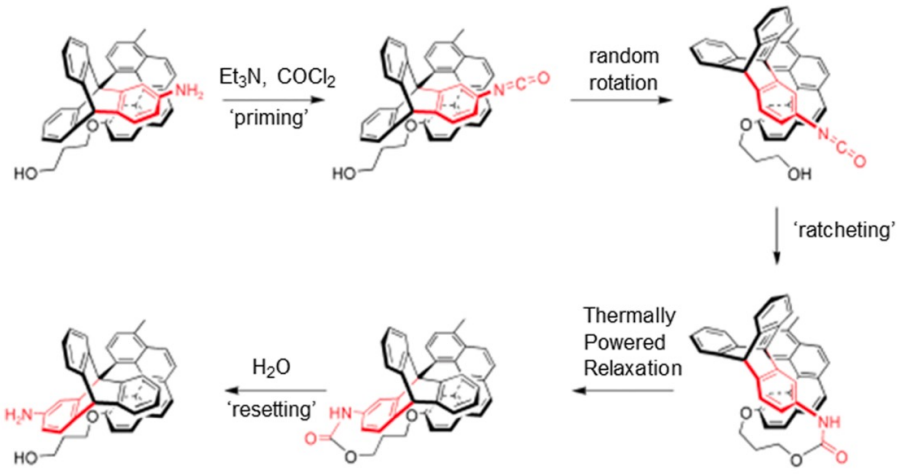

Figure 15: Chemically-driven directional 120° rotation of a triptycene rotor.[16]

The construction of molecular machines begins from a careful consideration of molecular geometry, shape, size, non-bonding interaction and electronic properties that dictate the mechanical functions of the system. Chemists can utilize these inherent properties to combine molecules into systems capable of transducing energy and performing works such as molecular gears. In this purpose, 9-triptycene derivatives have been considered as interesting building blocks for the synthesis of molecular motors. Indeed, 9-triptycene is a well-known part of gear molecules with a rigid structure similar to a three-bladed gear, corresponding to the benzene rings, which extends symmetrically in three directions and can rotate freely three times. This allows to design machines involving correlated motions in the form of gearing, achieved when the cogs are tightly intermeshed. Rotation motion in molecular gears implies that two or more adjacent rotors give up their individual degrees of freedom to enter in synchronous regime, where their velocity and direction of rotation of any element is dependent on the rotational characteristic of its closest neighbors (Figure 16).

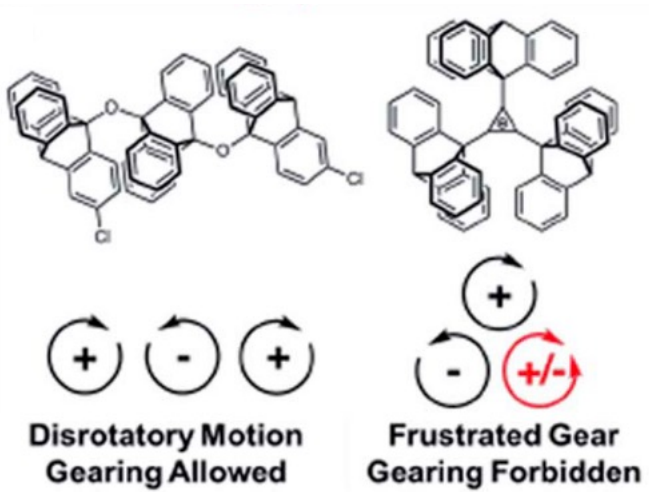

Figure 16: Illustration of the importance of the structure upon the correlated motion of gears.[22]

From a structural point of view, triptycene units can either adopt parallel or bent orientations, resulting in spur or bevel gears, respectively (Figure 17). In spur gears, triptycenes lie in parallel alignment with the cog of one triptycene fitting into the space that exists between two cogs of an adjacent one. In contrast, bevel gears consist of two triptycene gears linked by a single atom or a cis-alkene derivative, resulting into intermeshed cogs. This structural feature is due to the design of the stator, thought to induce a proper positional relationship between the rotators to allow them to undergo a synchronous disrotatory motion. The first molecular bevel gear was reported by the groups of Mislow and Iwamura,[23] who designed and synthesized a molecule containing two triptycyl groups joined through their bridge head carbons to a central stator. In these structures, rotators are linked by a single atom or cis-alkene derivative that confirmed the importance of the stator nature on the gearing process. Indeed, studies confirmed that some

stators impose a sufficient strain angle on the 9-triptycyl groups to prevent them from deviating from their intermeshed configuration, which causes errors in their rotation known as gear slippage. Therefore, the choice of the stator is central to avoid any widening of the angle that can arise from the steric hindrance exerted by the triptycene groups.

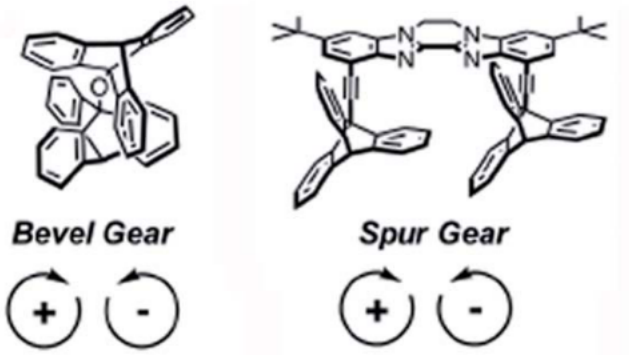

Figure 17: Illustration of bevel gears and spur gears depending on the structure of the stator.[22]

Since then, many other examples of complex multirotor gears with multiple kind of structural platforms have been published. These include more sophisticated gear systems, such as Ru complex with four triptycyl groups or multirotor gear consisting of six triptycenes circularly arranged around a central benzene ring.[24] Also, some bevel gears covalently linked to a bridging heteroatom or group 14 element (X = O, S, CH, CO, NH, PH, SiH_2, GeH_2, $GeF_{2, ...}$) have been reported.[25] One ingenious example of covalently linked system is a silicon-centered bistriptycene which can undergo a switchable gearing triggered by fluorination/defluorination (Figure 18).[26] The change of configuration by a chemical stimulus, especially a cis/trans isomerization is used in many molecular systems to control motion. Indeed, it represents an interesting tool for the design of molecular machines and can be useful to create switchable systems. In the case of molecular gears, this can lead to the possibility of interconversion between two structures where conformational changes control the engagement/disengagement of the gears.

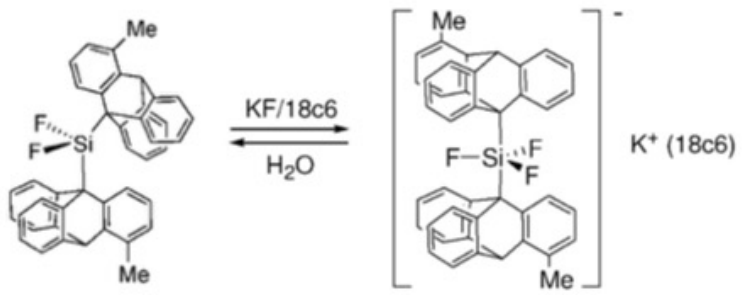

Figure 18: Reversible clutch function in a molecular gear system by a silane-silicate interconversion.[26]

The elaboration of molecular gears requires a meticulous consideration of structural aspects to obtain a system capable to perform a synchronous rotation. Indeed, the careful choice in the nature of the stator is central in the synthesis of stimuli-responsive clutchable gear system, so promising for the design of molecular machines. In this context, Ube et al. synthesized an external stimuli-responsive gear system with a controlled switching motion.[27] It consists in a Pt^{II}-centered molecular gear with two coordinating azaphosphatriptycenes derivatives as rotators. Metal ions can serve as center of molecular motion due to their coordination geometry, reversible bonding nature and external stimuli responsiveness. Indeed, such compounds are capable to change their coordination geometry by ultraviolet irradiation and heating conditions, allowing a reversible interconversion between a cis-engaged and a trans-disengaged state of gearing (Figure 19).

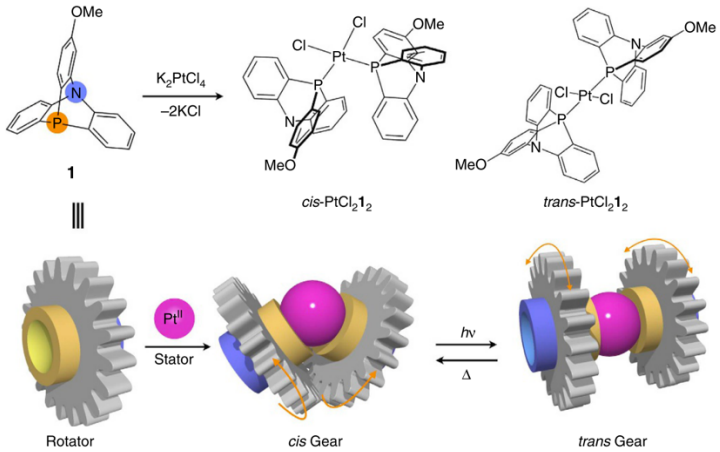

Figure 19: Schematic representation of the Pt^{II}-centered molecular gear with two azaphosphatriptycene rotators.[27]

In this work, the photo- and thermally-driven photoisomerization could be described by methods such as ^{1}H, ^{13}C and ^{31}P nuclear magnetic resonance (NMR) spectroscopy as well as X-rays crystallographic analysis. However, the complete analysis of the rotational dynamics remains difficult to obtain by classical characterization methods. More specifically, the rotation energy barriers and rates provide a tough challenge due to the barely visible differentiation of the cycles in NMR spectroscopy during their rotational motion. As a result, quantum chemistry investigations of the system properties provide new clues on its behaviors.[28] Namely, the investigation of this metal-centered molecular gear by density functional theory (DFT) provides further indication on the structural geometry of isomers and their corresponding energies, giving an evaluation of the energy barrier and the rate constant of the isomerization reaction. Also, the same method can be applied to the isomers independently to access to the dynamical characteristics of the gear rotation and slippage and the corresponding potential energy curves.

PART II – Research objectives

In the aim of getting a better fundamental understanding of their properties, this Master thesis is focusing on the design of different 9-phosphatriptycene building blocks (Figure 20) for platinum-centered square planar complexes and the investigation of their use as molecular machines. As shown in the previous section, these platinum complexes are known for their ability to undergo dynamic isomerization, allowing a controlled engagement-disengagement of the cogs.

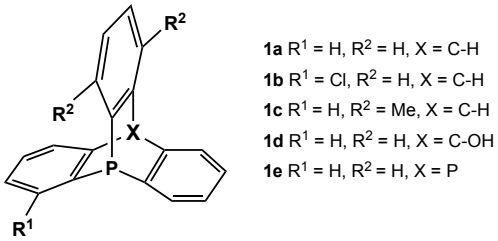

Figure 20: Representation of the aimed ortho-substituted 9-phosphatriptycenes.

Therefore, several *ortho*-substituted 9-phosphatriptycene derivatives were synthetized in order to tune the physico-chemical properties of the complexes. This was followed by coordination reactions on precursors of metal complexes to determine the most efficient conditions to obtain the desired molecular machines. Once complexes are obtained, the dynamical ligands exchange is investigated by NMR spectroscopy and XRD. In parallel, quantum chemical calculations performed on the complexes provided an overview of their structural and thermodynamic properties to give a first look of the steric and electronic effects on the rotary motion around the Pt-P bonds (Figure 21).

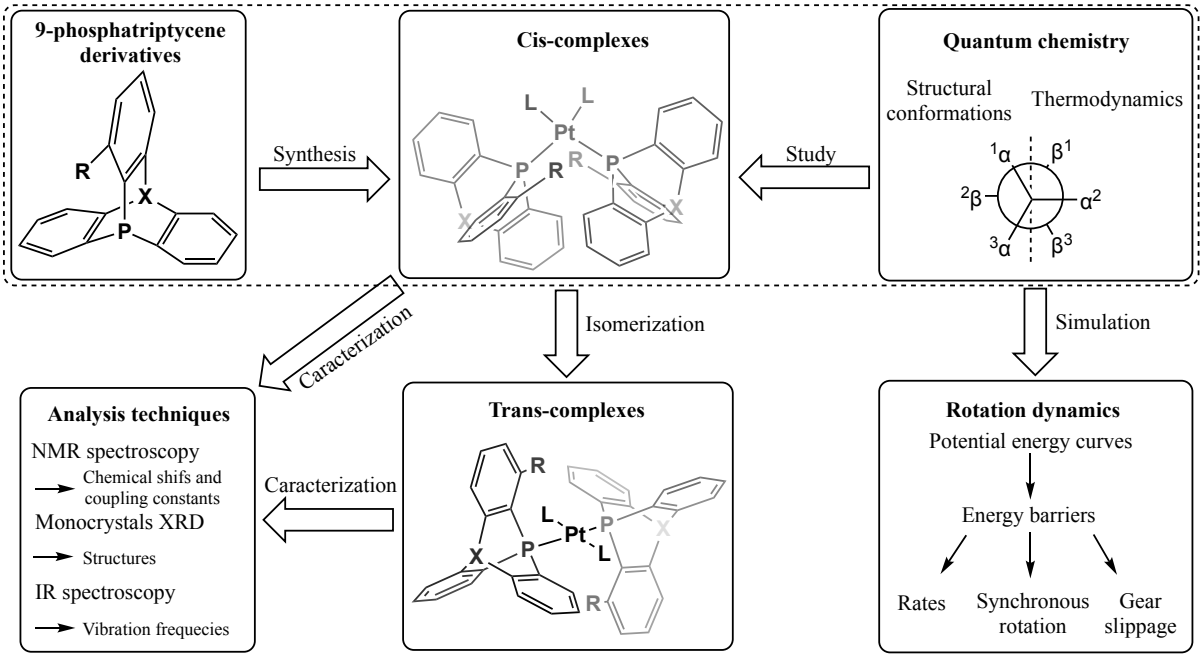

Figure 21: Schematic representation of the research objectives presented in this work (surrounded by dotted lines) and for further investigation.

PART III – Experimental results and discussion

1. Synthesis of 9-phosphatriptycene ligands

Phosphines constitute an important class of chemical compounds in organic chemistry with various applications. For instance, their oxidation constitutes the driving force of several important organic reactions such as the Mitsunobu, the Appel or the Staudinger reactions.[29] As Lewis bases, phosphines also display affinities for a wide variety of Lewis acids, leading to the formation of strong covalent bonds. Consequently, they exhibit strong coordinating properties toward transition metals, making them the most widespread ligands in transition metal catalysts used for major organic reactions as the Suzuki-Miyaura, the Buchwald-Hartwig and the Negishi cross-coupling reactions. Beside that, a large number of transition-metal-free organic reactions involved phosphines as organocatalysts for both "classical" and asymmetric catalysis.[30] It includes recent applications in the area of frustrated Lewis pairs, which provide new prospects in phosphine organocatalysis for small molecules activation and catalyzed hydrogenations.[31]

This is for the latter purpose and the need of finding new bulky Lewis bases that the synthesis of *ortho*-substituted 9-phosphatriptycene (henceforth simply called "phosphatriptycene") derivatives was first developed. Those unique cage-shaped compounds display considerable modifications of reactivity and properties compared to ordinary triarylphosphines.[32] These ring-strained structures impose a larger hindrance due to the aryl rings π-systems orthogonal to the phosphorus atom and their strain prevents any rotation of the aryl rings that could decrease the steric shielding. Due to this orthogonality, no conjugation between rings and the phosphorus lone pair is possible and *ortho*-substituents have a minor electronic effect on P lone pair. The electronic properties are also modified by the pyramidalization of the trivalent phosphorus atom via the structural constraint, which will be discussed in the next section.

The multistep synthetic pathway shown in Scheme 1 allows to obtain a variety of *ortho*-substituents for X = C-H (**1a-c** in Figure 20) phosphatriptycenes in gram scale. This synthesis path presents the particularity to be efficient to access phosphatriptycenes with either an attractor or a donor group as *ortho*-substituent. Indeed, they both can be incorporated in the structure in different steps of the synthesis. This differentiation is crucial for the efficiency of the next reaction steps, as discussed below. Three bulky ligands (**1a-c**) were synthetised following this general path with commercially available reagents to afford chlorine, methyl and hydrogen *ortho*-substituted ligands.

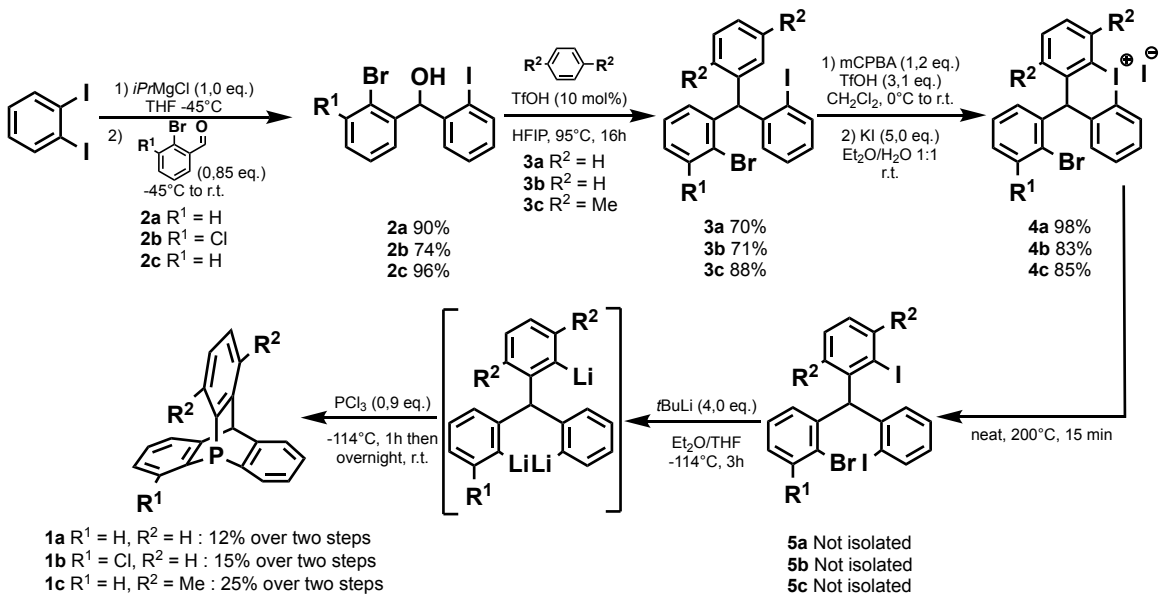

Scheme 1: General synthesis pathway of ortho-substituted 9-phosphatriptycenes.

The synthesis of the phosphatriptycenes starts from the formation of an *ortho*-halogenated diphenylmethanol precursor (**2a-c**), itself prepared from 1,2-diiodobenzene and a 2-bromobenzaldehyde derivative with high yields. The mechanism of this step begins with a I/Mg exchange to form a (2-iodophenyl)magnesium chloride intermediate, which can then perform a nucleophilic attack on the aldehyde group. The low temperature of -45°C (using an acetonitrile/$N_{2(l)}$ cooling bath) ensures the stability of the Grignard intermediate and avoids undesired degradation. As shown by the structure of the reactants, this step allows to incorporate an electron-withradwing group (a chlorine atom in **b**) in the final structure by making the Grignard species reacting with the bromobenzaldehyde derivatives substituted in the right position. Other suitable attractor groups can be added following the same procedure, such as F or CF_3 for example.[32]

The following step is based on the method of Moran,[33] and consists in the Friedel-Crafts alkylation of the **2a-c** reactants with benzene (for **a** and **b**) or *p*-xylene (for **c**) to produce the triarylmethane precursors (**3a-c**). In this step, the benzhydrylium ion generated from the reaction between **2a-c** and trifluoromethanesulfonic acid in HFIP (hexafluoroisopropanol) give access to the desired product with good yields. The presence of HFIP as solvent is necessary to carry on the reaction. Indeed, this solvent forms H-bond clusters in interaction with the Brønsted acid catalysts, which accelerates and enables the reaction on the electronically deactivated diphenylmethanol. In addition, this reaction needs a sufficiently activated phenyl ring to alkylate the benzhydrylium ion, which justifies that deactivating attractor groups must be integrated in the structure during the previous step. Finally, *p*-xylene is preferred to toluene to access to *ortho*-methylated phosphatriptycene. Indeed, due to the regioselectivity occurring

in Friedel-Crafts alkylation, toluene would be alkylated on both *ortho* and *para* position of its methyl group, leading to a mixture of regioisomers. This problem is not encountered in benzene and *p*-xylene, where all unsubstituted positions are identical and afford the desired product (**3a-c**).

The third step consisting in the formation of an iodonium ring (**4a-c**) is the key transformation of the synthesis since it is a unique pathway to afford this kind of *ortho*-halogenated triarylmethane (**5a-c**). This reaction, described by Peters,[34] consists in the electrophilic aromatic substitution of the most activated aryl ring present in the structure on a highly electrophilic iodane. The latter is obtained by oxidation, turning the iodine atom into an hypervalent iodosyl group (-IO), before protonation by triflic acid, loss of water and nucleophilic attack of the aryl ring. After that, a treatment in the presence of potassium iodide allows an exchange of counter-ion to access the desired compound (**4a-c**) for the next transformation.

Next, it is possible to halogenate the latter triarylmethane (**4a-c**) by opening the ring in the presence of a nucleophilic halide. An important part of this work was to investigate this crucial step to identify suitable conditions. Indeed, a substantial drop in the yield of this reaction was observed due to the formation of side-products, such as I_2, clearly recognisable by its dark purple colour. In fact, the complexity of formed products suggested that a radical mechanism either governed or at least contributed to the thermal decomposition process. A detailed investigation of the mechanism can be put forward to explain the formation of these side-products. It appears that most diaryliodonium ions can react with nucleophiles via two paths, a polar and a radical one, following the Scheme 2.[35]

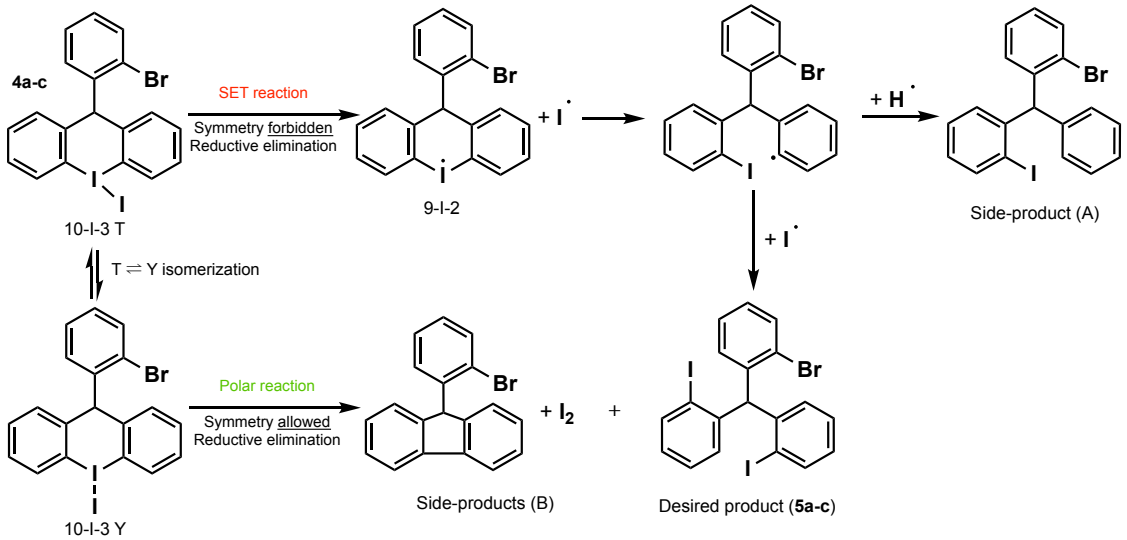

Scheme 2: Representation of polar and SET processes of iodonium ring opening. Hypervalent iodines are named following a N-X-L notation where N stands for the number of electrons around the central atom X and L is the total number of ligands. R substituents are here omitted in the structures. Scheme adapted from reference [35].

As shown, the **4a-c** precursor can be represented under the form of a hypervalent 10-I-3 intermediate (where 10 stands for the number of electrons around the central I atom and 3 is the total number of ligands), which may undergo reductive elimination via the polar or the single electron transfer (SET) process. The reductive elimination is normally forbidden for the lower energy T-shape (where the iodine presents a trigonal bipyramidal geometry) conformation of the tricoordinate iodine (**10-I-3 T**), but allowed for the higher energy Y-shape iodine (where iodine is in the centre of a tetragonal pyramid) conformer (**10-I-3 Y**). Consequently, the process (polar or SET) which mediates the reaction depends on the activation energy barrier of the Berry pseudorotation needed for the permutation around the tricoordinate iodine atom (Scheme 3).[36] In the case of cyclic diaryliodoniums, this energy barrier is highly dependent on the strain of the ring. In the present case, due to the rigidity of the six-membered ring, the system has difficulties to adopt the Y-shape required to undergo the polar reaction. This structural rigidity induces a low reactivity of the **4a-c** reactant, causing the necessity of carrying out the reaction at a high temperature. Unfortunately, at elevated temperature, the hypervalent derivatives prefer decomposing homolytically via the SET path to give complex mixture of products.

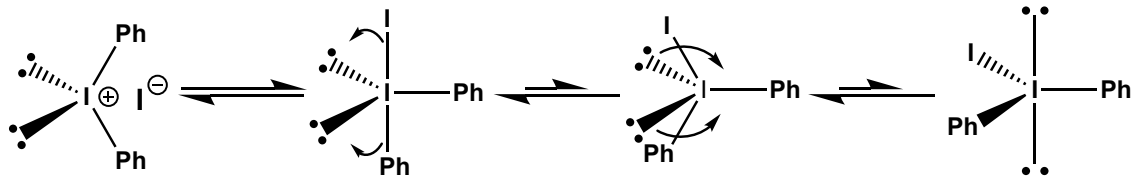

10-I-3 T 10-I-3 Y

Scheme 3: Representation of the Berry pseudorotation occurring in a diaryliodonium ring. Scheme adapted from reference [36]b.

The first intermediate following the formation of the trivalent iodine (III) intermediate is believed to be the T-shaped, as are diaryliodonium compounds in the solid state. In this structure, with the bulkiest of the two aryl ligands and the two lone pairs lying in the less encumbered equatorial position. Since apical-equatorial interactions are symmetry forbidden in trigonal bipyramidal structures, the system is forced to undergo a permutation transformation via a tetragonal pyramidal intermediate. Finally, a new Y-shaped structure is reached, in which the iodine atom, the nucleophile and both substituents lie in one plane. As the interaction between two substituents lying in the same plane is symmetry allowed, the nucleophile will tend to bind with the bulkiest phenyl ring to decrease the steric strain, possibly giving the desired product. As a result, the favoured reaction path will be determined by the difference in the activation energy barriers of the T ⇌ Y isomerization with the homolytic decomposition of

the trivalent iodine (SET path). Unfortunately, in the case of a six-membered ring, these two barriers are comparable and by-products are always expected. As shown in Table 1, changing the reaction conditions by decreasing the temperature or changing the solvent of the reaction could not avoid their formation (roughly 50% of the crude is composed of radical decomposition products)[35] but only makes the reactions run slower or not at all.

*Table 1: Experimental reaction conditions tested for iodonium ring opening. The complete or incomplete state of the reaction is based on the consumption of **4a/c** determined by thin layer chromatography (TLC).*

Molecule	Conditions	Conversion
4a	Neat, 200°C, 15 min	Complete
4a	Toluene, 95°C, 20h	Complete
4a	Benzene, 65°C, 7 days	Incomplete
4c	Neat, 200°C, 15 min	Complete
4c	Toluene, 95°C, 20h	Complete
4c	Benzene, 65°C, 7 days	Incomplete

Once the iodonium ring opened, and the **5a-c** precursors isolated,[1] the last step can be performed. It consists in the three-fold nucleophilic attack on an electrophilic phosphorus as PCl_3. Despite efforts to ensure the stability of the lithiated triphenylmethane reactant by low temperature conditions (-114°C, ethanol/$N_{2(l)}$ cooling bath), the reaction exhibits low yields. The difficulty comes from the third nucleophilic attack on the phosphorus atom. Indeed, the last substitution needs the molecule to adopt a very unfavorable ring-strained conformation sometimes leading to a degradation of the lithium intermediate before the completion of the reaction (Scheme 4).

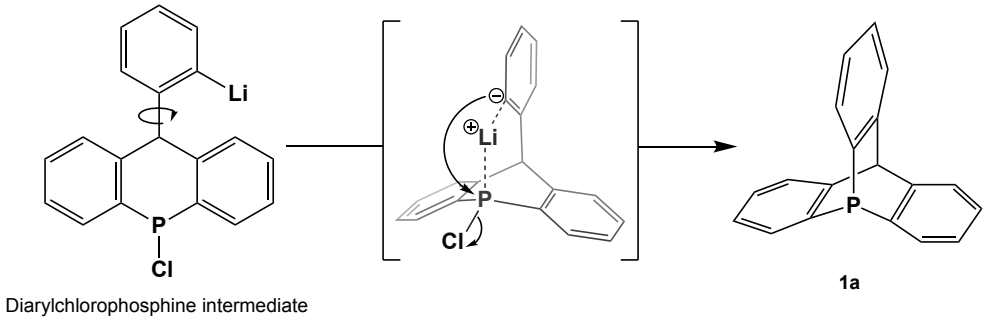

Scheme 4: Illustration of the strained conformation (in brackets) during the third nucleophilic attack.

[1] Precursors 5a-c were not isolated in satisfactory purity. The large amount of by-products at similar polarities (R_F values close in range) prevented a clean purification by silica gel column chromatography.

2. Synthesis of Pt-centered complexes

2.1 Effects of the pyramidalization

As mentioned above, 9-phosphatriptycene derivatives constitute a class of ring-strained phosphines with unique structural and electronic properties.[32] Whereas stereoelectronic properties of phosphines can be readily modulated by varying the nature of the groups linked to the phosphorus atom (alkyl, aryl, halogen, …) as well as their substituents, the cage-shaped structure of phosphatriptycenes provides new opportunities. Indeed, the phosphorus atom, fixed in the 9-position of the tricyclic bridgehead of the [2.2.2]-bicyclooctane motif, is strongly pyramidalized. This geometry has a strong effect on the electronic state of the phosphorus lone pair, which acquires a higher *s*-character than other phosphines (Figure 22). Because *s*-orbitals present a lower energy than the p-orbitals, the electrons are further stabilized and make phosphatriptycenes weaker Lewis bases compared to usual triarylphosphines. It results in phosphatriptycenes being weak σ-electron donor (because the overlap between s and p orbital is less efficient than p-p orbital overlap) and strong π-acceptor ligands. This feature is interesting for the elaboration of transition-metal catalysts that require low σ-donating ligands such as Stille couplings or Heck reactions.[37]

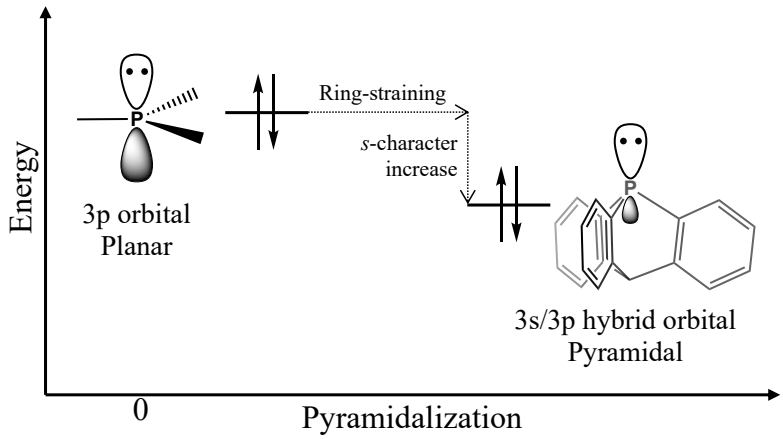

Figure 22: Walsh diagram of phosphine. Figure adapted from reference [38].

Ortho-substituted 9-phosphatriptycene derivatives are very adequate building blocks for molecular machines because of i) their robust scaffold where the *ortho*-position fixed in a rigid position can serve to tune the steric effects by changing the substituent and, ii) their steric and electronic properties modulated by the pyramidalization, which confer them unique behaviors towards transition metals. Whereas the first aspect will be further discussed in part III, the second is central in the synthesis of the desired platinum-centered molecular gears and their properties.

2.2 Reaction of complexation

Following the synthesis of the ligands (**1a-c**), two commonly used platinum precursors were tested in different conditions in order to afford the desired complexes (**6a-c** and **7a-c**) represented in Scheme 5.

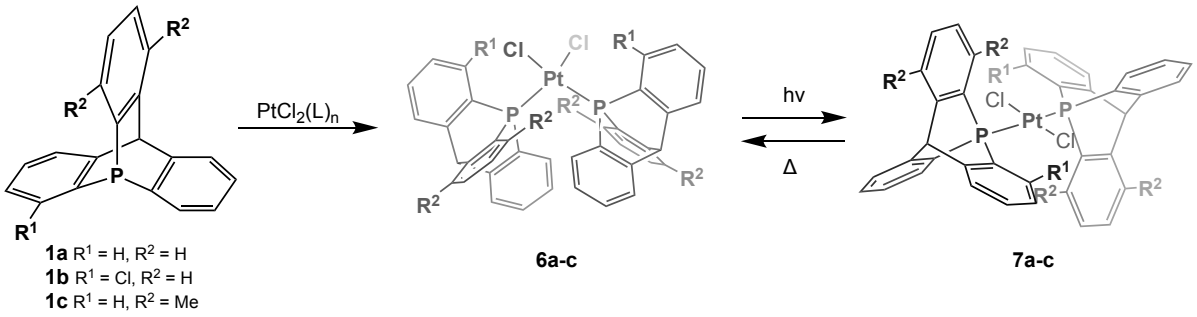

Scheme 5: Reaction of complexation on a $PtCl_2$ metal precursor.

These conditions, gathered in the Table 2, afford indication on the major challenges for accessing such molecular machines. Indeed, the search for working conditions to run the complexations was impeded by i) the difference of solubility between reactants leading to heterogenous mixture in some cases, and ii) the low reactivity of 9-phosphatriptycenes towards metal precursors due to the steric and electronic properties as discussed above. Despite intense efforts, no phosphatriptycene-metal complex was isolated pure and could be fully characterized by NMR due to insolubility in all organic solvents (list of all tested solvents) as well as in water.

Table 2: All reaction run for 20h, observations based on the presence of ligands in ^{31}P NMR.

Ligand	Precursor	Solvent	Temperature	Observations
1a	K_2PtCl_4	EtOH/H_2O	70°C	Completed
1b	K_2PtCl_4	EtOH/H_2O	70°C	Completed
1c	K_2PtCl_4	EtOH/H_2O	70°C	Completed
1c	K_2PtCl_4	EtOH/H_2O	r.t.	No reaction
1a	$PtCl_2$	Benzene	r.t.	Completed
1b	$PtCl_2$	Benzene	r.t.	Completed
1c	$PtCl_2$	Benzene	r.t.	Completed
1c	$PtCl_2$	Benzene	70°C	Completed

The first metal precursor tested, K_2PtCl_4, is probably one of the most widely used precursors to form organometallic compounds. Unfortunately, it presents the disadvantage of having a very low solubility in organic solvent which leads to the necessity to carry on the reaction in a

homogenous mixture of ethanol/water (1:1)[27] where the phosphatriptycenes were not suitably solubilized. In addition, potassium tetrachloroplatinate (II) being a square planar 16-electrons complex, the two phosphatriptycene ligands need to displace a chlorine atom during their binding to the metal. These ligand substitutions, occurring via an association and dissociation mechanism (Exemplified by the case of cisplatin in Scheme 6), are unfavored by the low σ-donating ability of the phosphatriptycenes, and did not occur at room temperature. Both above mentioned problems could be solved by increasing the temperature of the reaction. In fact, the higher temperature enables a better dissolution of the reactants as well as contributing to the displacement of the chlorine ligands. Thus, the reaction of complexation could be done, as confirmed by the extinction of the ^{31}P NMR signal of the phosphatriptycene.

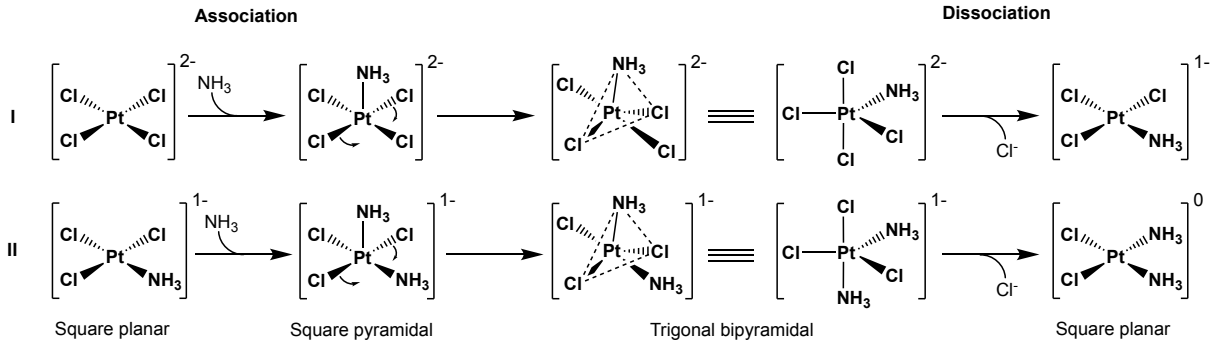

Scheme 6: Illustrative example of the two associative substitutions of ligand occurring in the synthesis of cisplatin from the K_2PtCl_4 precursor.

To avoid the difficulties linked to the use of K_2PtCl_4, a second metal precursor was tested for the reaction with the phosphatriptycenes. The latter, $PtCl_2$, is a 12-electron complex and, as a result presents a higher reactivity. Indeed, it does not need to displace any chlorine atom and can directly bind with the phosphatriptycene ligands. Its reactivity is also its weakness, since it needs to be stored and manipulated under inert atmosphere to avoid possible degradation. Despite that, platinum (II) dichloride also presents the advantage of being partially soluble in organic solvent such as benzene, the commonly used solvent for reaction with this metal precursor. As a result, when the complexation reaction of $PtCl_2$ with the phosphatriptycenes was attempted either at room temperature or at a temperature of 70°C, the same results were obtained and, in all cases, the ^{31}P signal of the phosphatriptycene disappeared, confirming the complexation.

2.3 Accessing the cis-complexes

As shown by the reaction represented in Scheme 5, the conditions detailed in Table 2 enable to form the cis-isomer of the aimed complexes (**6a-c**). In fact, the formation of the cis-

isomer as unique product is not trivial, and comes from a careful consideration of the selected metal precursor.[39] This can be explained by long-established concepts of inorganic chemistry which are i) the trans-"influence", defined in 1966 by Pidcock et al.,[40] as the ability of a ligand to weaken the metal-ligand bond trans to itself and, ii) the trans-"effect", which affects the rate of substitution reactions of the ligand in the same position. Since there is no definitive reason why an "influence" should describe a thermodynamic property and an "effect" refers to a kinetic property, the correct use of these terms is a common source of confusion and their distinction is rarely made.[41] As a result, these concepts took a general sense to cover both kinetic and equilibrium phenomena and adopted the unified term of "trans-philicity". It is noteworthy to say that a ligand exhibiting a high trans-effect does not necessarily show high trans-influence (Figure 23). However, the opposite case is real, as a high trans-influencing weakens the trans bond and thereby enhances the rate of substitution of the same trans ligand.

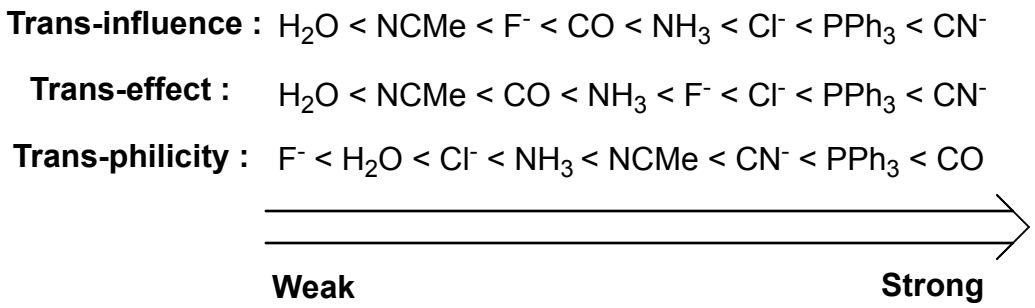

Figure 23: "Trans-effects" scale for some selected common ligands. Figure adapted from reference [41].

Although a considerable amount of research was done to scale these effects for various ligands, it has been difficult to produce a systematic set of data. Still, the numerous works concerning the evaluation of their magnitude based on experimental measurements (chemical shifts, stretching vibrational frequencies, coupling constants, …) or theoretical calculations lead to a systematic correlation with electronic properties of the considered ligands. Indeed, the strength of the effects is dictated by the σ-donation and π-back-donation of the ligands. As the synthesis of new complexes from 16-electron square planar (such as K_2PtCl_4) involves an associative ligand substitution, the consideration of all ligands effects is crucial to form the desired product. For instance, the reaction of ammoniac with potassium tetrachloroplatinate (II) gives the cisplatin complex, whereas the reaction of tetraamine platinum (II) in presence of chloride ion gives the trans product (Scheme 7).

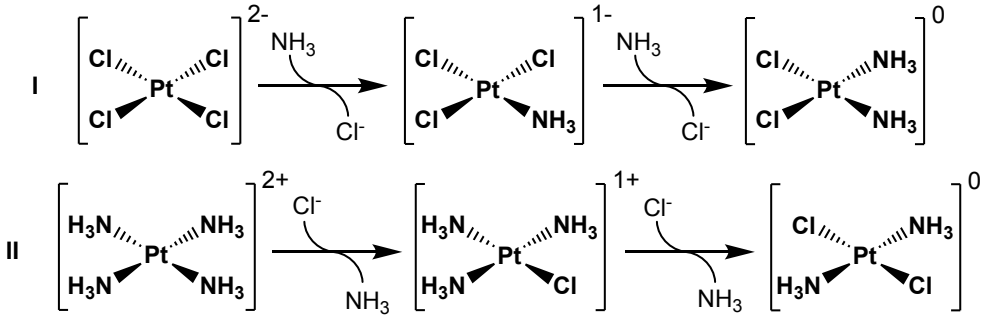

Scheme 7: Illustration of the trans-effects inducing the formation of different isomers depending on the metal precursor.

As already presented in Scheme 6, the mechanism of ligand substitution operates via a trigonal bipyramidal intermediate. In this intermediate, the most trans-inducing ligand (Cl in this case (cf. Figure 23)) always sits at an equatorial site where the two others are occupied by the incoming ligand (NH_3) and the leaving one (Cl as well). The propensity of the trans-inducing ligand to occupy an equatorial site actually arises from its π-acidity. Indeed, these positions are placed as the π*-orbitals of the ligand are in direct interaction with the d-orbitals of the metal. The latter provide a great electron source (when occupied) for the π-acceptor ligands, which receive the benefits of a back-bonding (Figure 24) and stabilize the intermediate.

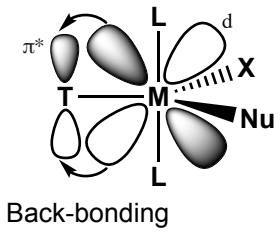

Figure 24: Illustration of the overlap between partially filled d-orbitals of the metal and the π-orbitals of the trans-inducing ligand.*

Once in this position, the trans-inducing ligand can exert its strong σ-basicity. This leads to the electronic enrichment of the complex, resulting in the destabilization of the bond trans to the ligand, and finally to an easy substitution reaction. Consequently, these two electronic properties work together to facilitate the substitution of the leaving ligand, one (π-acidity) by stabilizing the intermediate, the other (σ-basicity) by destabilizing the leaving ligand. This confirms the tricky differentiation between the thermodynamic and kinetic effects of some ligands.

To summarize, the formation of the desired cis- or trans-complex from square planar metal precursors begins with the careful consideration of its coordinated ligands, as well as the one that will be added during the associative substitution. However, the reason why

phosphatriptycene ligands form cis-isomers, has not been determined yet. Actually, it can be assumed that they exhibit a reactivity similar to common triarylphosphines. By comparing the trans effects scales shown in Figure 23, it appears that triarylphosphines derivatives (which exhibit very strong effects) only conduct to cis-isomers by reaction with K_2PtCl_4 (Scheme 8), which is also the case of phosphatriptycenes. However, due to their lower σ-basicity, phosphatriptycenes will destabilize to a lower extent the bond trans to their position, which means that the substitution process should be much slower.

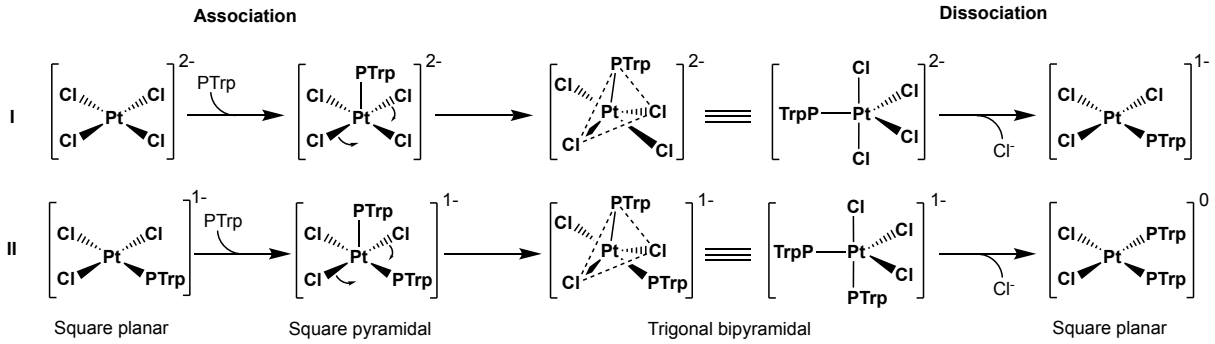

Scheme 8: Illustration of the two associative substitutions of ligand occurring in the present synthesis of molecular gears from the K_2PtCl_4 precursor.

2.4 Investigation of the isomerization process

Consequently, it is now necessary to find a way to access to the trans-isomers of the aimed complexes. One solution would be to use other metal precursors, such as the Zeise's salt or cis-bis(benzonitrile)platinum (II) chloride,[42] which afford the desired trans-product in reaction with phosphines. However, this solution does not afford any clutch-like function of the gears, as desired in the present work. Cis-trans isomerization of platinum (II) complexes has received great attention in last decades with earlier reports on the thermal interconversion,[43] followed by the photochemical in the next years.[44] Many research studies focus on d^8 square planar platinum and palladium (II) complexes of the MX_2L_2 type (X = Cl, Br, I; L = phosphine) where the cis isomers are generally known to be thermodynamically more stable than their trans counterparts. In fact, the equilibrium position favorable for cis-trans isomers of this type of complexes has proven to depend of the electronic properties of the ligands and the solvent polarity.[45] However, the trans complexes can be obtained via photo-induced isomerism with polychromatic light and are easily distinguishable from the cis by a series of characterization methods (spectroscopies, melting point, …).

It is believed that the cis to trans isomerization occurs via either an intramolecular path or an intermolecular one.[46] In the first path, the photoirradiation triggers a conformational change toward a tetrahedral photostationary state (pathway I in Scheme 9), for which the stability is dependent on the dielectric constant of the solvent. Indeed, the less polar is the solvent, the greater is the proportion of formed trans isomer in the mixture. It is explained by the fact that the latter has a very low dipole moment in the ground state (square planar structure) and thus would prefer a non-polar surrounding. As a result, the irradiation triggers the formation of the stationary state and then, the use of non-polar solvents favors the formation of the trans compound by its stabilization. The second path hypothesized that the solvent could have another role in the isomerization process. It is possible that adequate solvents could coordinate the metal, leading to a 5-coordinate trigonal bipyramidal geometry as the one encountered in the substitution mechanism (pathway II in Scheme 9). Consequently, it results in the substitution of the solvent ligand, similar in term of trans effects to the one occurring in the formation of new complexes. These processes present the advantage of being totally exempt of all new chemical compound addition to trigger the isomerization, making them "traceless". However, the photochemical stationary state is not thermodynamically favored, making the complete isomerization of cis isomers in trans difficult to reach.

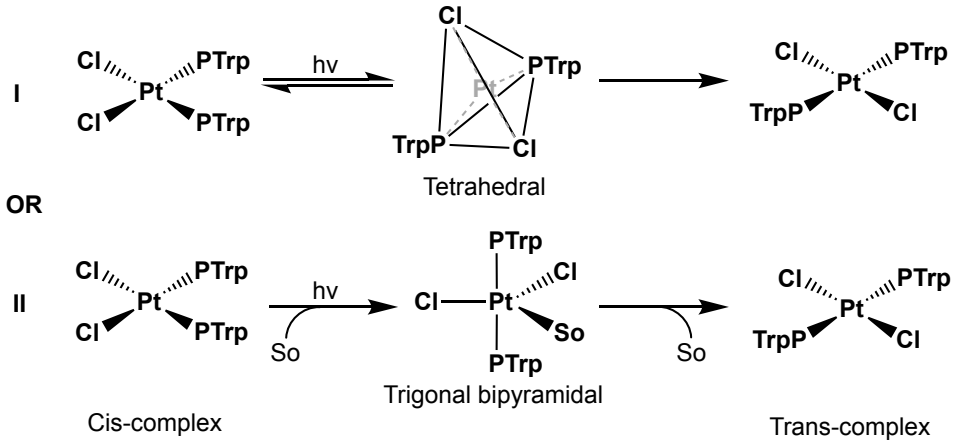

Scheme 9: Representation of the proposed mechanistic path for the cis to trans isomerization. Scheme adapted from the reference [46]. So = Solvent molecule.

As the clutch-like function of the gears is only completed when the system can reversibly switch between the cis and trans isomers, it is necessary to find a way to switch back to the first one. As shown in Scheme 5, the reversible process from trans to cis is thermally-conducted. Like the photoisomerization, it is believed that this process can occur via multiple paths.[46] Actually, these processes occur via a substitution mechanism, which tends to give the most favorable product. As discussed previously, due to the electronic properties of the ligands, the substitution mechanism goes through a stabilized trigonal bipyramidal intermediate where the position of

the ligands will determine the formed product, the cis in the present case. Therefore, as the substitution is an intermolecular reaction, an external ligand is needed to form the intermediate and give the cis-product. One of the paths considers an excess of ligand (here the phosphatriptycene) to access the trigonal bipyramidal intermediate. Since the aim is to provide a "traceless" isomerization, this path will not be more developed. The second proposed path is similar to the one encountered for the photoisomerization where a molecule of solvent is involved (Scheme 10). This path occurs in two steps, where the first one (step I in Scheme 10) is the substitution of the phosphatriptycene ligand by the solvent. This step is the slowest of the two (the rate-determining step) because it displaces a phosphine ligand, which is a very stabilized ligand for transition metals, as discussed before. After that, the displaced phosphatriptycene can again act as a nucleophile (step II in Scheme 10) to reach a second intermediate, where trans effects can induce the departure of the solvent molecule, inducing the formation of the cis-product. The last path once again suggests that the isomerization is highly dependent on the solvent polarity. Indeed, it has been proven that polar solvents exhibiting high binding potential can assist the trans to cis isomerization.[45]

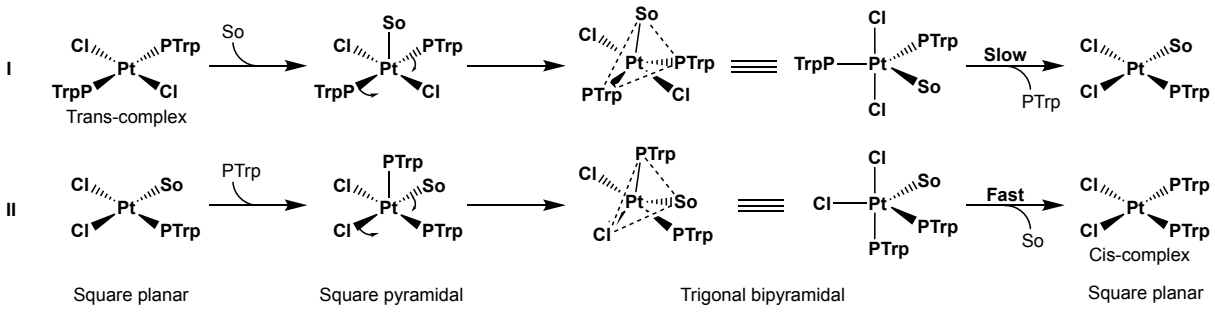

Scheme 10: Representation of the proposed mechanistic path for the trans to cis isomerization with the participation of a molecule of solvent. Scheme adapted from the reference [46].

Unfortunately, despite numerous efforts to synthetize the 9-phosphatriptycene platinum complexes, we realized that all complexes were very poorly soluble in common organic solvents chosen on a wide range of polarity. Indeed, these $PtCl_2L_2$ complexes display very low solubility, even in the presence of very bulky organic ligand (L) such as phosphine.[47] Therefore, the synthetized phosphatriptycene derivatives make no exception, preventing all characterization needing a prior solubilization.

3. Toward soluble molecular gears

Because of the insolubility of the desired Pt-complexes, it was necessary to think about alternative routes to synthetize and characterize soluble molecular gears. Due to the simplicity of their structure, composed of a $PtCl_2$ and two phosphatriptycenes rotators, it was thought that the modification of one of these components should lead to a modification of the physico-chemical properties of the complex, including solubility.

The first proposed solution was to change the chlorine substituents present on the metal by two methyl groups. It was reasoned that this difference could contribute to solubilize the formed complex in organic solvents. Therefore, the reaction between one of the synthetized phosphatriptycene (**1c**) and a $PtMe_2(NCPh)_2$ metal precursor was tested to finally show that no reaction occurs between the species. Since there was no difference in solubility between the compounds and that the reaction was also attempted at high temperature, it was then concluded that the poor basicity of the phosphatriptycene was in cause. This idea was confirmed when the reaction of the same precursor with the tris(o-tolyl)phosphine was successfully achieved at room temperature. In was then concluded that the chloride ligand present on the other precursors can attract the electrons from the metal, making it more electropositive and then favors the complexation reaction. It turns out that the chlorine atoms were actually essential for the reaction to occur. Following that observation, it was concluded that the used metal precursor must bear chlorine atoms to be sufficiently reactive toward the phosphatriptycenes.

In this case, the better solubility cannot arise from a change of the ligands beared by the metal, but could arise from a change of the metal itself. Indeed, as previously mentioned,[45] palladium (II) dichloride complexes are also widely used metal for the synthesis of square planar complexes and could provide an interesting alternative to the platinum. Few results have been obtained concerning the complexation of palladium (II) dichloride but these are encouraging. Indeed, the reaction of trans-bis(benzonitrile)palladium (II) with a phosphatriptycene (**1c**) affords a partially soluble complex, as confirmed by ^{31}P NMR by the replacement of the ligands signal by a much smaller one downfield. In addition, attempts to solubilize the formed complex in acetonitrile finally lead to the obtention of suitable crystals for crystallographic analysis (Figure 25).

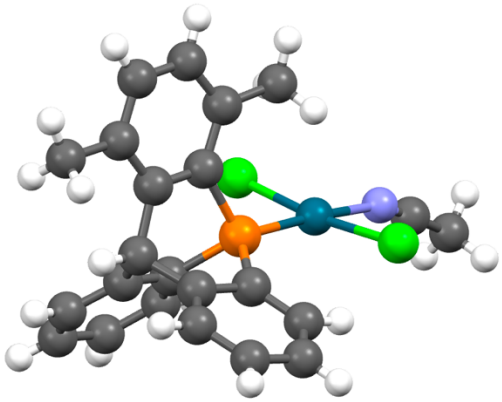

Figure 25: Molecular structure of the Pd-centered complex as obtained by crystallographic analysis.

As seen, the current structure revealed to be a trans isomer. Since the reaction of triarylphosphines with the same metal precursor normally leads to the formation of the trans isomer,[42] the latter structure (resulting of the ligand substitution of one phosphatriptycene by a solvent molecule) should normally conduct to the cis form. Indeed, this substitution occurred in the dark and then should follow the same mechanistic path as the one presented in Scheme 10 (I). It is believed that this difference with the expected scheme arise from the differences of electronic properties of the phosphatriptycenes with the common phosphines, mentioned before. In fact, from these properties could arise two scenarios. The first is that the formed product with phosphatriptycenes is not the trans as for common phosphine but the cis isomer, due to the nitrile ligands (cf. Figure 23) beared by the metal precursor. The second would be that the product of complexation is indeed the trans product as expected, but the acetonitrile ligand exhibits a strong enough trans-"effects" (cf. Figure 23) to compete with the phosphatriptycene. Both these scenarios can explain the observed differentiation in the substitution mechanism with the solvent (formation of the trans product instead of the cis) and are both possibly caused by the strong trans-"effect" of the nitrile group of the ligands.

Besides that, the solution could also comes from the modification of the rotators (*i.e.* the ligands of the metal complexes). Indeed, as mentioned in the literature,[47] the presence of certain kind of substituents on triarylphosphines and phosphatriptycenes leads to the obtention of soluble complexes. This idea was confirmed by a quick but significant test where two different triphenylphosphine derivatives (the tris(p-methoxy)phosphine **8a** and the tris(o-tolyl)phosphine **8b**) were complexed on a platinum (II) dichloride precursor (Scheme 11).

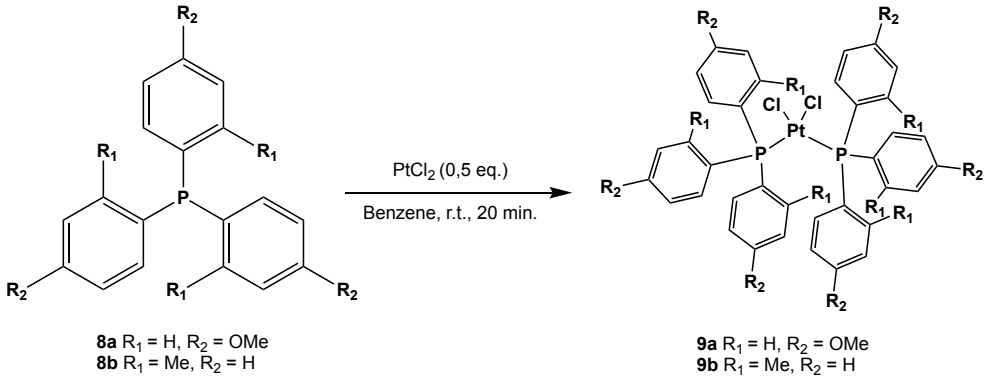

Scheme 11: Reaction of the reactions used to obtain soluble triarylphosphines Pt-complexes.

These tests led to the observation that the addition of substituents such as methoxy groups (in **8a**) can generate enough interactions with the solvent such as hydrogen bonds, to help the solubilization of the complex (**9a**). On the other hand, the addition of non-polar groups such as methyl groups (in **8b**) does not provide any stabilization of the complex (**9b**) by the solvent, this one being totally insoluble. It was then concluded that the same kind of interactions between the solvent and the complexes has to be generated to ensure its solubility in organic solvent. Indeed, all the reported structure of soluble platinum (II) dichloride complexes bearing on phosphatriptycenes derivatives include functional groups or atoms susceptible to interact with the solvent through strong non-covalent interactions (hydrogen bonds and other electrostatic interactions).

As a result, the synthesis of a new 9-phosphatriptycene derivative was planned to provide a new opportunity in the characterization of the molecular gears. The latter is based on a previously described synthesis affording an unsubstituted 9-phosphatriptycene with an alcohol function on the carbon of the second bridgehead position (Scheme 12).[32]

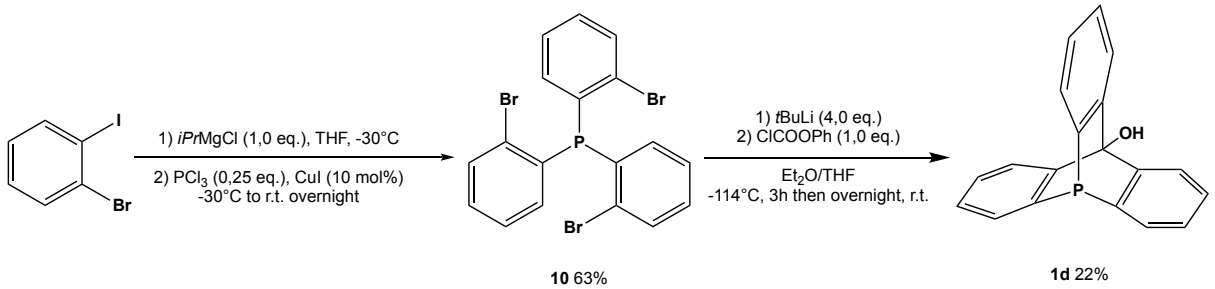

Scheme 12: Synthesis pathway to obtain the 9-phospha-10-hydroxytriptycene.

This synthetic path presents the net advantage of being much shorter than the previously described one, with only two steps to access the phosphatriptycene from a commercial compound. The synthesis starts with the formation of tris(2-bromophenyl)phosphine (**10**), prepared from the reaction of three equivalents of 1-bromo-2-iodobenzene on PCl_3. It begins

with a I/Mg exchange to form a (2-iodophenyl)magnesium chloride intermediate. The low temperature of about -30°C (using an acetone/$N_{2(l)}$ cooling bath) guarantees the stability of the Grignard intermediate and avoids undesired degradation. The formed Grignard can subsequently react with the electrophilic phosphorus of PCl_3 in the presence of a catalytic amount of copper (I) iodide. The presence of CuI is crucial to complete the reaction.

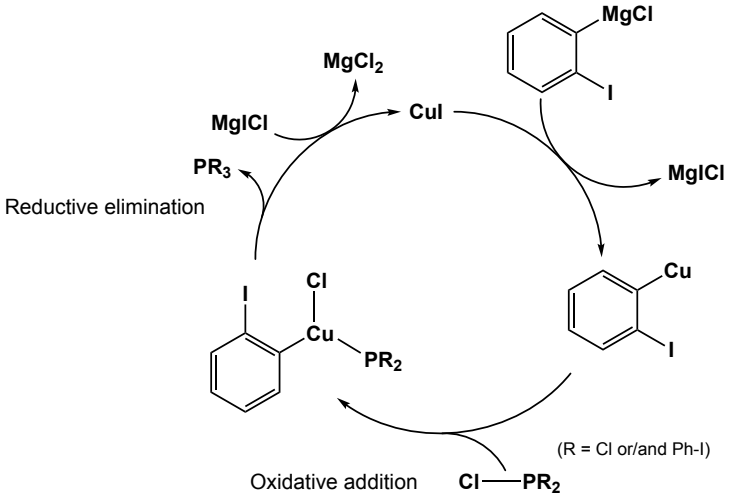

Scheme 13: Proposed catalytic cycle of CuI during the addition reaction.

From a mechanistic point of view, it is believed that the reaction proceeds through a catalytic cycle[48] (Scheme 13) where an organocopper intermediate resulting from the Mg/Cu exchange can facilitate the reaction between the aryl rings and the phosphorus atom. The catalyst is very important for the addition of the third aryl ring on the very bulky diarylchlorophosphine intermediate (PR_2 where R = Ph-I) because this reaction does not occur without it. After the addition on the phosphine, the CuI catalyst is regenerated via a salt metathesis reaction in the presence of MgICl, which precipitate as $MgCl_2$.

Once the triarylphosphine precursor (**10**) is synthesized, the last step can be performed. As it was the case for the previous synthesis path, it consists in the three-fold nucleophilic attack on an electrophilic atom, a carbon one here, giving the desired alcohol group. Once again, despite efforts to ensure the stability of the lithiated triphenylphosphine reactant by low temperature conditions (-114°C, ethanol/$N_{2(l)}$ cooling bath), the reaction exhibits low yields. The difficulty comes again from the third nucleophilic attack, difficult to do due to the unfavourable ring-strained structure. Once again, the obtained complexes of this ligand in reaction with the $PtCl_2$ metal precursor exhibited a low solubility, showing that the addition of only one hydroxy group is not sufficient to allow a solubilization. The next step is then to take direct inspiration from the literature to solubilize the complex, and transform this alcohol into a methoxy group, as it will be discussed in Part V.

In parallel, another phosphatriptycene derivative was considered as a potential ligand for transition metal. The latter, the so-called diphosphatriptycene, belongs to the family of the 9,10-diheteratriptycene and presents the particularity of having two phosphorus atoms on its bridgehead positions. This molecule can be synthesized similarly to the ones described before by making the three-fold nucleophilic attack on the electrophilic phosphorus of PCl_3, from the already described triarylphosphine (**10**) (Scheme 14).

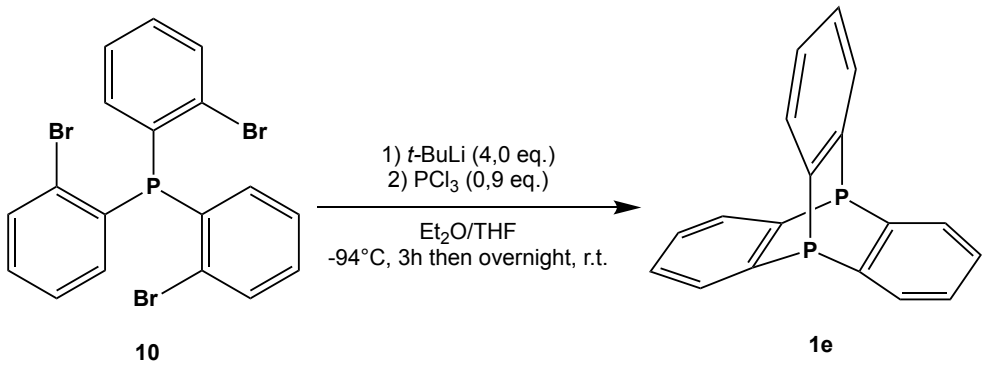

10 **1e**

Scheme 14: Synthesis pathway to obtain the 9-10-diphosphatriptycene.

Due to the presence of the two phosphorus atoms on these positions, it is believed that both of them exhibit a lower pyramidalization than their counterparts (phosphatriptycenes **1a-e**). Indeed, the C-P bonds length, larger than the C-C ones, bring the three aryl rings closer to the second phosphorus atom and then change the bond angles. This has been confirmed by the crystallographic analysis of the product (Figure 26), which shows the perfect symmetry of the molecule.

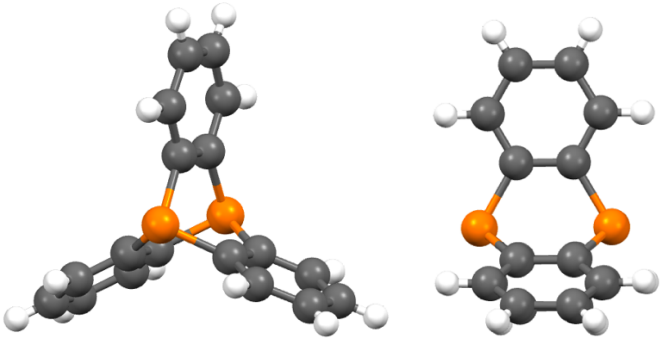

Figure 26: Molecular structure of the Pd-centered complex as obtained by crystallographic analysis.

As a result, due to the change of their pyramidalization, both phosphorus atom exhibit changes in their electronic properties compared to the other 9-phosphtriptycenes (**1a-e**). Once again, this affirmation was confirmed by ^{31}P NMR, where the phosphorus are deshielded compared to their more pyramidalized counterparts. However, even if their signal is downfield, it is believed that their σ-basicity is stronger because of their lowest pyramidalization (cf. Figure 22). These unique electronic properties bring interesting new prospects for the elaboration of new molecular gears with transition metal as stator, as more discussed in Part V.

PART IV – Theoretical results and discussion

1. Studied structures and calculation methods

The theoretical part of this master thesis consists in a *Density Functional Theory* (DFT) investigation of the properties of the targeted complexes. It includes cis isomers (**6a-c**) of the different 9-phosphatriptycene derivatives (where X = C-H) as well as the corresponding trans isomers (**7a-c**), much more difficult to obtain experimentally. Their properties are analyzed through a complete investigation of their possible conformers, by studying their relative energies and the structural factors influencing it. This provides an overview of most influential features on rotational motions in the aim of getting a better understanding of their working process.

A preliminary comparative DFT study of exchange-correlation (xc) functionals and relativistic effective core potentials (RECPs) on cisplatin as model compound established that the M06-2X functional combined with LanL2TZ(f)[49] for Pt center and 6-311G(d)[50] for other atoms is the most suited method for describing Pt-based complexes. All the results obtained with the Gaussian 16 set of programs[51] were compared to structural and vibrational experimental data to finally show that this xc functional displays the best compromise between accuracy and computational costs. This xc functional belongs to the Minnesota M06-class of density functional as hybrid meta-GGA with an exchange term that includes 54 % of the exact Hartree-Fock exchange.[52] Therefore, this method was chosen for the computational investigation of complexes properties using a tight convergence threshold for geometry optimization.

2. Investigation of complexes conformations

In the aim of defining rotation dynamics of isomers, several geometry optimizations were performed from different starting points, varying by the substituents position around the P-Pt-P axe. This method provides an exhaustive series of possible conformers for both cis and trans isomers (**6a-c** and **7a-c**). These conformers correspond to local minima on the potential energy surface when a rotational motion is engaged. After optimization calculations, all complexes present a square planar molecular geometry on the platinum center and exhibit a near-symmetrical structure around it. As expected, cogs in cis-isomers are tightly intermeshed, which allow a synchronized rotational motion of the gears while trans-isomers ones are sufficiently separated in space to display a complete disengagement. Their structures are

presented in Table 3 as well as the equilibrium between their most representative conformations, also pictured in Figure 27.

Table 3: Structure of the studied complexes in their cis- (left) and trans- (right) isomer form.

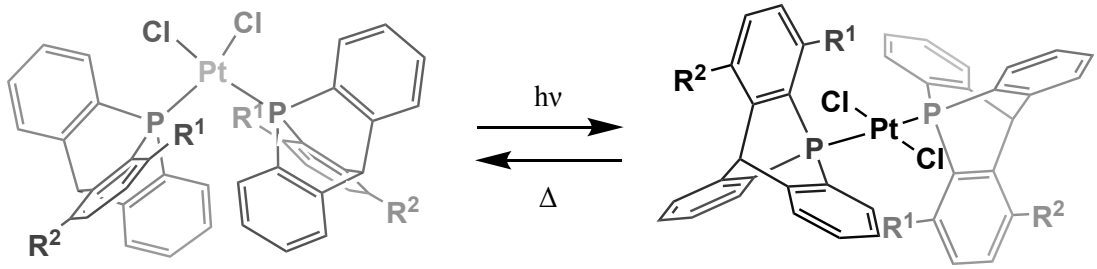

6a-c **7a-c**

Compounds 6 and 7	Substituents	
	R^1	R^2
a	H	H
b	Cl	H
c	Me	Me

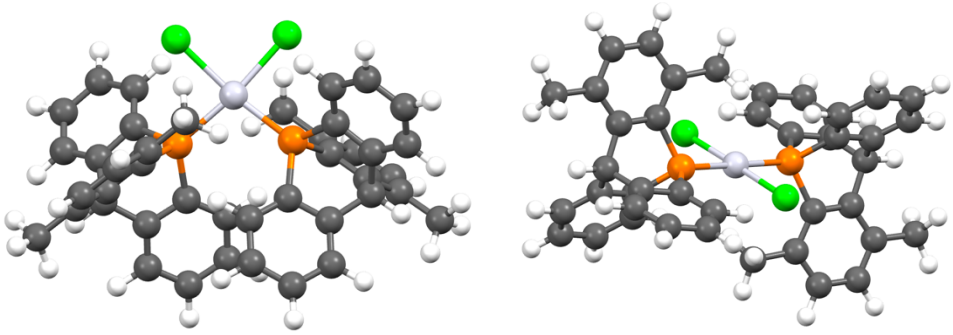

6a-c **7a-c**

Figure 27: Representation of the cis- (left) and trans- (right) isomers for complex N°.

Legend: Orange = Phosphorus; Light grey = Platinum; Green = Chlorine; Dark grey = Carbon; White = Hydrogen

Cis-isomers (**6a-c**) are characterized by the shorter angle between phosphine ligands leading to the engagement of their cogs. The latters are distributed around the rotation axis in three particular positions described below in Table 4. Depending on their position, cycles are located i) near the central chlorines of the stator, ii) in the space between two cycles of the opposite gear or iii) parallelly to the inferior cycle of the opposite gear. It is expected that their position causes varying repulsive interactions affecting the rotation dynamics. Trans-isomers (**7a-c**) are characterized by a longer distance between the gears, supposing less interactions in the structure. These isomers have also critical positions of the cogs, with cycles situated either beside the central chlorines of the stator or in spaces between two cycles of the opposite gear.

Consequently, it is expected that the major contribution on rotation dynamics arise from the stator-cogs interaction since the gears are sufficiently spaced (the stator being the Pt-Cl_2 core of the complex).

The structure optimization started from different rotamers allowing to define all stable conformations of both isomers. The latters exhibit the same distribution of their cogs around the rotation axes, independently of the substituents position. As a result, it is possible to describe them equally by pseudo-Newman projection represented in Figure 28. These show the spatial organization of ligands cycles beside the Cl_2-Pt-P_2 plane and provide a useful tool for the following discussions. As seen, gears are named α and β for which the cogs can be distinguished into three pairs, numbered from 1 to 3, corresponding with each other by the similarity of their structure and chemical environment.

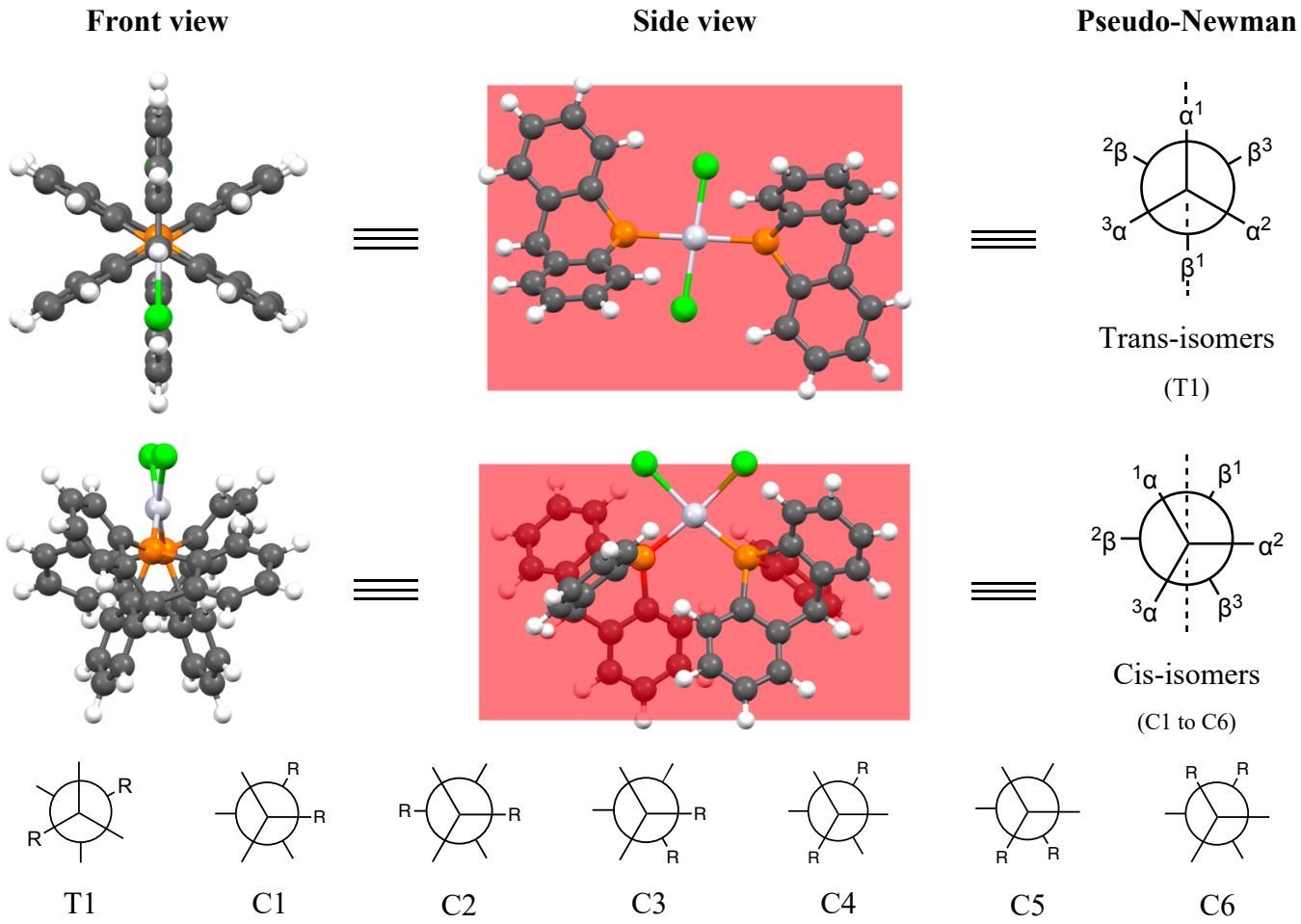

Figure 28: Structure of isomers (n°) as obtained at the M06-2X/6-311G/Lanl2TZ(f) (gas phase) level and the corresponding pseudo-Newman projections. Letters written in projections correspond to cycles denomination and dotted line to the central plane (in red).*

First optimization results on trans-complexes showed that they all present a similar antiperiplanar conformation along the P-Pt-P axis. In this conformation represented in Figure 27, substituents are placed opposite to each other to minimize steric interactions between them. This structure was reached for many starting points of the optimization regardless of the substituent, which means that i) this conformation is the most stable because the steric hindrance between gears is minimized and that ii) the gears are sufficiently separated in space to perform a quasi-free rotation. Similarly, calculations on cis-isomers exhibited a staggered conformation but the resulting conformer depends on the starting point due to the steric hindrance of this isomer which impede the free rotation of gears. As a result, starting by all significative rotamers, six different conformers were found once redundant ones were removed. Due to the absence of substituents in **6a** and **7a**, all their respective conformers have equivalent structure.

3. Thermodynamics

Since each conformer are local minima on the potential energy surface, they correspond to encountered structures in the rotation motion. As a result, the analysis of their relative energies gives more indication on the complexes rotation dynamics. In this part, complexes are compared with each other to get a first insight of structural factors impacting the global energies. Also, the relative energies of the conformers are compared between gas phase and their equivalent in a solvent (chloroform, $CHCl_3$), modelled using the IEFPCM[53] approach, to see whether it causes electrostatic stabilizations. As shown in Table 2, cis-isomers are generally less stable than the corresponding trans-isomer except for C2 conformers. The ranking of stability of the different conformers can be determined as: C5 < C4 ≈ C3 ≈ C6 < C1 < C2. As seen, the unsubstituted cis-isomer shows a stability almost similar to its trans-isomer, leading to think that substituent-induced steric clashes are the major factor of destabilization in these complexes. This observation is verified in all conformers and especially in the case of C5 where steric clashes are probably the most important due to the presence of substituents on the inferior cycles. Following this same idea, it can be seen that C4 and C3 also exhibit a significant destabilization due to the close proximity of their substituents. They both present a substituent on one of the inferior cycles and the second could explain the difference of stability between them. The further destabilization of C4 compared to C3 is attributed to the fact that its second substituent is directly interacting with the central chlorines, which is not the case of C3. Thus, as seen in Figure 29, inferior cycle-cycle and superior cycles-chlorines interactions are

impacting factors on relative energies of conformers. By comparing C5 with C6 conformers where substituents are in the inferior and the superior positions, respectively, it is clear that steric hindrance between inferior cycles is more impacting stabilities than cycles-chlorines interactions. Finally, C1 and C2 are the most stable since the first have only one cycle-chlorines interaction and the second avoids all previously discussed steric clashes.

Table 4: Relative energies (kJ/mol) and dipole moments (D) obtained at the M06-2X/6-311G/Lanl2TZ(f) (gas phase) level for the different complexes. All relative energies were calculated as the differences with respect to the corresponding trans-isomer.*

Complex	Projection	ΔE	ΔH^0	ΔG^0	μ
Trans					
H		0,0	0,0	0,0	0,0
Cl		0,0	0,0	0,0	0,0
Me		0,0	0,0	0,0	0,1
Cis					
C1					
H	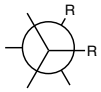	-8,3	-7,8	1,4	11,8
Cl		3,5	6,5	12,9	12,2
Me		-5,2	-4,2	7,7	11,6
C2					
Cl	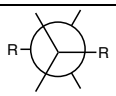	-3,4	-3,2	0,0	13,0
Me		-14,8	-13,9	-2,6	11,8
C3					
Cl	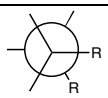	6,6	6,5	12,9	12,2
Me		10,9	11,3	20,7	11,4
C4					
Cl		4,7	4,9	11,8	12,4
Me		11,0	11,2	20,0	11,4
C5					
Cl	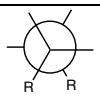	17,1	16,1	23,3	10,9
Me		31,5	31,1	42,2	11,2
C6					
Cl	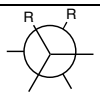	9,8	9,2	13,6	13,2
Me		4,2	3,3	10,1	11,4

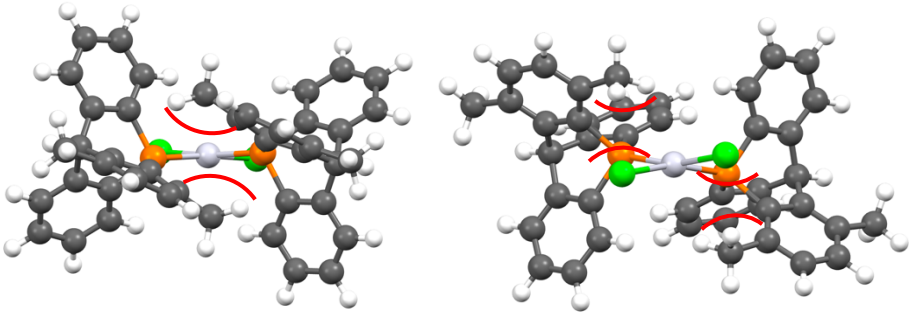

Figure 29: Illustration of the existing steric clashes in complex 1c between the inferior cycles in C5 (left) (lower view) and between cycles and central chlorines in C6 (right) (upper view).

Energies value presented in Table 5 show that cis-isomers have a lower free energy in chloroform than the corresponding trans-isomers except for conformers C5, C4 (Me) and C3 (Me). Therefore, as previously shown, the ranking of stability of different conformers is: C5 < C4 ≈ C3 ≈ C6 < C1 < C2. As in gas phase, substituent-induced steric clashes must destabilize some conformers to explain the order of stability. However, it can be seen that the solvent has a significant effect on energies since it allows the stabilization of all cis-isomers. In the absence of substituents, the more stable character of the cis-isomers is entirely attributed to its larger dipole moment, which allows stabilizing electrostatic interactions with the solvent while the non-polar trans-isomer is much weakly stabilized. When *ortho*-substituents are added on the triptycene gears, steric clashes between i) the two substituents, ii) the substituents and the central chlorine atoms and iii) the substituents and the inferior phenyl rings impact the conformers stability. In some conformers (C5, C4 and C3), steric clashes cause enough destabilization to counterbalances the favorable electrostatic interactions with the solvent and result in the cis-isomers being less stable than the trans ones.

Since steric clashes are the main factor determining energies, chlorine-substituted complexes should exhibit stability similar than their methyl-substituted counterparts. However, C1 and C6 do not seem to follow this theory. As seen in their structure, they present substituents in interaction with the central chlorines (Figure 30). This interaction should be slightly more important in the case of a methyl and, as a result, leads to a decrease of stability by steric interactions. Since it is not what is observed, the difference in energies between substituents must arise from a different reason. A further investigation of the complexes structure showed that intramolecular electrostatic interactions could justify the energy differences between substituents.

Table 5: Relative energies (kJ/mol) and dipole moments (D) obtained at the M06-2X/6-311G/Lanl2TZ(f)/IEFPCM (solvent = $CHCl_3$) level for the different complexes. All relative energies were calculated as the difference with the corresponding trans-isomer.*

Complex	Projection	ΔE	ΔH^0	ΔG^0	μ
Trans					
H		0,00	0,0	0,0	0,2
Cl		0,00	0,0	0,0	0,0
Me		0,00	0,0	0,0	0,9
Cis					
C1					
H	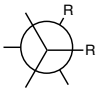	-29,6	-29,1	-25,1	16,4
Cl		-18,1	-18,4	-9,9	18,5
Me		-23,3	-22,3	-10,7	16,2
C2					
Cl	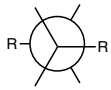	-25,6	-25,9	-18,6	18,1
Me		-34,0	-33,8	-22,7	16,4
C3					
Cl	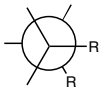	-14,2	-14,5	-5,6	17,1
Me		-9,7	-9,5	0,7	16,0
C4					
Cl		-15,2	-15,2	-4,3	17,3
Me		-9,0	-9,3	0,2	15,9
C5					
Cl		-0,5	-2,4	4,0	15,2
Me		10,0	8,2	16,2	15,6
C6					
Cl		-14,8	-15,2	-5,2	18,6
Me		-16,3	-16,3	-6,3	16,1

As shown by atomic natural partial charges gathered in Table 6, difference of partial charge between central chlorine and the closest substituent is larger in the case of methyl than chlorine substituents. In fact, the methyl groups bear positive charges while their hydrogens directly point toward the negative central chlorines, inducing electrostatic stabilization. In the case of chlorine substituents, the smaller positive charge on the atoms create less interactions and do

not counterbalance the destabilization by steric hindrance. As a result, repulsive forces are more important than electrostatic ones leading to a global destabilization and an increase of distances between the substituent and central chlorine.

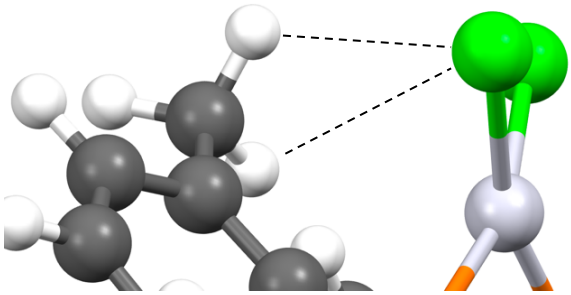

Figure 30: Illustration of the existing electrostatic interactions in complex 6b between the substituent and the closest central chlorine.

Table 6: Natural partial charges (δ) and distances (distances d in Å) in selected cis-isomers using the M06-2X/6-311G/Lanl2TZ(f) (gas phase) method. Values for methyl groups are given for the closest hydrogen atom from the central chlorine.*

Complex	Projection	δ_{Cl}	δ_{R}	$\Delta\delta_{R\text{-}Cl}$	$d_{R\text{-}Cl}$
C1					
Cl	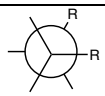	-0,42	0,07	0,48	3,304
Me		-0,44	0,24	0,69	3,220
C4					
Cl		-0,40	0,06	0,46	3,349
Me		-0,43	0,25	0,68	3,248
C6					
Cl		-0,43	0,07	0,49	3,330
Me		-0,44	0,25	0,69	3,264

As conclusion to this part, each conformer representing local minima on the potential energy surface corresponds to the encountered structure in the rotation motion. The ranking of stability of the different conformers was determined as: C5 < C4 ≈ C3 ≈ C6 < C1 < C2, leading to the conclusion that substituent-induced steric clashes are the major factor of destabilization in these complexes. Then, it was determined that steric clashes between i) the substituents on the inferior phenyl rings, ii) the substituents and the central chlorine atoms and iii) the two substituents, are respectively the more impacting factors on relative energies. Finally, the solvent shows its significant effect on energies by its stabilization of all cis-isomers by electrostatic interactions.

4. Geometrical structure investigations

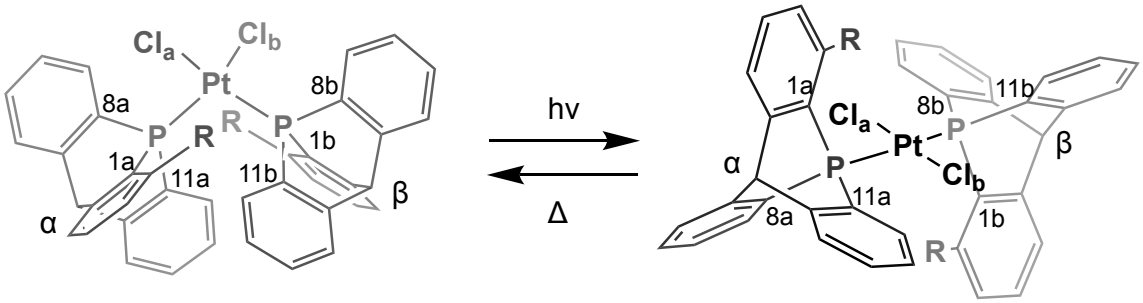

Figure 31: Structure of cis (left) and trans isomers (right). In molecules, α and β correspond to the gears where carbon atoms are numbered to facilitate next discussions.

As discussed in the thermodynamic part, most of the destabilization arises from steric clashes in the complexes. These repulsive interactions have been highlighted in a complete structure investigation of the conformers where the distortions have been attributed to repulsive forces. As shown in Figure 31, carbon atoms on the gears can be numbered and attributed to the different cycles, which allows an easier analysis of the effects.

4.1 Trans isomers

Table 7: Structural parameters (distances d in Å and angles in degrees) of the stator in the optimized trans-isomers as determined using the M06-2X/6-311G/Lanl2TZ(f) (gas phase) method.*

Trans	Projection	$d_{Pt\text{-}P}{}^{9a}$	$d_{Pt\text{-}P}{}^{9b}$	$d_{Pt\text{-}Cl}{}^{a}$	$d_{Pt\text{-}Cl}{}^{b}$	P^{9a}-Pt-P^{9b} angle	Cl^{a}-Pt-Cl^{b} angle
T1							
H		2,319	2,319	2,364	2,364	179,1	175,9
Cl		2,314	2,314	2,371	2,371	180,0	180,0
Me		2,326	2,321	2,367	2,367	177,9	174,8

In Tables 7 and 8, bond lengths and angles values show that trans-isomers have very symmetrical structures around the Pt center with i) the C^{1a} containing cycle (α^3) corresponding to the C^{1b} cycle (β^3), ii) the C^{11a} (α^1) corresponding to the C^{8b} (β^1) and finally iii) C^{8a} (α^2) corresponding to C^{11b} (β^2). Despite the unsubstituted ones, each cog presents different distance and angle values from the others with the larger ones for the R containing cycles (α^3 and β^3), intermediates for cycles interacting/clashing with central the chlorines (α^1 and β^1) and the smaller ones for non-interacting cycles (α^2 and β^2). These variations seem to be good indicators of existing steric clashes in the structures since repulsive interactions with the stator must induce bond distortions in the 9-phosphatriptycene gears.

Table 8: Structural parameters (distances d in Å and angles in degrees) of the gears in the optimized trans-isomers as determined using the M06-2X/6-311G/Lanl2TZ(f) (gas phase) method.*

Gear α								
Trans	$d_{P^9\text{-}C^{1a}}$	$P^9\text{-}C^{1a}\text{-}C^1$ angle	$d_{P^9\text{-}C^{11a}}$	$P^9\text{-}C^{11a}\text{-}C^{11}$ angle	$d_{P^9\text{-}C^{8a}}$	$P^9\text{-}C^{8a}\text{-}C^8$ angle	$Cl^a\text{-}Pt\text{-}P^9$ angle	$Cl^b\text{-}Pt\text{-}P^9$ angle
T1	α^3 cycle		α^1 cycle		α^2 cycle			
H	1,829	125,2	1,841	127,0	1,829	125,2	84,2	95,8
Cl	1,842	128,2	1,839	126,8	1,830	124,7	84,1	95,9
Me	1,844	125,9	1,841	127,5	1,832	125,3	84,4	95,6
Gear β								
Trans	$d_{P^9\text{-}C^{1b}}$	$P^9\text{-}C^{1b}\text{-}C^1$ angle	$d_{P^9\text{-}C^{8b}}$	$P^9\text{-}C^{8b}\text{-}C^8$ angle	$d_{P^9\text{-}C^{11b}}$	$P^9\text{-}C^{11b}\text{-}C^{11}$ angle	$Cl^a\text{-}Pt\text{-}P^9$ angle	$Cl^b\text{-}Pt\text{-}P^9$ angle
T1	β^3 cycle		β^1 cycle		β^2 cycle			
H	1,829	125,2	1,841	127,0	1,829	125,2	95,8	84,2
Cl	1,842	128,2	1,839	126,8	1,830	124,7	95,9	84,1
Me	1,844	125,9	1,841	127,5	1,832	125,3	95,6	84,4

It appears that unsubstituted gears (R = H) present two pairs of cycles with the same structure (α^3 and α^2 or β^3 and β^2). Following the idea that repulsive interactions induce distortions, the third cycles must be in the most destabilizing position. Indeed, as shown in Figure 31, cycles α^1 and β^1 are directly interacting with the closest central chlorine, causing deformations in the stator. One chlorine is pushed by the closest cycle, increasing the corresponding Cl-Pt-P angle, while the second is pushed in the opposite direction by the second gear. Thus, this interaction takes place at both sides of the Pt center, leading to the observed symmetry of trans-isomers. The presence of substituents also impacts the geometry due to the important bond deformation in α^3 and β^3 cycles in substituted complexes. As it is shown, Cl and Me substituents have almost the same impact on gears structure. In these cases, all cycles can be distinguished from the others because of their difference of interaction with the stator. This leads to the conclusion that i) the position of the cycles is still as important as for the unsubstituted ligands and that ii) the substituent has more interactions with the stator than with the opposite gear. As a result, considering a rotational motion, the most destabilizing conformers must be the ones with the substituents clashing with the central chlorines.

As conclusion, trans-isomers exhibit very symmetrical structures. In these complexes, cycles placed in the closest position to the central chlorines are the most destabilized due to steric clashes with the stator. As a result, considering a synchronized rotation motion of the gears, it would exist two identical transition states corresponding to structure where substituents are pointing towards the central chlorines. Finally, these repulsive interactions with the stator generate the rotational activation barriers and impede the rotational motion.

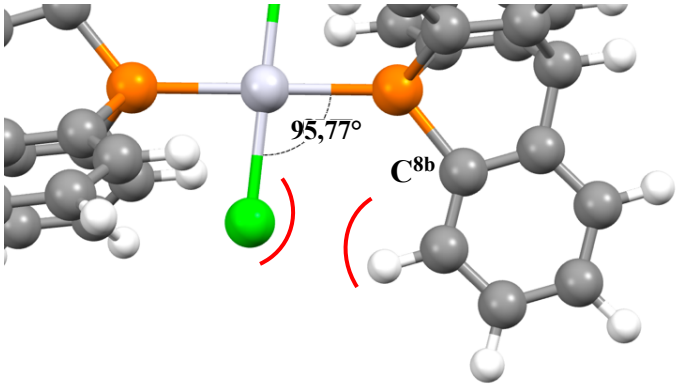

Figure 32: Interaction between the cycle β^1 and the closest central chlorine taking place in trans-isomers.

4.2 Cis isomers

Tables 9 to 11 show bond lengths and bond angle values in the cycles of the cis-isomers. As it was the case of trans-isomers, bond variations are indicators of steric clashes existing in the structure and most particularly between i) two adjacent substituents, ii) the substituents and the central chlorine atoms, and iii) the inferior phenyl rings. As a result, these distortions can directly be related to the relative energies discussed in Table 4 as the causes of observed destabilizations. By taking the unsubstituted isomer (R = H) as a reference for its symmetry, it can be seen as previously that all cycles are distinguishable from the others by their values, which depend on their positions. Once again, the presence of substituents increases the repulsive interactions between cycles and cause new distortions in complexes. By comparing values in both tables, only C2, C5 and C6 isomers present symmetrical structure with C^{1a} (α^2) corresponding to C^{1b} (β^2), C^{8a} (α^1) to C^{8b} (β^1) and C^{11a} (α^3) to C^{11b} (β^3). In these structures, it appears that some positions of the substituents are more likely to afford steric clashes than the others.

Table 9: Structural parameters (distances d in Å and angles in degrees) of the stator in the optimized trans-isomers as determined using the M06-2X/6-311G/Lanl2TZ(f) (gas phase) method.*

Complex	Projection	$d_{Pt-P}{}^{9a}$	$d_{Pt-P}{}^{9b}$	$d_{Pt-Cl}{}^{a}$	$d_{Pt-Cl}{}^{b}$	P^{9a}-Pt-P^{9b} angle	Cl^{a}-Pt-Cl^{b} angle
Cis							
C1							
H	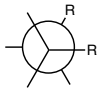	2,232	2,232	2,376	2,376	102,5	88,9
Cl		2,233	2,228	2,374	2,391	103,1	89,8
Me		2,238	2,235	2,385	2,390	103,1	89,3
C2							
Cl	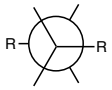	2,227	2,227	2,380	2,380	102,9	88,9
Me		2,232	2,232	2,387	2,387	102,4	88,1
C3							
Cl	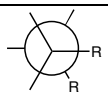	2,231	2,257	2,374	2,377	105,4	87,4
Me		2,238	2,269	2,379	2,376	105,3	87,0
C4							
Cl		2,250	2,236	2,371	2,383	104,9	88,1
Me		2,257	2,245	2,372	2,386	105,0	88,0
C5							
Cl	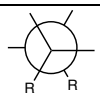	2,263	2,263	2,369	2,369	108,7	86,8
Me		2,266	2,266	2,371	2,371	107,7	86,8
C6							
Cl	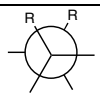	2,214	2,214	2,391	2,391	102,9	91,8
Me		2,224	2,224	2,393	2,393	103,1	91,4

Tables 9 to 11 show bond lengths and bond angle values in the cycles of the cis-isomers. As it was the case of trans-isomers, bond variations are indicators of steric clashes existing in the structure and most particularly between i) two adjacent substituents, ii) the substituents and the central chlorine atoms, and iii) the inferior phenyl rings. As a result, these distortions can directly be related to the relative energies discussed in Table 4 as the causes of observed destabilizations. By taking the unsubstituted isomer (R = H) as a reference for its symmetry, it can be seen as previously that all cycles are distinguishable from the others by their values, which depend on their positions. Once again, the presence of substituents increases the repulsive interactions between cycles and cause new distortions in complexes. By comparing

values in both tables, only C2, C5 and C6 isomers present symmetrical structure with C^{1a} (α^2) corresponding to C^{1b} (β^2), C^{8a} (α^1) to C^{8b} (β^1) and C^{11a} (α^3) to C^{11b} (β^3). In these structures, it appears that some positions of the substituents are more likely to afford steric clashes than the others.

Table 10: Structural parameters (distances d in Å and angles in degrees) of the gear α in the optimized cis-isomers as determined using the M06-2X/6-311G/Lanl2TZ(f) (gas phase) method.*

		Gear α					
Complex	Projection	$d_{P^9\text{-}C^{1a}}$	$P^9\text{-}C^{1a}\text{-}C^1$ angle	$d_{P^9\text{-}C^{8a}}$	$P^9\text{-}C^{8a}\text{-}C^8$ angle	$d_{P^9\text{-}C^{11a}}$	$P^9\text{-}C^{11a}\text{-}C^{11}$ angle
Cis							
C1		α^2 cycle		α^1 cycle		α^3 cycle	
H	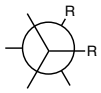	1,821	124,2	1,838	126,7	1,838	126,2
Cl		1,844	127,8	1,842	126,2	1,841	125,9
Me		1,845	125,9	1,842	126,9	1,840	126,3
C2		α^2 cycle		α^1 cycle		α^3 cycle	
Cl	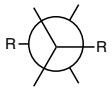	1,841	128,0	1,837	125,8	1,841	126,2
Me		1,841	125,9	1,838	126,5	1,843	127,0
C3		α^2 cycle		α^1 cycle		α^3 cycle	
Cl	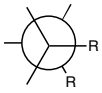	1,841	128,2	1,840	126,1	1,838	126,0
Me		1,846	126,4	1,839	126,8	1,839	126,5
C4		α^3 cycle		α^2 cycle		α^1 cycle	
Cl		1,864	129,4	1,824	123,6	1,840	126,3
Me		1,864	127,5	1,827	124,3	1,840	126,9
C5		α^3 cycle		α^2 cycle		α^1 cycle	
Cl	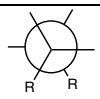	1,861	129,4	1,827	123,8	1,838	126,1
Me		1,860	127,7	1,831	124,4	1,836	126,7
C6		α^1 cycle		α^3 cycle		α^2 cycle	
Cl		1,843	128,5	1,836	126,3	1,818	123,7
Me		1,848	127,0	1,835	126,7	1,820	124,4

Following the idea that largest bond lengths and angle values are attributed to the most hindered positions, the order of destabilization of these would be: middle positions (α^2 and β^2) < upper positions (α^1 and β^1) < lower positions (α^3 and β^3). These results confirmed the observations discussed in Table 4 about the energies and their relation with steric clashes. These observations are further confirmed by values in other isomers. In the isomer C1 the largest deformation

occurs in β^1 cycle in both conformers, once again leading to the conclusion that the closer to the central chlorines the substituted cycle is, the larger the steric hindrance and the destabilization will be.

Table 11: Structural parameters (distances d in Å and angles in degrees) of the gear β of the optimized cis-isomers as determined using the M06-2X/6-311G/Lanl2TZ(f) (gas phase) method.*

		Gear β					
Complex	Projection	$d_{P^9\text{-}C^{1b}}$	$P^9\text{-}C^{1b}\text{-}C^1$ angle	$d_{P^9\text{-}C^{8b}}$	$P^9\text{-}C^{8b}\text{-}C^8$ angle	$d_{P^9\text{-}C^{11b}}$	$P^9\text{-}C^{11b}\text{-}C^{11}$ angle
Cis							
C1		β^1 cycle		β^3 cycle		β^2 cycle	
H	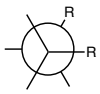	1,838	126,6	1,838	126,2	1,821	124,2
Cl		1,849	129,3	1,837	126,3	1,824	124,0
Me		1,854	127,7	1,837	126,9	1,823	124,5
C2		β^2 cycle		β^1 cycle		β^3 cycle	
Cl	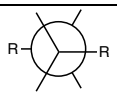	1,841	128,0	1,837	125,8	1,841	126,3
Me		1,841	125,9	1,838	126,5	1,843	127,0
C3		β^3 cycle		β^2 cycle		β^1 cycle	
Cl	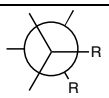	1,868	129,8	1,826	123,7	1,836	125,8
Me		1,872	128,2	1,826	124,2	1,835	126,3
C4		β^1 cycle		β^3 cycle		β^2 cycle	
Cl		1,851	129,2	1,837	126,4	1,826	124,3
Me		1,855	127,5	1,836	126,7	1,828	124,9
C5		β^3 cycle		β^2 cycle		β^1 cycle	
Cl	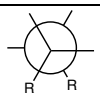	1,861	129,4	1,827	123,8	1,838	126,1
Me		1,860	127,7	1,831	124,4	1,836	126,7
C6		β^1 cycle		β^3 cycle		β^2 cycle	
Cl	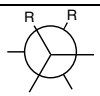	1,843	128,5	1,836	126,3	1,818	123,7
Me		1,848	127,0	1,835	126,7	1,820	124,4

The same kind of observation can be made for the C3 isomer where the most destabilized is the β^3 cycle. Therefore, substitution on the lower cycle induces more distortion of the structure than in the horizontal plane. Finally, isomer C4 confirms which position of the substituent has the strongest impact upon relative energies. Indeed, C4 isomer presents a substituent in both positions and a direct comparison between them shows that the previously suggested order of

destabilization is correct, with the lower position of substituent being the most destabilizing position.

To conclude, structural variations showed that the existing clashes between i) the inferior phenyl rings, ii) the substituents and the central chlorine atoms and iii) two adjacent substituents are respectively the most impacting factor on structure. Also, it was confirmed that these distortions are directly impacting the energies presented in Table 4 as causes of destabilization in the complexes. As a result, the two first factors have to be considered as the possible barriers impeding rotational motion. A further discussion about the rotation dynamics will highlight the impact of these possible transition states and the differences between the rotation motion containing them.

4.3 Spacing angles between cogs

Results presented in Table 12 shows similarities with the ones discussed above. As previously, spacing angles between cycles are distinguishable from the other by the variations of their values, indicating that these could be indicators of steric clashes induced by both the stator and the opposite gear.

It can be seen that trans-isomers exhibit once again structural symmetry. In these isomers, cycles are not necessarily separated by different angle values showing that the stator induces the major effect on separation angles. The presented values show that substituents on the opposite gear also increase the angles but less than the stator due to the large distance between gears. Therefore, as it was concluded before, central chlorines cause steric clashes with the closest cycle that induce an increase of the C^{1a}-C^{8a} and C^{1b}-C^{11b} angles and a deformation of the gear.

For cis-isomers, unsubstituted gears (R = H) present expected parameter values without the deformation induced by the substituents. This particular case possesses, as the other cis-isomers, three different angle value for each gear which can be separated as one containing the central chlorines and the upper cycle of the opposite gear (α^2-α^1 and β^2-β^1 angles), a second containing the opposite lower cycle (α^2-α^3 and β^2-β^3 angles), and the last containing the opposite horizontal cycle (α^1-α^3 and β^1-β^3 angles). At first sight it seems that these angles depend on both the interactions with the stator and between gears. For unsubstituted gears, the lower cycle induces slightly more hindrance than the central chlorines and their adjacent cycle

which is in agreement with the previous observations. Also, it appears that angles in front of horizontal cycles are always the smaller ones while the two others value depend on the considered conformer. It is probably because this position causes less structure deformations due to the low interaction with the second gear.

Table 12: Spacing angles between cycles plane (angles in degrees) of the optimized cis- and trans- isomers as determined using the M06-2X/6-311G/Lanl2TZ(f) (gas phase) method.*

Complex	Projection	C^{1a}-C^{8a} angle	C^{1a}-C^{11a} angle	C^{8a}-C^{11a} angle	C^{1b}-C^{8b} angle	C^{1b}-C^{11b} angle	C^{8b}-C^{11b} angle
Trans		α^3-α^2	α^3-α^1	α^2-α^1	β^3-β^1	β^3-β^2	β^1-β^2
H		122,1	119,0	119,0	119,0	122,1	119,0
Cl		125,2	116,8	117,8	116,8	125,2	117,8
Me		125,9	116,4	117,5	117,1	126,0	116,7
Cis							
C1		α^2-α^1	α^2-α^3	α^1-α^3	β^1-β^3	β^1-β^2	β^2-β^3
H	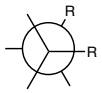	122,7	126,6	110,7	110,7	122,7	126,6
Cl		126,0	124,4	109,6	111,0	123,7	125,2
Me		125,7	124,5	109,7	111,3	122,9	125,7
C2		α^2-α^1	α^2-α^3	α^1-α^3	β^2-β^1	β^2-β^3	β^1-β^3
Cl	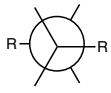	126,2	124,1	109,6	126,2	124,1	109,6
Me		126,8	123,6	109,6	126,8	123,6	109,6
C3		α^2-α^1	α^2-α^3	α^1-α^3	β^3-β^2	β^3-β^1	β^3-β^1
Cl	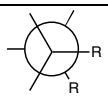	124,5	126,9	108,5	125,1	109,0	125,6
Me		125,8	125,0	109,3	123,8	110,0	125,8
C4		α^3-α^2	α^3-α^1	α^2-α^1	β^1-β^3	β^1-β^2	β^2-β^3
Cl		125,2	108,3	126,3	110,1	123,4	126,5
Me		124,9	109,0	125,7	111,0	122,0	126,9
C5		α^3-α^2	α^3-α^1	α^2-α^1	β^1-β^3	β^1-β^2	β^2-β^3
Cl	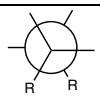	126,4	109,5	123,5	126,4	109,5	123,5
Me		125,2	111,1	122,7	125,2	111,1	122,7
C6		α^1-α^3	α^1-α^2	α^3-α^2	β^3-β^2	β^3-β^1	β^3-β^1
Cl	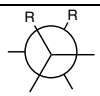	107,2	126,2	126,5	107,2	126,2	126,5
Me		108,2	124,5	127,2	108,2	124,5	127,2

As discussed before, the presence of substituents induces changes in comparison to this unsubstituted case. This is evidenced in structures C4, C5 and C6 where the widest angle

depends on the substituent positions. In both isomers, it corresponds to the angles where the substituents of the opposite gear are situated. It shows that the position of substituents must be an impacting factor upon angles. This is confirmed in substituted C1 isomer for its gear α, where the largest angle is the one containing both opposite substituent and central chlorines. However, deviations are observed in C3 conformer, which bring nuances to this last observation. In this structure, the largest angle in gear α depends on the substituent nature. For the Cl-substituted molecule, the wider is the inferior one containing the opposite substituent (α^2-α^3) while in the case of Me, it is the one interacting with the central chlorines (α^2-α^1). Since these complexes exhibit similar structures, the difference must arise from the substituent's nature. The case of Cl is similar to the ones discussed before (C4, C5 and C6) with the wider angle depending on the opposite substituent position. In the case of Me-substituted gear α, it is the upper angle which is wider than the others. An explanation to this behavior could be that methyl substituent on the gear β generates enough hindrance to force the left one to rotate without distorting it. This small rotation has as effect to bring closer its substituent from the central chlorines plane and their adjacent cycle. Then, the association of these entities could generate enough steric hindrance to increase this angle until a balance between rotation and distortion is found. Thus, the system tends to rotate to separate substituents before increasing the spacing angles that could destabilize the structure by changing the phosphorus atom geometry.

To conclude, spacing angles between cycles indicate the presence of steric clashes induced by both the stator and the opposite gear. In the case of trans-isomers, the opposite gears are sufficiently far apart not to cause large distortion in the opposite rotator, which means that the stator induces the major effects on spacing angles. It is no longer the case in the cis-isomers, where the widest angle also depends on the opposite substituent position. As previously shown, the most impacting factors of steric clashes are the inferior opposite cycles and the central chlorines. Moreover, in some cases, the repulsive interactions between adjacent substituents are large enough to force the gears to rotate before beginning to change their structure. However, when a rotation motion is engaged, cycles are forced to go through a position where the cogs are likely to bend. These positions are the same as described before and correspond to the transition states in the rotational motion.

PART V – Conclusions and perspectives

1. Conclusion

The increasing interest of chemists for new artificial molecular machines, makes their development one of the contemporary goals of nanoscience. In this context, early pioneering works conducted to the construction of the so-called "molecular gears". Since, the construction of such molecular motors begins from a careful consideration of molecular properties, research works rapidly put forward triptycene scaffolds as interesting candidates. Indeed, they exhibit rigid structures with many functionalizable positions that can dictate the mechanical properties of the system. In the same context, the change of configuration by an external stimulus represents one of the greatest challenges for the design of machines capable of performing significant work. Therefore, the present Master thesis aimed the development of new platinum-centered square planar complexes with phosphatriptycene derivatives as ligands, and the investigation of their potential use as molecular machines by both experimental and theoretical chemistry.

Several *ortho*-substituted 9-phosphatriptycenes derivatives (**1a-c**) were synthetized in gram scale after five steps from a commercially available aromatic compound (Scheme 15). In this synthesis path, the fourth step, consisting in the opening reaction of a diaryliodonium ring by a nucleophile, turns out to be a competitive reaction between a polar and a radical one. A detailed investigation of the mechanism revealed the obtained side-products were characteristics to the high temperature employed to run the process. However, some other conditions were tested, and finally confirmed that the thermal energy is actually needed to overcome an intramolecular isomerization barrier, highly defavorable in the case of an intrinsically rigid 6-membered ring.

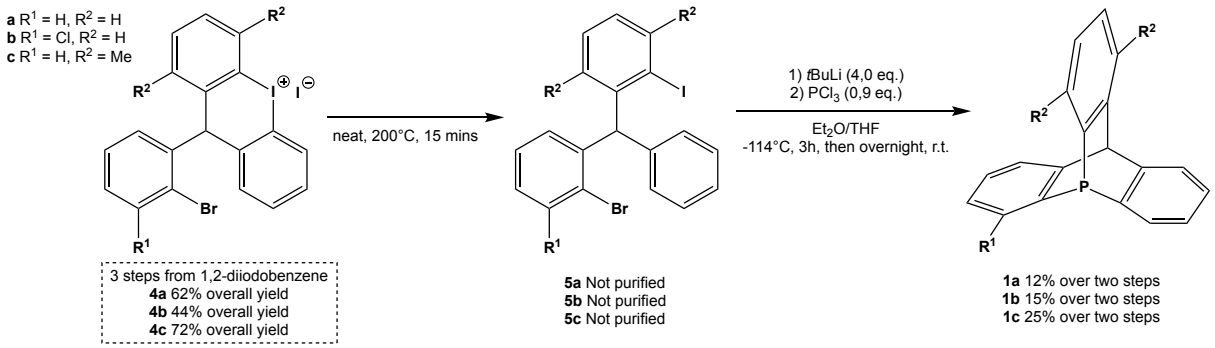

*Scheme 15: Synthesis of 9-phosphatriptycene **1a-c**.*

Despite the complexity of the mixture of products obtained during this thermally activated reaction, the desired ones could be sufficiently purified to successfully form the phosphatriptycene ligands in the next step (**1a-c**). Eventually, the latter were used for the

complexation of two platinum (II) precursors, K_2PtCl_4 and $PtCl_2$, of which the advantages and disadvantages of use were discussed. It appeared that the main difficulties encountered for the reaction with K_2PtCl_4, the difference of solubility in organic solvent and the lack of reactivity of the phosphatriptycenes, were perfectly resolved by the use of $PtCl_2$ instead. In addition, the mechanism of the ligand substitution reaction, prevalent in the case of square planar metal precursor has been investigated. The explanation of some fundamental concepts of this mechanism such as the trans-"effects", their origins and their consequences on the formed intermediates, could justify the formation of the preferential cis isomer and the lower reaction rate of phosphatriptycenes compared to common phosphines. Moreover, this associative substitution of ligands turned to be at the base of the isomerization processes taking place in square planar complexes. This kind of isomerization, generally thermally- or photo-induced, and occurring via either an intramolecular or an intermolecular path, is typically dependent on the properties of the solvent, such as its dielectric constant or its binding potential.

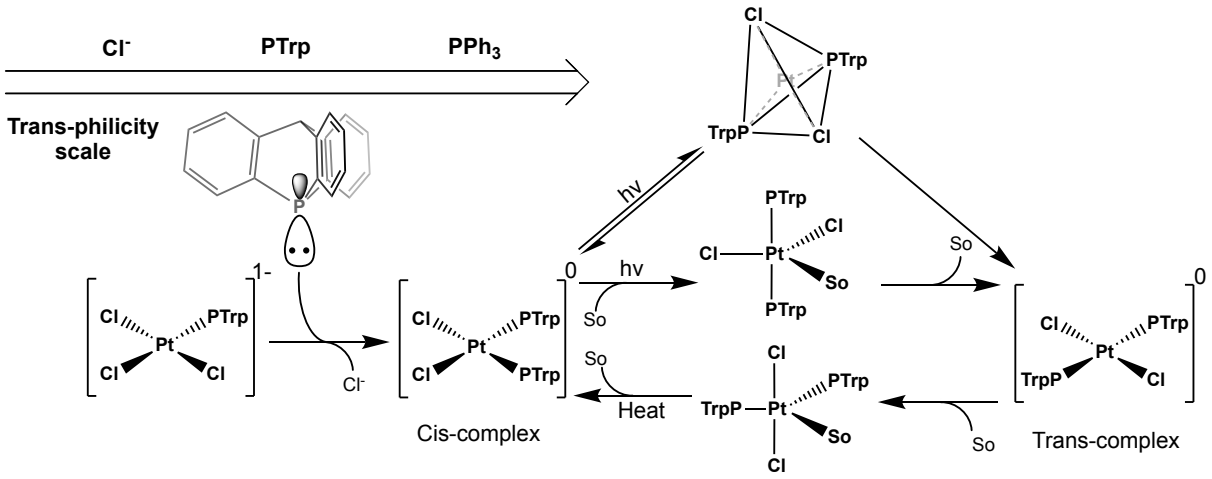

Scheme 16: Cis-trans isomerization process and trans-*philicity scale of selected ligands.*

In parallel, the theoretical investigation of the aimed molecular gears allowed to overcome some of the difficulties encountered at the experimental level due to their low solubility. Indeed, DFT investigation enabled to get an overview of the possible conformers of both cis and trans isomers (**6a-c** and **7a-c**), their structure, as well as their energies. The detailed analysis of their geometry allowed to correlate some of their structural parameters with their respective energies, identifying the possible causes of destabilization in the structure as the steric clashes between i) the two inferior rings and ii) the superior rings with the central chlorines. Also, calculations in chloroform using the IEFPCM method confirmed the role of the solvent on the stability of isomers by electrostatic interactions. As a result, quantum chemistry enabled to show the most influential features on rotational motions, giving a better understanding of their working process.

2. Perspectives

In the present work, two molecules have displayed great interest for the design of new molecular gears. Indeed, the 9-phospha-10-hydroxytriptycene exhibited interesting possibilities for the better solubilization of the complexes by the transformation of the alcohol into a methoxy group (Scheme 17).

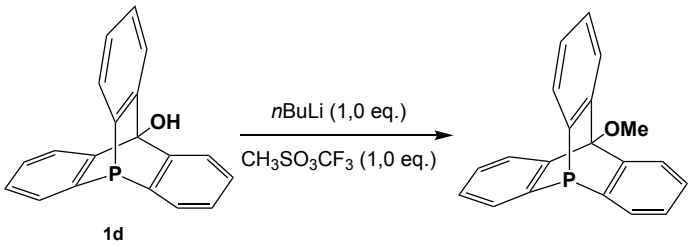

Scheme 17: Proposed synthesis for the methylation of the 9-phospha-10-hydroxytriptycene.

The latter reaction has already been attempted and the desired product was presumed present in the form of traces in the crude. However, the product still needs to be isolated and identified as the desired one with suitable characterization. If it is the right one, an optimization of the reaction conditions can lead to the production of larger amount, enabling to test this product as ligand in platinum- (II) or palladium- (II) centered square planar complexes.

In addition, the 9,10-diphosphatriptycene shows interesting electronic properties of its phosphorus atoms due to the reduction of their pyramidalization. It is now important to rationalize these properties through measurements such as the Tolman electronic parameter to validate the possibility of performing a double reaction of complexation, one on each phosphorus atom.

Furthermore, once suitable complexes accessed, it will be necessary to complete the present work by the investigation of the parts which were not tackled here, as shown in the Figure 21 (Part II). It includes the investigation of the cis-trans isomerization by analysis technique as well as the complete computational investigation of the rotation dynamics.

PART VI – References

[1] J. Carson and J.F. Stoddart, The Nature of the Mechanical Bond: From Molecules to Machines, Wiley-Blackwell, **2016**.

[2] A. Coskun, M. Banaszak, R. D. Astumian, J. F. Stoddart and B. A. Grzybowski, *Chem. Soc. Rev.*, 2012, **41**, 19–30.

[3] H.J. Yoon, J. Kuwabara, J.H. Kim, and C.A. Mirkin, *Science*, 2010, **330**, 66–69.

[4] J.-M. Lehn, *Science*, 1993, **260**, 1762–1763.

[5] E. Fischer, *Ber. Dtsch. Chem. Ges.*, 1894, **27**, 2985–2993.

[6] J. Gross, G. Harder, A. Siepen, J. Harren, F. Vogtle, H. Stephan, K. Gloe, B. Ahlers, K. Cammann and K. Rissanen, *Chem. Eur. J.*, 1996, **2**, 1585–1595.

[7] (a) J.-M. Lehn, *Pure Appl. Chem.*, 1977, **49**, 857–870. (b) D. J. Cram and J. M. Cram, *Science*, 1974, **183**, 803–809. (c) C. J. Pedersen, *J. Am. Chem. Soc.*, 1967, **89**, 7017–7036.

[8] "The Nobel Prize in Chemistry 1987", NobelPrize.org., consulted the 6 Dec 2021. <https://www.nobelprize.org/prizes/chemistry/1987/summary/>

[9] K. Ariga, J. P. Hill, M. V. Lee, A. Vinu, R. Charvet and S. Acharya, *Sci. Technol. Adv.*, 2008, **9**, 1–96.

[10] E. V. Perez, C. Karunaweera, I. H. Musselman, K. J. Balkus and J. P. Ferraris, *Processes*, 2016, **4**, 1–68.

[11] (a) C. O. Dietrich-Buchecker, J. P. Sauvage and J. P. Kintzinger, *Tetrahedron Lett.*, 1983, **24**, 5095–5098. (b) P. Lucio Anelli, N. Spencer and J. Fraser Stoddart, *J. Am. Chem. Soc.*, 1991, **113**, 5131–5133. (c) N. Koumura, R. W. J. Zijistra, R. A. Van Delden, N. Harada and B. L. Feringa, *Nature*, 1999, **401**, 152–155.

[12] K. Kinbara and T. Aida, *Chem. Rev.*, 2005, **105**, 1377–1400.

[13] D. Okuno, R. Iino and H. Noji, *J. Biochem.*, 2011, **149**, 655–664.

[14] (a) M. Schliwa and G. Woehlke, *Nature*, 2003, **422**, 759–765. (b) 1 G. Bhabha, G. T. Johnson, C. M. Schroeder and R. D. Vale, *Trends Biochem. Sci.*, 2016, **41**, 94–105.

[15] (a) R. B. Vallee and P. Höök, *Nature*, 2003, **421**, 701–702. (b) 1 G. Bhabha, G. T. Johnson, C. M. Schroeder and R. D. Vale, *Trends Biochem. Sci.*, 2016, **41**, 94–105.

[16] S. Erbas-Cakmak, D. A. Leigh, C. T. McTernan and A. L. Nussbaumer, *Chem. Rev.*, 2015, **115**, 10081–10206.

[17] R. Brown, *Philos. Mag. Ann. Philos.*, 1829, **4**, 161–173.

[18] (a) B. Krishna Juluri, A. S. Kumar, Y. Liu, T. Ye, Y.-W. Yang, A. H. Flood, L. Fang, J. Fraser Stoddart, P. S. Weiss and T. Jun Huang, *ACS Nano*, 2009, **3**, 291–300. (b) Y. Liu, A. H. Flood, P. A. Bonvallet, S. A. Vignon, B. H. Northrop, H.-R. Tseng, J. O. Jeppesen, T. J. Huang, B. Brough, M. Baller, S. Magonov, S. D. Solares, W. A. Goddard, C.-M. Ho and J. Fraser Stoddart, *J. Am. Chem. Soc.*, 2005, **127**, 9745–9759.

[19] E. A. Neal and S. M. Goldup, *Chem. Commun.*, 2014, **50**, 5128–5142.

[20] T. Ross Kelly, M. C. Bowyer, K. Vijaya Bhaskar, D. Bebbington, A. Garcia, F. Lang, M. H. Kim and M. P. Jette, *J. Am. Chem. Soc.*, 2002, **116**, 3657–3658.

[21] T. R. Kelly, H. De Silva and R. A. Silva, *Nature*, 1999, **401**, 150–152.

[22] I. Liepuoniute, M. J. Jellen and M. A. Garcia-Garibay, *Chem. Sci.*, 2020, **11**, 12994–13007.

[23] H. Iwamura, T. Ito, H. Ito, K. Toriumi, Y. Kawada, E. Ósawa, T. Fujiyoshi and C. Jaimelc, 1984, **106**, 4712–4717.

[24] (a) H. Ube, R. Yamada, J. I. Ishida, H. Sato, M. Shiro and M. Shionoya, *J. Am. Chem. Soc.*, 2017, **139**, 16470–16473. (b) I. Liepuoniute, J. N. Sanders, M. A. Garcia-Garibay and K. N. Houk, *J. Org. Chem.*, 2020, **85**, 8695–8701.

[25] K. Okamura, Y. Inagaki, H. Momma, E. Kwon and W. Setaka, *J. Org. Chem.*, 2019, **84**, 14636–14643.

[26] W. Setaka, T. Nirengi, C. Kabuto and M. Kira, *J. Am. Chem. Soc.*, 2008, **130**, 15762–15763.

[27] H. Ube, Y. Yasuda, H. Sato and M. Shionoya, *Nat. Commun.*, 2017, **8**, 1–6.

[28] Z. Jia, Q. Guan, H. Wang and X. Wang, *Supramol. Chem.*, 2020, **32**, 569–577.

[29] J. J. Li, Name Reactions, 3rd ed., New-York: Springer, 2006.

[30] (a) H. Guo, Y. Chiao Fan, Z. Sun, Y. Wu and O. Kwon, "Phosphine Organocatalysis", Chem. Rev. 2018, 118, 20, 10049-10293. (b) H. Ni, W.-L. Chan and Y. Lu, "Phosphine-Catalyzed Asymmetric Organic Reactions", *Chem. Rev.* 2018, **118**, 9344-9411.

[31] D. Mahaut, A. Chardon, L. Mineur, G. Berionni and B. Champagne, *Chem. Phys. Chem.*, 2021, **22**, 1958–1966.

[32] (a) L. Hu, D. Mahaut, N. Tumanov, J. Wouters, L. Collard, R. Robiette and G. Berionni, *Dalt. Trans.*, 2021, **50**, 4772–4777. (b) L. Hu, D. Mahaut, N. Tumanov, J. Wouters, R. Robiette and G. Berionni, *J. Org. Chem.*, 2019, **84**, 11268–11274.

[33] V. D. Vuković, E. Richmond, E. Wolf and J. Moran, *Angew. Chemie - Int. Ed.*, 2017, **56**, 3085–3089.

[34] S. E. Creutz and J. C. Peters, *J. Am. Chem. Soc.*, 2014, **136**, 1105–1115.

[35] V. V. Grushin, *Chem. Soc. Rev.*, 2000, **29**, 315–324.

[36] (a) R. S. Berry, *J. Chem. Phys.*, 1960, **32**, 933–938. (b) V. V. Grushin, *Acc. Chem. Res.*, 2002, **25**, 529–536.

[37] T. Agou, J. Kobayashi & T. Kawashima, *Chem. Lett.*, 2004, 33, 1028- 1029.

[38] M. Yamamura and T. Nabeshima, *Bull. Chem. Soc. Jpn.*, 2016, **89**, 42-49.

[39] W. E. Hill, D. M. A. Minahan, J. G. Taylor and C. A. McAuliffe, *J. Am. Chem. Soc.*, 1982, **104**, 6001–6005.

[40] A. Pidcock, R. E. Richards and L. M. Venanzi, *Inorg. Phys. Theor.*, 1966, 1707–1710.

[41] A. C. Tsipis, *J. Comput. Chem.*, 2019, **40**, 2550–2562.

[42] W. E. Hill, D. M. A. Minahan, J. G. Taylor and C. A. McAuliffe, *J. Am. Chem. Soc.*, 1982, **104**, 6001–6005.

[43] J. H. Price, J. P. Birk and B. B. Wayland, *Inorg. Chem.*, 1978, **17**, 2245–2250.

[44] (a) P. Haake and T. A. Hylton, *J. Am. Chem. Soc.*, 1962, **84**, 3774–3775. (b) S. H. Mastin and P. Haake, *J. Chem. Soc. D Chem. Commun.*, 1970, 202.

[45] H. A. Nkabyo, B. Procacci, S. B. Duckett and K. R. Koch, *Inorganica Chim. Acta*, 2020, **512**, 1-15.

[46] P. D. Fleischauer, A. W. Adamson and G. Sartori, 2007, **17**, 1–56.

[47] R. A. Baber, A. G. Orpen, P. G. Pringle, M. J. Wilkinson and R. L. Wingad, 2005, **2**, 659–667.

[48] S. Konishi, T. Iwai and M. Sawamura, *Organometallics*, 2018, **37**, 1876–1883.

[49] P. J. Hay and W. R. Wadt, *J. Chem. Phys.*, 1985, **82**, 270–283.

[50] R. Ditchfield, W. J. Hehre and J. A. Pople, *J. Chem. Phys.*, 1971, **54**, 720–723.

[51] M. J. Frisch et al., Gaussian 16, Revision B.01, Gaussian, Inc., Wallingford CT, 2016.

[52] Y. Zhao and D. G. Truhlar, *Theor. Chem. Acc.*, 2008, **120**, 215–241.

[53] J. Tomasi, B. Mennucci and R. Cammi, *Chem. Rev.* 2005, **105**, 2999-3093

PART VII – Material and methods

1. Experimental section

1.1 Synthetic procedures and characterization

General laboratory procedure

All moisture-sensitive reactions were performed under an atmosphere of argon in flame-dried Schlenck flasks.

Analytical methods

^{1}H, ^{13}C, and ^{31}P NMR spectra were recorded on a Jeol 500 MHz NMR spectrometer and the observed signals are reported in parts per million (ppm) relative to the residual signal of the non-deuterated solvent. The following abbreviations are used to describe multiplicities s = singlet, d = doublet, t = triplet, q = quartet, quin = quintuplet, br = broad, m = multiplet.

Material

All anhydrous solvents were dried with a solvent purification system. Solvents, reagents and chemicals were purchased from Sigma-Aldrich, Carbosynth, FluoroChem and TCI and used without further purification.

1.2 9-phosphatriptycene (**1a**)

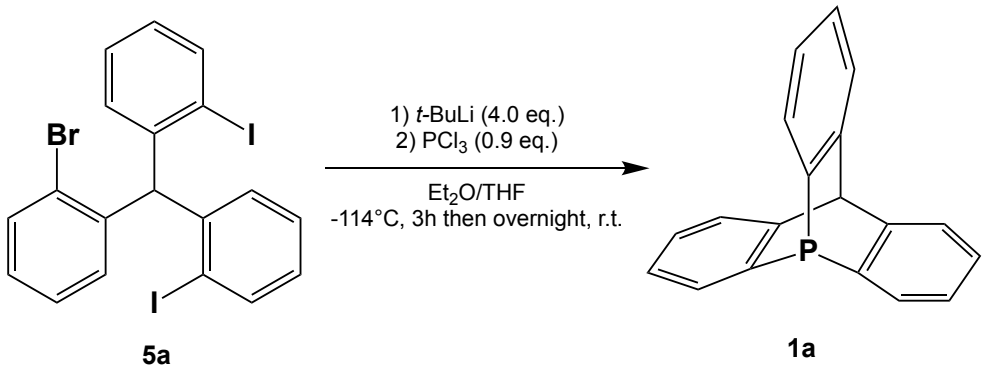

5a **1a**

Chemical formula: $C_{19}H_{13}P$

Molecular weight: 272.07 g/mol

Physical state: White solid

Prepared according to the literature.[2] In a pre-dried 100 mL Schlenck flask under Ar and equipped with a magnetic stirrer is added compound **5a** (3.00 g, 5.24 mmol, 1.0 eq.) in 50 mL of a 1:1 mixture of anhydrous THF and Et_2O. The resulting clear solution is cooled down to -114°C ($EtOH/N_{2(l)}$) before the dropwise addition of *t*-BuLi (1.9 M in hexane, 11.0 mL, 20.9 mmol, 4.0 eq.). After stirring at this temperature for 3h, PCl_3 (0.41 mL, 4.72 mmol, 0.9 equiv.) is added dropwise at -114°C. The resulting solution is stirred for one additional hour at -114°C before being allowed to warm up to room temperature overnight stirring. The reaction is quenched with aqueous NH_4Cl (30 mL) and the organic phase is extracted with AcOEt (3 x 30 mL). The combined organic phases are dried over $MgSO_4$ before filtration and evaporation of the solvents under reduced pressure. The crude product is purified by silica gel column chromatography (eluent = cyclohexane to cyclohexane/dichloromethane 9:1) to afford pure 9-phosphatriptycene **1a** as an off-white powder (154 mg, 12% over two steps).

^{1}H NMR (500 MHz, $CDCl_3$): δ 7.77-7.74 (m, 3 H), 7.50 (d, J = 7.4 Hz, 3H), 7.17-7.14 (m, 3 H), 7.07-7.05 (m, 3 H), 5.57 (s, 1H).

^{31}P NMR (202 MHz, $CDCl_3$): δ -64.4.

---

[2] L. Hu, D. Mahaut, N. Tumanov, J. Wouters, L. Collard, R. Robiette and G. Berionni, *Dalt. Trans.*, 2021, **50**, 4772–4777.

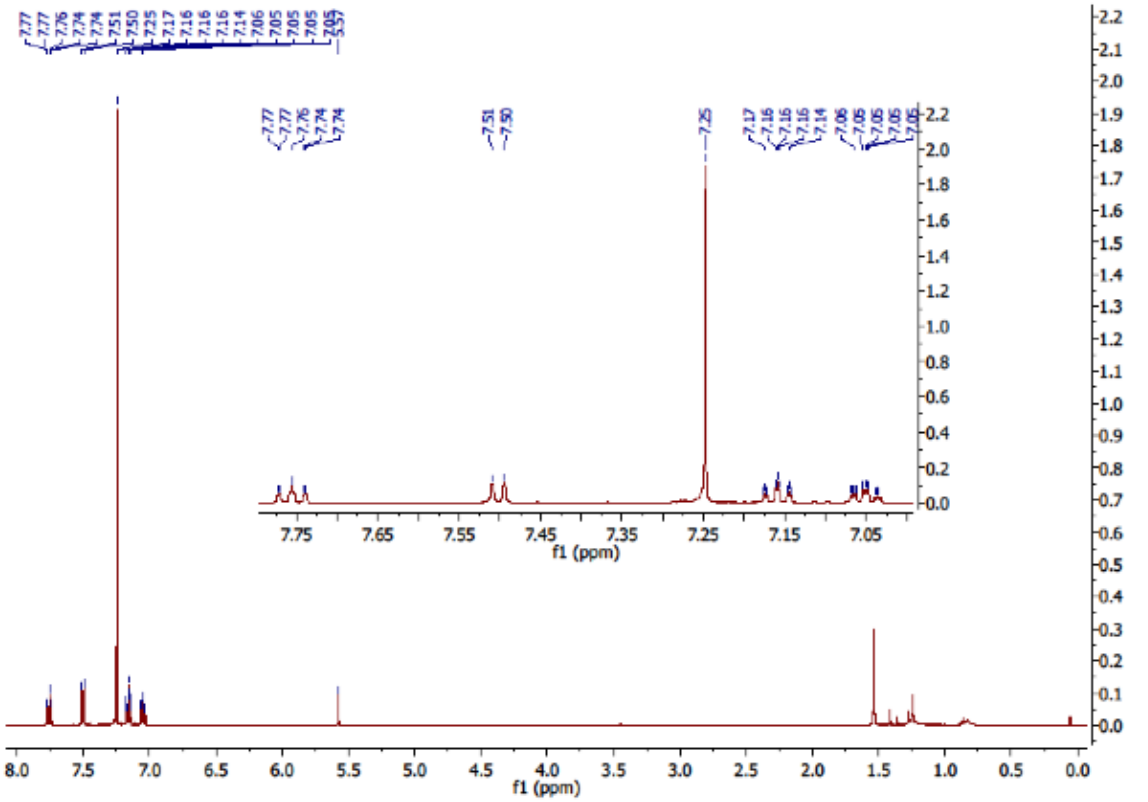
7.77
7.77
7.76
7.74
7.74
7.51
7.50
7.25
7.17
7.16
7.16
7.16
7.14
7.06
7.05
7.05
7.05
7.05
7.57
f1 (ppm)

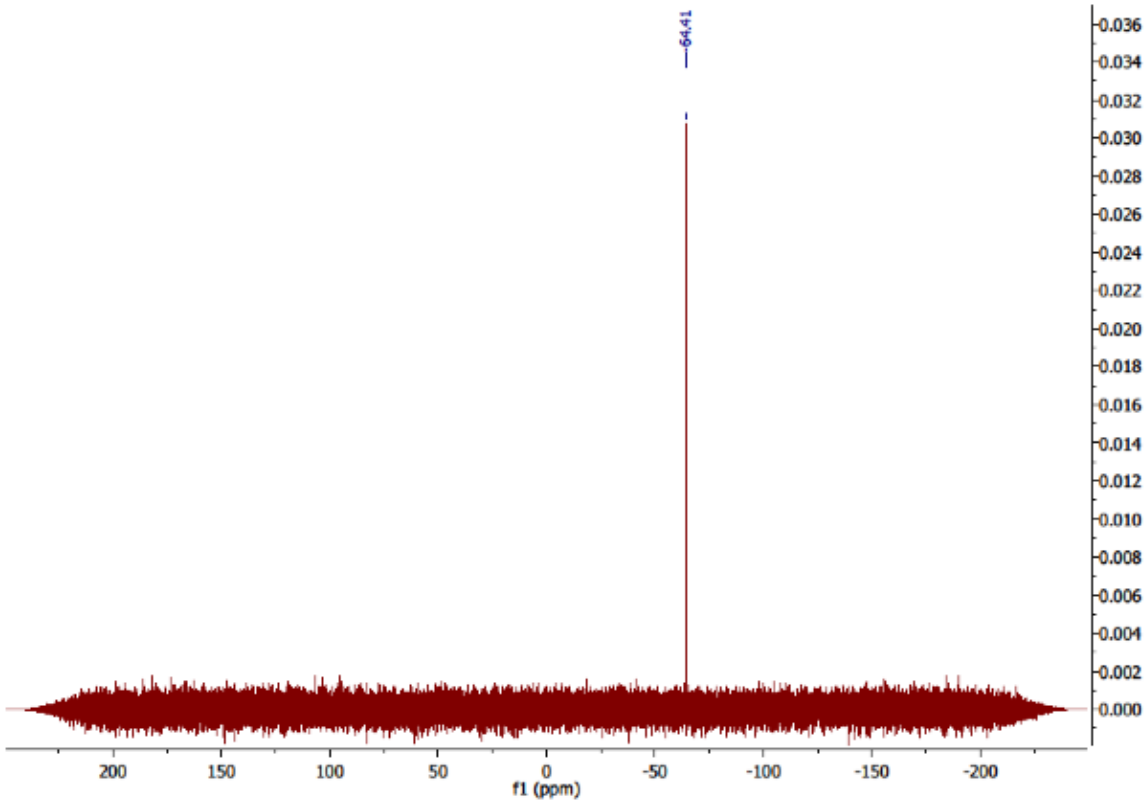
64.41
f1 (ppm)

1.3 1-chloro-9-phosphatriptycene (**1b**)

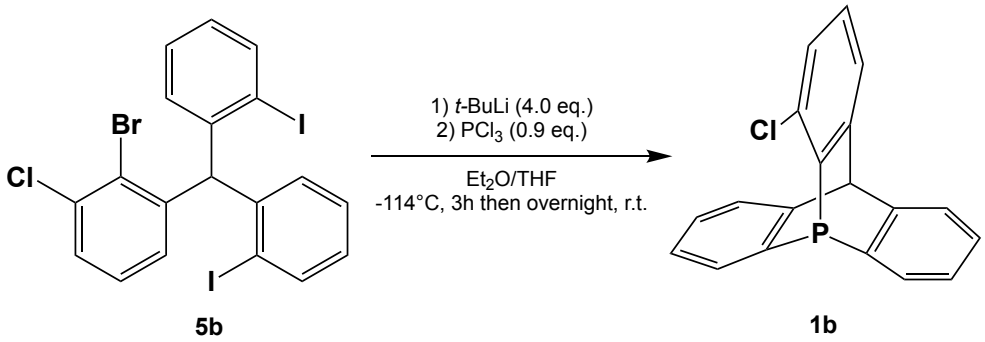

5b **1b**

Chemical formula: $C_{19}H_{12}ClP$

Molecular weight: 306.73 g/mol

Physical state: White solid

Prepared according to the literature similarly to **1a**. In a pre-dried 100 mL Schlenck flask under Ar and equipped with a magnetic stirrer is added compound **5b** (2.00 g, 3.28 mmol, 1.0 eq.) in 50 mL of a 1:1 mixture of anhydrous THF and Et_2O. The resulting clear solution is cooled down to -114°C ($EtOH/N_{2(l)}$) before the dropwise addition of *t*-BuLi (1.9 M in hexane, 7.0 mL, 13.1 mmol, 4.0 eq.). After stirring at this temperature for 3h, PCl_3 (0.27 mL, 4.25 mmol, 0.9 equiv.) is added dropwise at -114°C. The resulting solution is stirred for one additional hour at -114°C before being allowed to warm up to room temperature overnight stirring. The reaction is quenched with aqueous NH_4Cl (30 mL) and the organic phase is extracted with AcOEt (3 x 30 mL). The combined organic phases are dried over $MgSO_4$ before filtration and evaporation of the solvents under reduced pressure. The crude product is purified by silica gel column chromatography (eluent = cyclohexane to cyclohexane/dichloromethane 9:1) to afford pure 1-chloro-9-phosphatriptycene **1b** as an off-white powder (195 mg, 15% over two steps).

^{1}H NMR (500 MHz, $CDCl_3$) δ 7.81 (t, *J* = 8.0 Hz, 2H), 7.51 (d, *J* = 7.3 Hz, 2H), 7.40 (dd, *J* = 6.3, 1.8 Hz, 1H), 7.19 (t, *J* = 7.4 Hz, 2H), 7.10 – 7.06 (m, 4H), 5.58 (s, 1H).

^{31}P NMR (202 MHz, $CDCl_3$) δ -72.5.

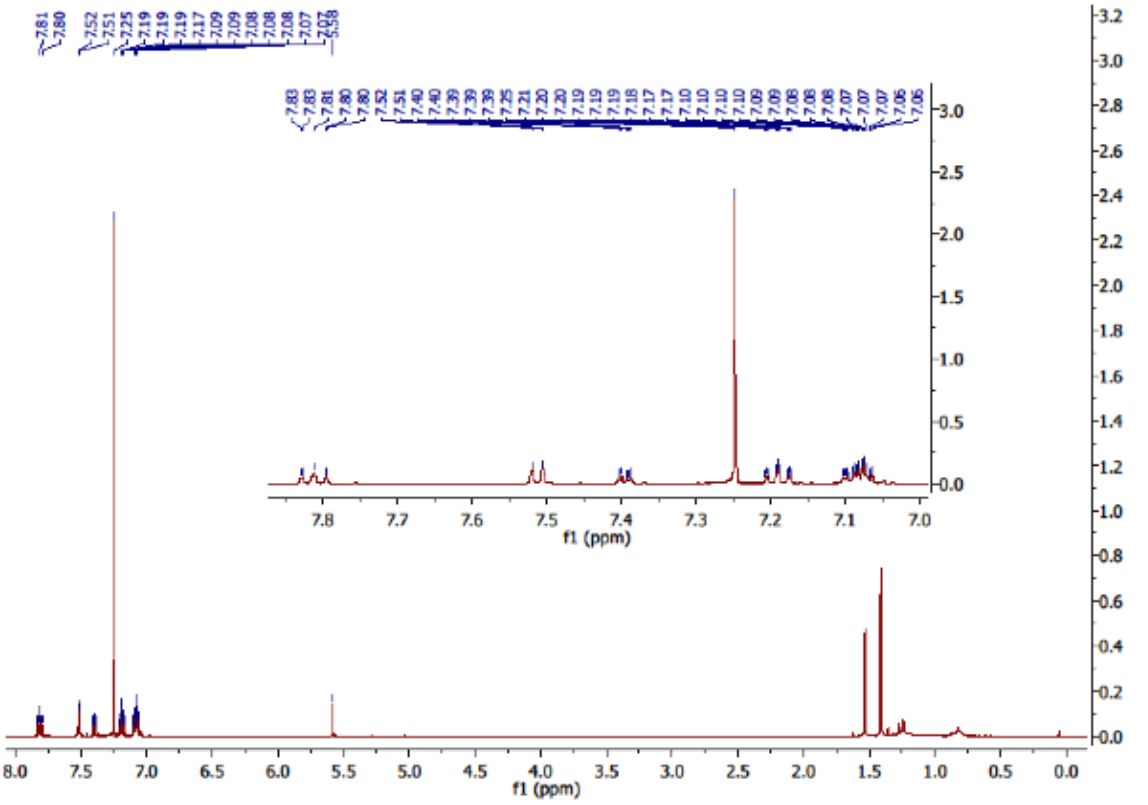
f1 (ppm)

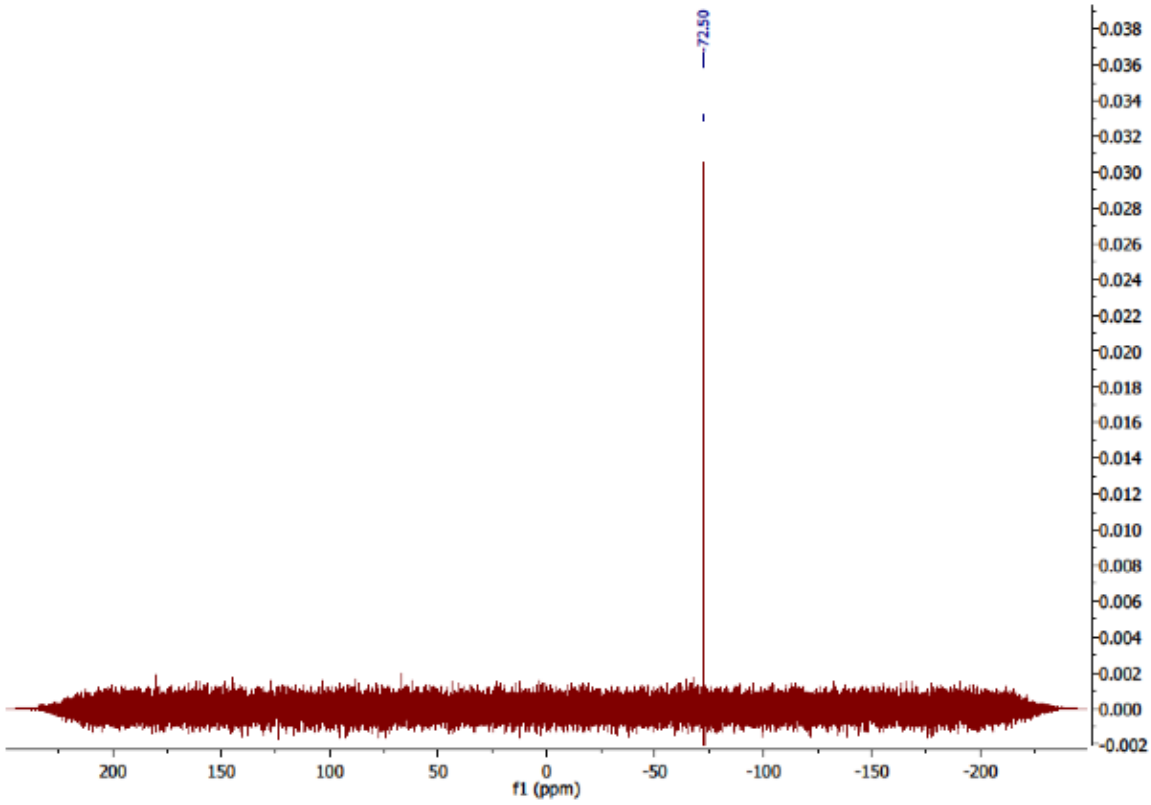
72.50
f1 (ppm)

1.4 1,4-dimethyl-9-phosphatriptycene (**1c**)

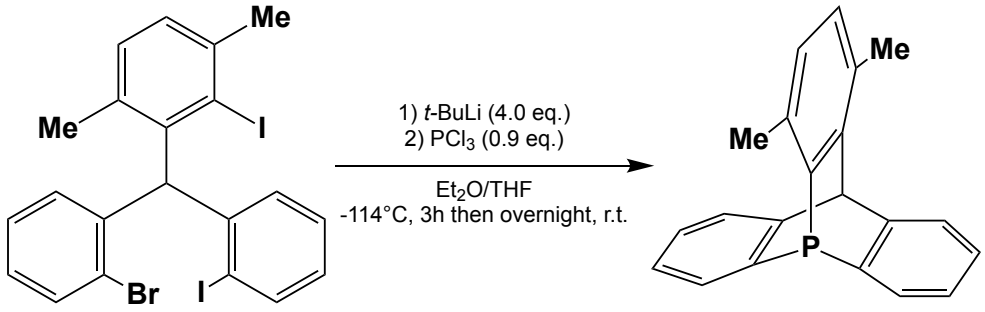

5c **1c**

Chemical formula: $C_{21}H_{17}P$

Molecular weight: 300.34 g/mol

Physical state: White solid

Prepared according to the literature similarly to **1a**. In a pre-dried 100 mL Schlenck flask under Ar and equipped with a magnetic stirrer is added compound **5c** (1.27 g, 2.11 mmol, 1.0 eq.) in 30 mL of a 1:1 mixture of anhydrous THF and Et_2O. The resulting clear solution is cooled down to -114°C ($EtOH/N_{2(l)}$) before the dropwise addition of *t*-BuLi (1.9 M in hexane, 4.4 mL, 8.44 mmol, 4.0 eq.). After stirring at this temperature for 3h, PCl_3 (0.17 mL, 1.90 mmol, 0.9 equiv.) is added dropwise at -114°C. The resulting solution is stirred for one additional hour at -114°C before being allowed to warm up to room temperature overnight stirring. The reaction is quenched with aqueous NH_4Cl (30 mL) and the organic phase is extracted with AcOEt (3 x 30 mL). The combined organic phases are dried over $MgSO_4$ before filtration and evaporation of the solvents under reduced pressure. The crude product is purified by silica gel column chromatography (eluent = cyclohexane to cyclohexane/dichloromethane 9:1) to afford pure 1,4-dimethyl-9-phosphatriptycene **1c** as an off-white powder (143 mg, 25% over two steps).

^{1}H NMR (500 MHz, $CDCl_3$) δ 7.75 (t, *J* = 7.9 Hz, 2H), 7.49 (d, *J* = 7.3 Hz, 2H), 7.15 (t, *J* = 7.4 Hz, 2H), 7.06 (tdd, *J* = 7.3, 2.2, 1.1 Hz, 2H), 6.88 (d, *J* = 7.7 Hz, 1H), 6.78 (dd, *J* = 7.7, 4.6 Hz, 1H), 5.90 (s, 1H), 2.63 (s, 3H), 2.55 (s, 3H).

^{31}P NMR (202 MHz, $CDCl_3$): δ -74.9.

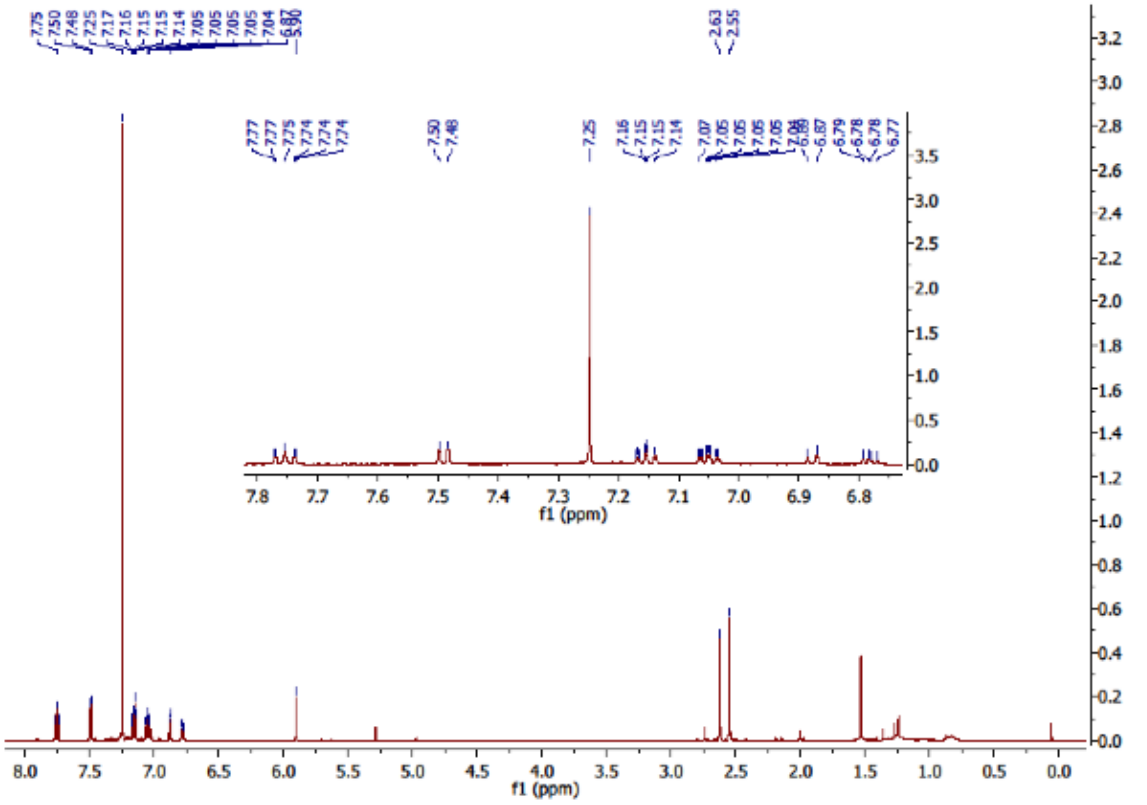
f1 (ppm)

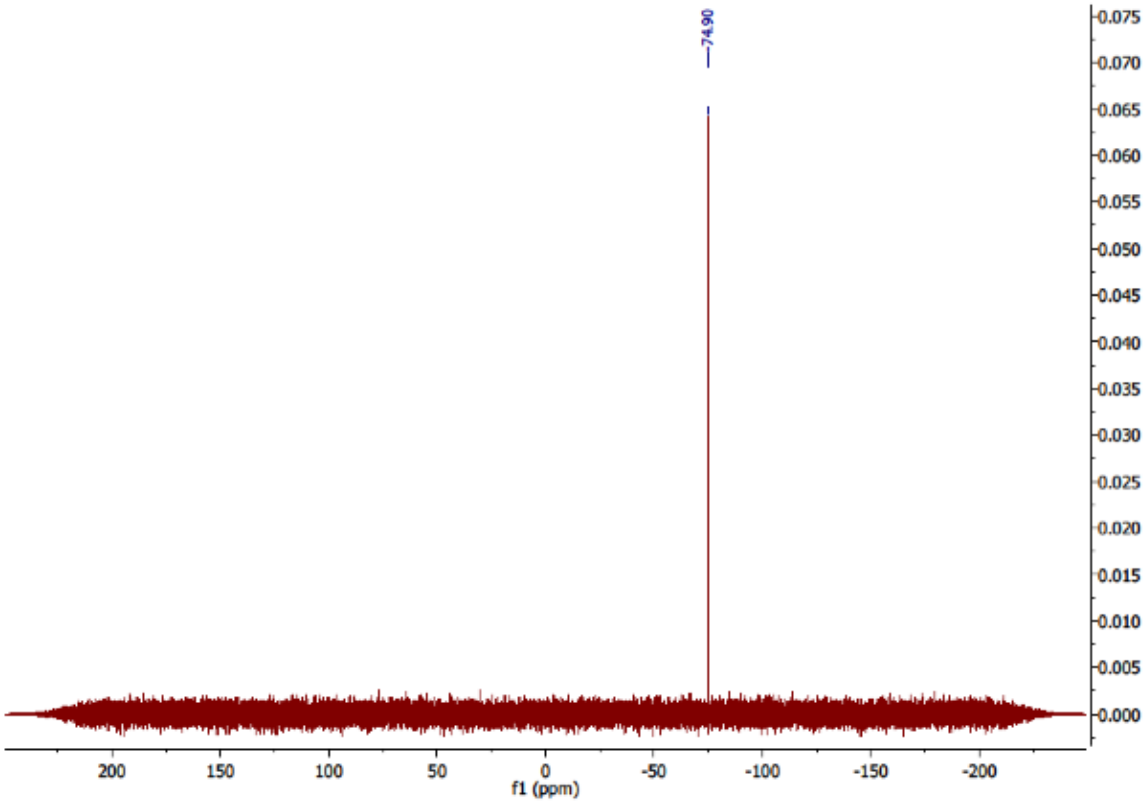
74.90
f1 (ppm)

1.5 9-phospha-10-hydroxytriptycene (**1d**)

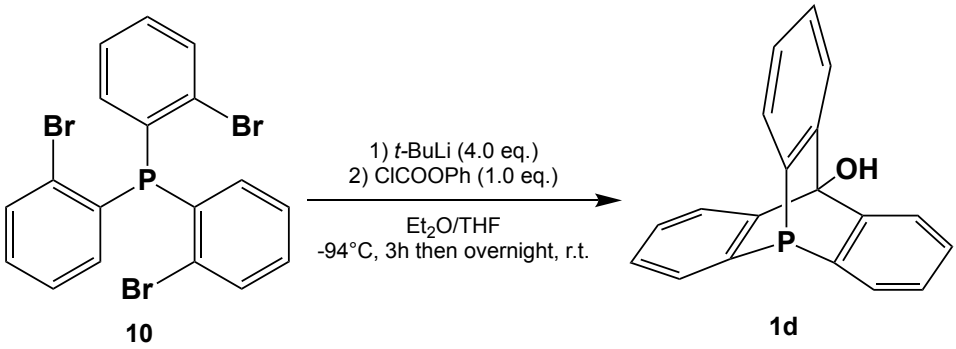

Chemical formula: $C_{19}H_{13}OP$

Molecular weight: 288.27 g/mol

Physical state: White solid

Prepared according to the literature.[3] In a pre-dried 100 mL Schlenck flask under Ar and equipped with a magnetic stirrer is added compound **10** (2.05 g, 4.10 mmol, 1.0 eq.) in 30 mL of a 1:1 mixture of anhydrous THF and Et_2O. The resulting clear solution is cooled down to -94°C (Acetone/$N_{2(l)}$) before the dropwise addition of *t*-BuLi (1.9 M in hexane, 8.7 mL, 16.4 mmol, 4.0 eq.). After stirring at this temperature for 3h, phenyl chloroformate (0.52 mL, 4.10 mmol, 1.0 equiv.) is added dropwise at -94°C. The resulting solution is stirred for one additional hour at -94°C before being allowed to warm up to room temperature overnight stirring. The reaction is quenched with aqueous NH_4Cl (30 mL) and the organic phase is extracted with AcOEt (3 x 30 mL). The combined organic phases are dried over $MgSO_4$ before filtration and evaporation of the solvents under reduced pressure. The crude product is purified by silica gel column chromatography (eluent = cyclohexane/AcOEt 15:1 to 5:1) to afford pure 9-phospha-10-hydroxytriptycene **1d** as an off-white powder (260 mg, 22% over two steps).

^{1}H NMR (500 MHz, $CDCl_3$) δ 7.78−7.73 (m, 6H), 7.27 (ddd, J =7.5, 4.9, 1.0 Hz, 3H), 7.10−7.07 (m, 3H).

^{31}P NMR (202 MHz, $CDCl_3$): δ -71.9.

---

[3] L. Hu, D. Mahaut, N. Tumanov, J. Wouters, R. Robiette and G. Berionni, *J. Org. Chem.*, 2019, **84**, 11268–11274.

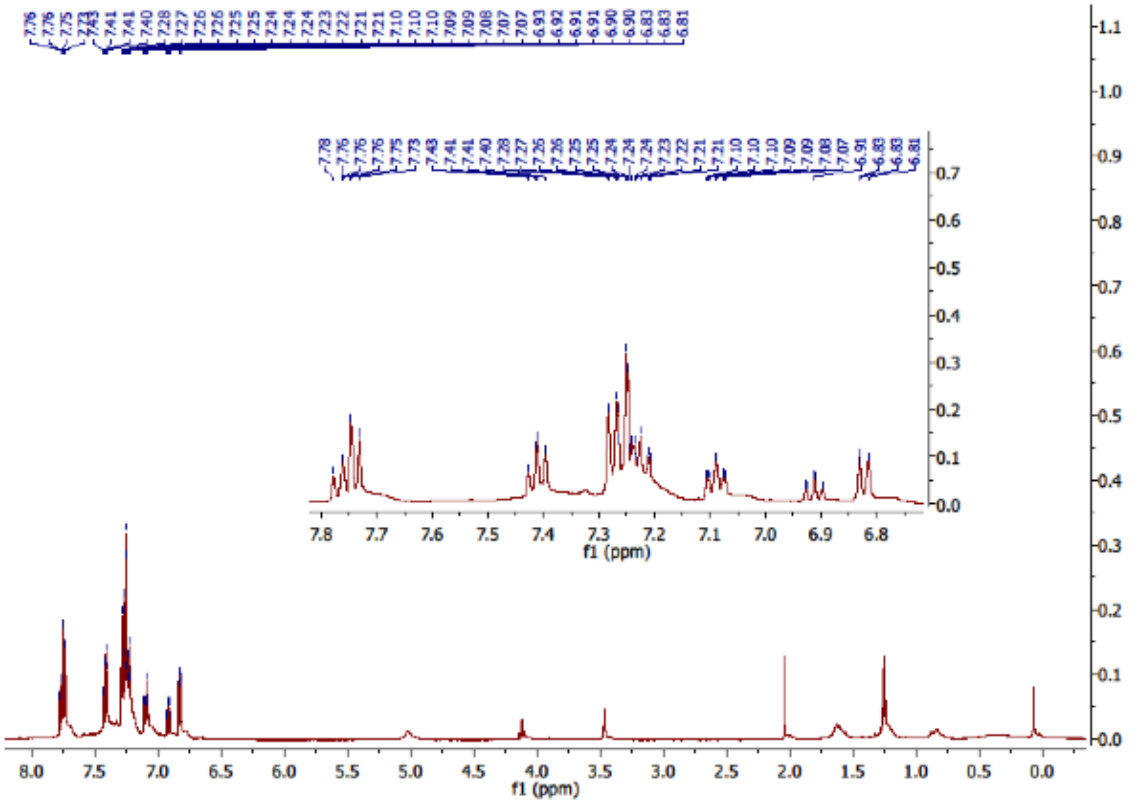
f1 (ppm)

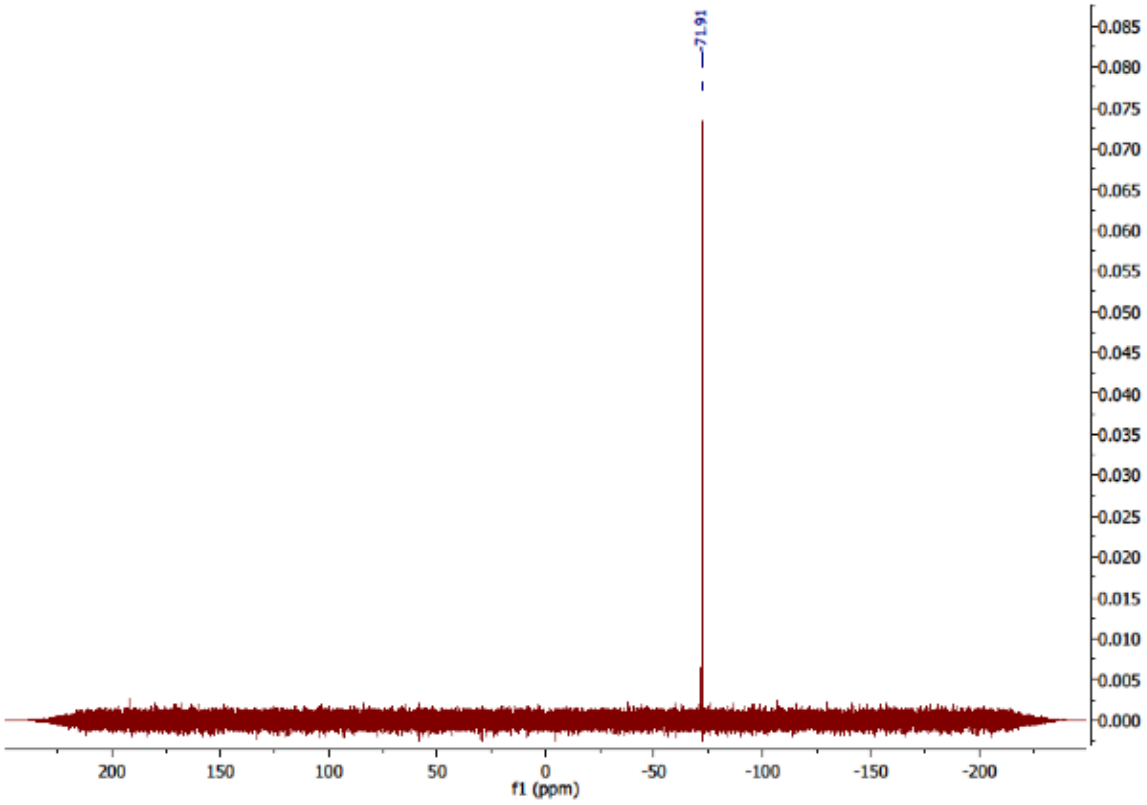
71.91
f1 (ppm)

1.6 9,10-diphosphatriptycene (**1e**)

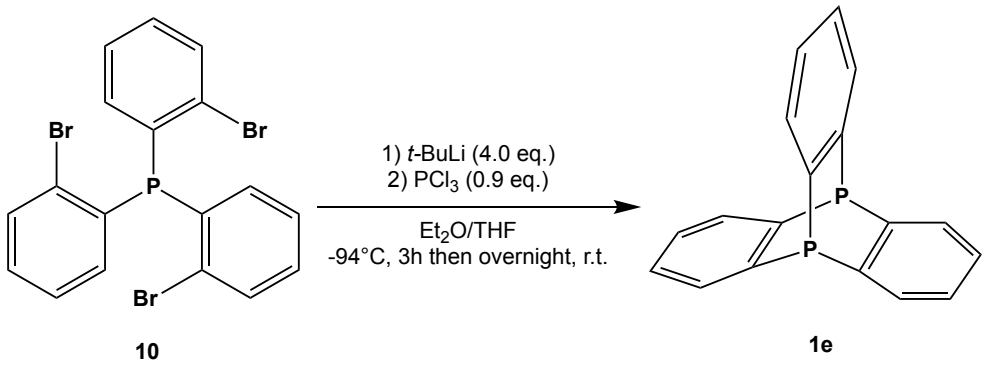

10 **1e**

Chemical formula: $C_{18}H_{12}P_2$

Molecular weight: 290.24 g/mol

Physical state: White solid

Prepared according to the literature similarly to **1a**. In a pre-dried 100 mL Schlenck flask under Ar and equipped with a magnetic stirrer is added compound **10** (1.70 g, 3.41 mmol, 1.0 eq.) in 30 mL of a 1:1 mixture of anhydrous THF and Et_2O. The resulting clear solution is cooled down to -94°C ($EtOH/N_{2(l)}$) before the dropwise addition of *t*-BuLi (1.9 M in hexane, 7.5 mL, 13.6 mmol, 4.0 eq.). After stirring at this temperature for 3h, PCl_3 (0.27 mL, 3.07 mmol, 0.9 equiv.) is added dropwise at -94°C. The resulting solution is stirred for one additional hour at -94°C before being allowed to warm up to room temperature overnight stirring. The reaction is quenched with aqueous NH_4Cl (30 mL) and the organic phase is extracted with AcOEt (3 x 30 mL). The combined organic phases are dried over $MgSO_4$ before filtration and evaporation of the solvents under reduced pressure. The crude product is purified by silica gel column chromatography (eluent = cyclohexane to cyclohexane/dichloromethane 7:3) to afford pure 9,10-diphosphatriptycene **1e** as an off-white powder (109 mg, 11% over two steps).

^{1}H NMR (500 MHz, $CDCl_3$) δ 8.03-7.96 (d, *J* = 31.9 Hz, 6H), 7.31-7.24 (d, *J* = 34.3 Hz, 6H).

^{13}C NMR (126 MHz, $CDCl_3$): δ = 145.4 (dd, J = 10.7, 5.0 Hz), 134.6 (ddd, J = 32.4, 19.3, 9.5 Hz), 128.53 (m).

^{31}P NMR (202 MHz, $CDCl_3$) δ -42.6.

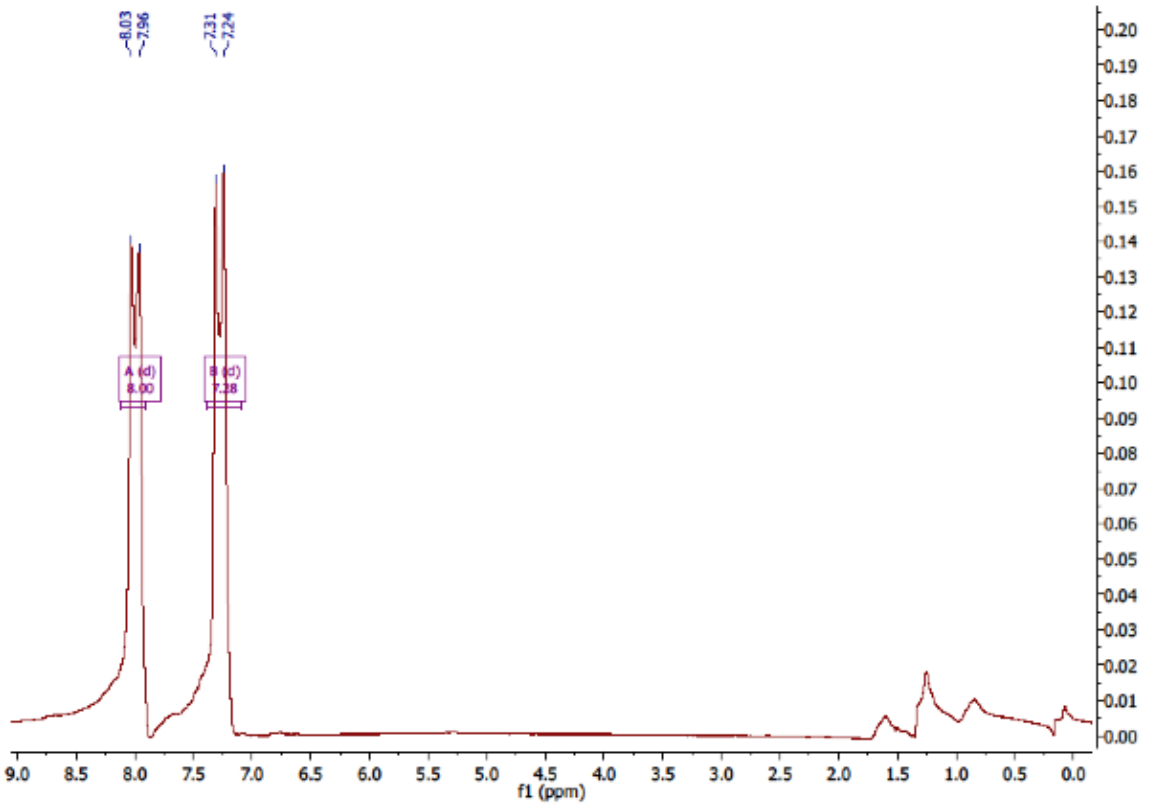
8.03
7.96
7.31
7.24
A (d)
8.00
B (d)
7.28
f1 (ppm)

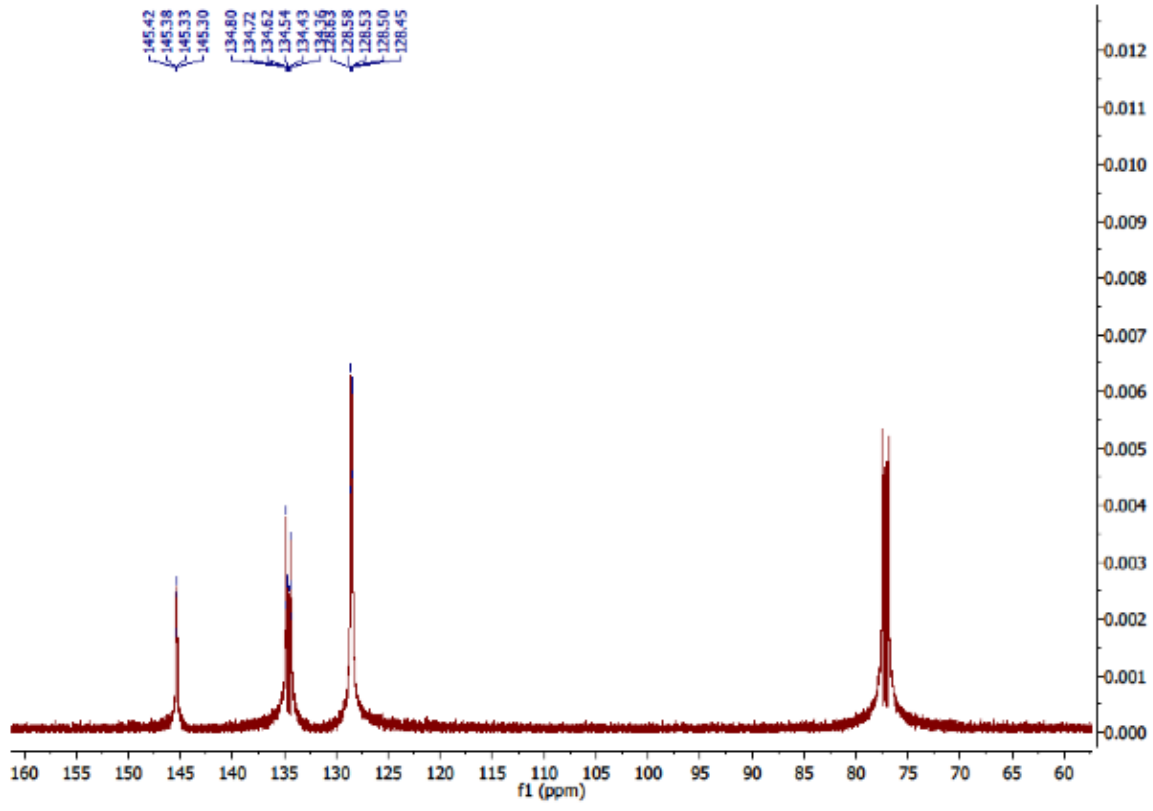
145.42
145.38
145.33
145.30
134.80
134.72
134.62
134.54
134.43
128.58
128.53
128.50
128.45
f1 (ppm)

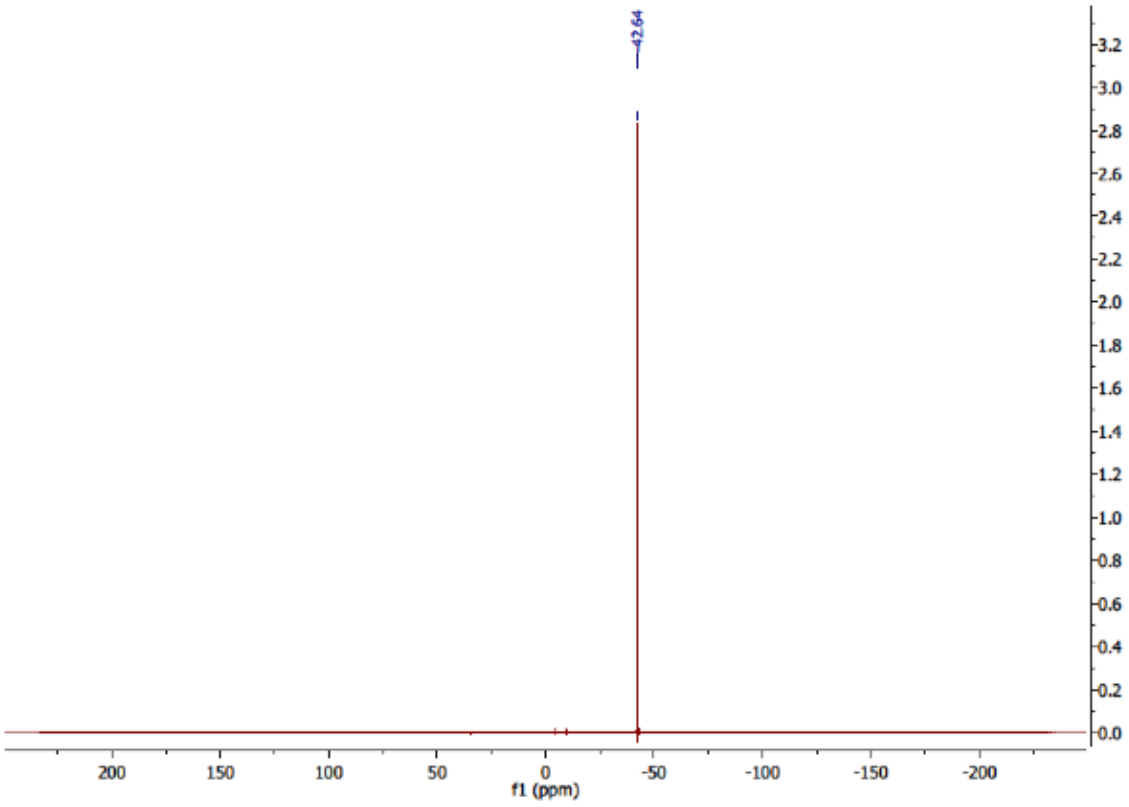
42.64
3.2
3.0
2.8
2.6
2.4
2.2
2.0
1.8
1.6
1.4
1.2
1.0
0.8
0.6
0.4
0.2
0.0
200
150
100
50
0
-50
-100
-150
-200
f1 (ppm)

1.7 Cis-$PtCl_2$(**1a-c**)$_2$ (**6a-c**)

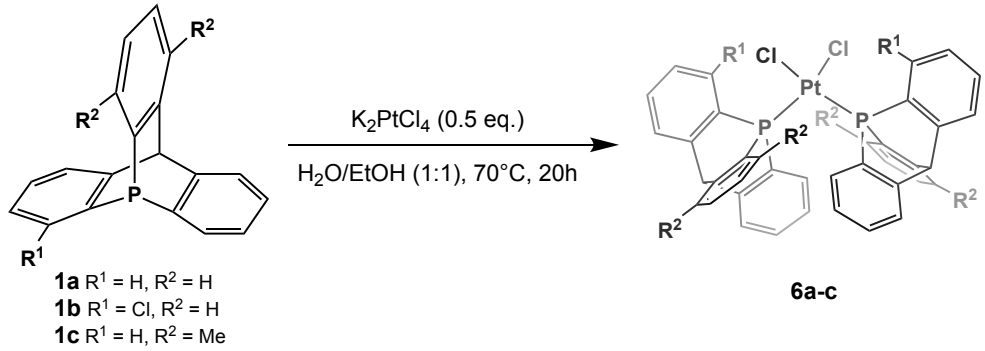

1a R^1 = H, R^2 = H
1b R^1 = Cl, R^2 = H
1c R^1 = H, R^2 = Me

6a-c

Physical state: White solid

Prepared according to the literature.[4] In a 10 mL flask under inert conditions (glove box) and equipped with a magnetic stirrer are dissolved compound **1a-c** (1.0 eq.) and K_2PtCl_4 (0.5 eq.) in 5 mL of a 1:1 mixture of H_2O and EtOH. The solution sealed and stirred at 70°C for 20h and then cooled to room temperature. The resulting precipitate was collected by filtration, washed with a mixture of H_2O and EtOH (1:1), and dried under vacuum to give **6a-c** as a white powder.

Due to the insoluble nature of the complexes, no exploitable NMR spectrum could be obtained for characterization with standard deuterated solvents.

[4] H. Ube, Y. Yasuda, H. Sato and M. Shionoya, *Nat. Commun.*, 2017, **8**, 1–6.

1.8 Cis-$PtCl_2$(**1a-d**)$_2$ (**6a-d**)

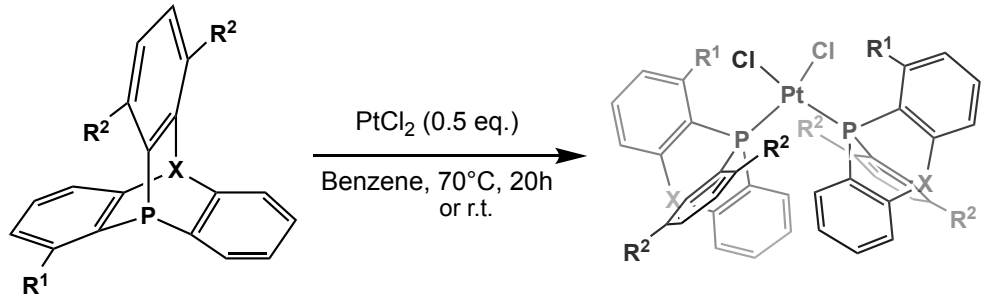

1a R^1 = H, R^2 = H, X = C-H
1b R^1 = Cl, R^2 = H, X = C-H
1c R^1 = H, R^2 = Me, X = C-H
1d R^1 = H, R^2 = H, X = C-OH

6a-d

Physical state: White solid

Prepared according to the literature.[5] In a 10 mL flask under inert conditions (glove box) and equipped with a magnetic stirrer are dissolved compound **1a-c** (1.0 eq.) and $PtCl_2$ (0.5 eq.) in 5 mL of toluene. The resulting solution sealed and stirred at 70°C (or r.t.) for 20h and then cooled to room temperature. The solvent is evaporated under reduced pressure and the resulting solid is washed with 2 x 10 mL of cold toluene before drying under vacuum to give **6a-d** as a white powder.

Due to the insoluble nature of the complexes, no exploitable NMR spectrum could be obtained for characterization with standard deuterated solvents.

[5] R. A. Baber, A. G. Orpen, P. G. Pringle, M. J. Wilkinson and R. L. Wingad, 2005, **2**, 659–667.

2. *Quantum chemical section*

2.1 Density functional theory

Introduction

This part introduces the method employed for all quantum calculations made in this master thesis, the density functional theory (DFT).[1-3]

The principle of density functional theory (DFT) is to replace the N-electron wavefunction dependent on N spin-space coordinates $\Psi(x_1, x_2, ..., x_N)$ by the electron density $\rho(r)$, dependent on one space coordinates. Indeed, the electron density, which corresponds to the probability of finding an electron in a portion of space, allows to replace the complex Schrödinger equation by much simpler one.

The Hohenberg and Kohn theorems

The Hohenberg and Kohn theorems[4] represent the theoretical basis of the density functional theory. The first of these theorems states that the external potential $V_{ext}(r)=V(r)$ can be determined (within a constant) by the electron density. This affirmation has as consequence that all the properties of the system can be expressed using only electron density as variable. Furthermore, since the electronic density gives the number of electrons of the system when integrated over the space ($N = \int \rho(r)\, dr$), it can also serve to determine the kinetic energy operator $\hat{T}$ and the electron repulsion operator V_{ee}. With the external potential and the kinetic energy operators known, we have now access to the Hamiltonian of the system and to all its properties through the Schrödinger equation:

$$\hat{H} = \hat{T} + \hat{V} \quad \Rightarrow \quad \hat{H}\Psi = E\Psi \tag{1}$$

The energy can then be expressed as a functional of the electron density:

$$E_v[\rho(r)] = T[\rho(r)] + V_{ne}[\rho(r)] + V_{ee}[\rho(r)] \tag{2}$$

where V_{ne} is the electron-nuclei attraction term, which corresponds usually to the external potential. The last equation can be recast to split the V_{ee} terms into a coulomb $J[\rho(r)]$ and a non-classical term. Further manipulations of the equation introduce the Hohenberg and Kohn functional ($F_{HK}[\rho(r)]$), which is a universal functional independent of the given system.

$$E_v[\rho(r)] = T[\rho(r)] + V_{ne}[\rho(r)] + J[\rho(r)] + nonclassical\ term$$
$$E_v[\rho(r)] = \int \rho(r)v(r)dr + F_{HK}[\rho(r)] \quad (3)$$

The second Hohenberg-Kohn theorem states that the electron density of the ground state is the one that minimizes the total energy of the system, giving insight into how to actually calculate the electron density of a given system:

$$\mu = \frac{\delta E_v[\rho(r)]}{\delta\rho(r)} = v(r) + \frac{\delta F_{HK}[\rho(r)]}{\delta\rho(r)} \quad (4)$$

So, using approximate densities, this energy will always remain higher than the exact energy of this ground state, it is the concept of the variation principle. Solutions can thus be obtained by the resolution of this equation and provide a solution tending towards the exact ground state energy. However, F_{HK} contains a non-classical part called the exchange-correlation, that is not known. In order to solve this equation, approximate Hohenberg-Kohn functionals must be used and another approach employed.

The Kohn-Sham method

The principle of the Kohn-Sham method[5] consists in substituting the real system of interacting electrons by a fictitious one of independent electrons having the same density. Kohn-Sham spin-orbitals ($\theta_i(x)$) are then re-introduced to describe that density and the squares of their norm sum up to give the Kohn-Sham density:

$$\rho(r) = \sum_{i}^{N} \int |\theta_i(x)|^2 d\omega \tag{5}$$

The latter expression, written in term of one-electron functions, is the exact ground state density of the system. Due to their independent character, the global wavefunction of the system assumes the form of a Slater determinant:

$$\Psi = \frac{1}{\sqrt{N!}} det|\theta_1(x_1), \theta_2(x_2), \dots, \theta_N(x_N)| \tag{6}$$

The Hamiltonian of this fictitious system is said to be independent because it does not possess any two-electron term:

$$\widehat{H}_S = \sum\nolimits_{i}^{N} \frac{-1}{2} \nabla_i^2 + \sum_{i}^{N} v_{eff}(r_i) \tag{7}$$

It does however possess, in addition to the kinetic energy operator, an effective potential. In order to define this parameter, several steps are needed. Starting from the Kohn-Sham equivalent of equation (3) and using the variation principle, the Hohenberg-Kohn functional can be defined:

$$F[\rho(r)] = T_S[\rho(r)] + J[\rho(r)] + E_{XC}[\rho(r)] \tag{8}$$

Which gives the exchange-correlation (XC) energy functional $E_{XC}[\rho(r)]$:

$$E_{XC}[\rho(r)] = T[\rho(r)] - T_S[\rho(r)] + V_{ee}[\rho(r)] - J[\rho(r)] \tag{9}$$

This functional is the one that must be chosen at the beginning of each DFT calculation. The functional derivative of the energy functional $E_v[\rho(r)]$ with respect to the electron density defines the effective potential:

$$v_{eff} = v(r) + \int \frac{\rho(r')}{|r - r'|} dr' + v_{xc}(r) \qquad \text{with} \qquad v_{xc}(r) = \frac{\delta E_{XC}[\rho(r)]}{\delta \rho(r)} \tag{10}$$

where $v_{xc}(r)$ is the exchange-correlation potential. The effective potential corresponds to the potential that "surrounds" all the electrons. It is a key part of the Kohn-Sham equation (shown below in its canonical form):

$$\left[\frac{-1}{2}\nabla^2 + v_{eff}(r)\right]\Theta_n(x) = \varepsilon_n\Theta_n(x) \qquad (11)$$

Solving the Kohn-Sham equation gives the electronic density of the system. Since the effective potential depends on this density, the resolution starts from a guest density, and proceeds self-consistently. It is an iterative process, a SCF (Self-Consistent Field) cycle is carried out as follows: from the guess density, the effective potential is evaluated (10) and inserted in the Kohn-Sham equation (11) which is resolved. The energy is the evaluated, a new density is proposed and the cycle starts again until convergence towards the minimum energy, following the variation principle.

In the effective potential, the exact expression of the exchange-correlation functional is approximated, leading to approximate densities and energies. This term accounts for electron correlation effects. Many exchange-correlation functionals have been developed with several levels of approximation, as discussed in the next section. If the exact XC functional was known, the Kohn-Sham method would be an exact method.

Exchange-correlation functionals

As said, many exchange-correlation (XC) functionals have been designed over the years and scaled as a function of their chemical accuracy in a Jacob's ladder. The crudest approximation is associated with the *Local Density Approximation* (LDA) which tries to describe non-uniform systems by applying uniform-electron-gas results for infinitesimal portions of the non-uniform electron distribution. More accurate functionals are based on the *Generalized Gradient Approximation* (GGA), which depends on both the density as in the previous case but also includes a dependence on its gradient. For some of these functionals, empirical parameters can be introduced to reproduce some specific properties. In *meta-GGAs* (mGGAs), a dependence on the kinetic energy density is introduced, improving the accuracy of several properties with respect to GGA functionals. In some of these XC functionals, a

certain percentage of exact Hartree-Fock exchange is introduced, increasing the non-locality of the method. It gives rise to the long-range corrected hybrid functionals which split the exchange potential into short- and long-range terms with different HF exchange percentages. This allows a better description of the charge-transfer effects due to the exact -1/r asymptotic dependence of the exchange potential while retaining more DFT exchange at short range prevents from errors similar to the HF method. In double hybrids functionals, the correlation functional is partially described by MP2 while HF exchange is still added to the exchange functional. These latter functionals improve significantly the results but their computational cost is far higher than that of the other functionals. Empirical dispersion corrections can also be included to describe the London dispersion forces.

Increasing the complexity of the functional does not necessary lead to better results. Indeed, some functionals are just more suited to describe a given system. In this work, the M06-2X functional was used. It is a hybrid meta-GGA functional that is suited, according to its developers, to describe main- group thermochemistry, kinetics and noncovalent interactions.[6] Also, a preliminary comparative DFT study of functionals on cisplatin as model compound established that the M06-2X functional is the most suited XC for describing Pt-based complexes.

Atomic basis sets

The choice of an atomic basis set is crucial to settle any SCF-LCAO-MO calculation. Indeed, these basis sets describe the molecular orbitals (in the LCAO scheme), necessary to obtain the electronic density and wavefunction of the system. They are defined as contractions of gaussian functions, aiming to simulate the exact atomic orbitals and solving the Schrödinger equation. The basis sets have been divided in several families with respect to their composition.

The minimal basis sets (or simple ζ) include a single basis function for each occupied atomic orbital in a given atom. One of these basis sets is STO-3G (Slater Type Orbital) where each basis function is a contraction of three gaussian primitive functions. In addition, Double or Triple ζ basis sets include two or three of these basis functions, respectively, for each orbital of a given atom.

A further improvement of these basis set comes from the understanding that most of the chemistry of an atom is performed by the valence orbitals, so they should be more flexible than the core ones. It results in the split valence basis sets, which differentiate the number of basis functions between the core orbitals (usually described with simple ζ) and the valence orbitals (with double or triple ζ). Therefore, basis sets with two or three valence atomic orbitals are called valence double- and triple ζ basis sets, respectively.

In numerous cases, a better description can be obtained by taking account of the environment effects on the atom. It is done by including polarization functions to these basis sets, which implement p functions on hydrogen or d and f functions on atoms from the second and third periods. The addition of these functions allows to correct the imprecisions made due to the omittance of molecular events such as hybridation of the orbitals. Furthermore, diffuse functions can also be added to the basis sets. They allow a better description of the outer part of the orbitals and the electronic density. In this case, s and p functions are added on atoms from the second and third periods while only s functions are applicable on hydrogen atoms.

J. A. Pople developed a series of basis sets such as STO-3G, 6-31G, 6-311G(d,p), 6-311++G(3df,3pd), etc, mainly valence double or triple ζ. During this master thesis, the 6-311G(d) basis sets was mainly used. It is a Pople valence triple ζ basis set which possesses one contraction of six gaussians for the core orbitals while the valence orbitals are described by three basis functions, one by a contraction of 3 gaussians, and the two others by a single gaussian function. A set of five polarization functions are added: d orbitals for the atoms of the second and third period. In addition, an *Effective Core Potential* (ECP), or pseudopotential, was used as an approximation to simplify the description of more complex systems. It consists in the description of complex relativistic effects, occurring in the inner electronic layer and the corresponding nucleus, by an effective potential. The Schrödinger equation contains then a much simpler effective potential term instead of the Coulombic potential term for core electrons, normally found in the latter equation and becoming hard to solve in the case of large systems such as transition metal atoms. Their utilization brings many advantages such as the reduction of the basis set size, the reduction of the number of electrons and the inclusion of relativistic effects, all reflected by a diminution of the computational cost. In the present work, the LanL2TZ(f) was determined as the most suitable ECP to describe the platinum atom. The latter contains a Triple ζ basis function for the valence electron as well as f polarization functions.

2.2 Solvent effects and the polarizable continuum model

Since most systems are not in gas phase but in condensed ones, such as liquid medium, an adequate description of the solvent effects is also crucial. A fundamental quantity that describes the interactions between the system and its surroundings is the enthalpy of solvation (ΔG_S^0), that characterizes the energetic transition caused by the modification of the properties of the solute, when going from gas phase to the solution.

$$K_S = \frac{[X]_{Sol}}{[X]_{Gas}} = e^{-\Delta G_S^0(X)/RT} \quad (12)$$

where K_S is the equilibrium constant for going from gas phase to solution and $[X]_{Sol}$ and $[X]_{Gas}$ represent the concentrations of the X compound in solution or in gas phase, respectively.

The free enthalpy of solvation describes the modification of the studied system on all levels: structure, reactivity, responses to perturbation, etc. Thus, it is divided in several contributions: the electrostatic interactions between the solute and the solvent molecules, the cavitation energy (the energy needed to form the cavity in solution that will contain the solute without solute-solvent interactions), the dispersion forces (the interactions between induced dipoles) that represents the major contribution, and finally the changes in the bulk solvent structure.

Solvents effects can be described using two models: the explicit and the implicit one. The first simulates the solvent molecules, gives better and more precise results, but demand more computational resources, while the latter does not simulate the solvent molecules and it is less time-and energy consuming.

The Polarizable Continuum Model (PCM) is an implicit solvation method. In this model a cavity containing the solvated molecule is delimited by circulating a probe sphere around the solute molecule. This sphere has a radius equal to the van der Waals radius of the atoms

constituting one solvent molecule. The circulation delimits two surfaces, an inner one which is the solvent exclusion surface and an outer, accessible for the solvent molecules (Figure 1).

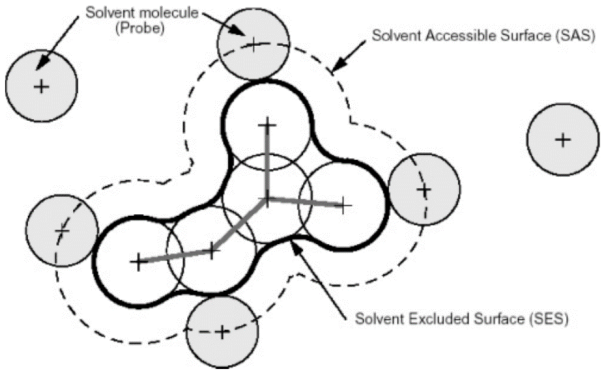

Figure 1 - Cavity formed by circulating a probe solvent molecule around the studied compound. Picture extracted from reference [7].

In this method, the explicit solute-solvent interactions can be replaced by a continuum characterized by a dielectric constant ε. The latter will apply an electric field on the solute, simulating the solvent effects. The mathematical development of the PCM model is now put in an integral equation formalism (IEF, in the IEFPCM approach). The subtlety in the PCM approach is that the charge distribution of the solute also induces a polarization of the dielectric continuum which in turn polarizes the solute charge distribution. It is thus a self-consistent model that must be solved in an iterative manner until finding an equilibrium.

2.3 Thermochemistry and equilibrium constants

The thermochemistry is the study of the thermodynamic functions of a given chemical system. These are macroscopic values, resulting from the state and the energy of the matter at the microscopic level. Statistical thermodynamics is the tool which allow to pass between the microscopic and macroscopic chemistry. The partition function (Ω) is of paramount importance in this field as it contains all the information of the system, and is defined as follows:

$$\Omega = \sum_i g_i e^{\frac{-\varepsilon_i}{kT}} \tag{13}$$

$$\Omega = \Omega_{trans}\, \Omega_{vib}\, \Omega_{rot}\, \Omega_{el} \tag{14}$$

where g_i is the degeneration of the i level of energy, ε_i, k, is the Boltzmann constant and T, the temperature. This last equation highlights that the partition function is the product of several contributions (trans = translation; vib= vibrations; rot = rotation; el = electronic). Each state function of the system (internal energy, free Gibbs enthalpy, entropy, enthalpy, …), calculated in this work, can be expressed as a function of the partition function.

2.4 Bibliography

[1] R. G. Parr and W. Yang, "Density-Functional Theory of Atoms and Molecules", New York: Oxford University Press, 1989.

[2] W. Koch and M. C. Holtausen, A Chemist's Guide to Density Functional Theory, 2nd ed., Weinheim: Wiley-VCH, 2001.

[3] P. Geerlings, F. De Proft and W. Langenaeker, *Chem. Rev.,* 2003, **103**, 1793-1873.

[4] A. Hohenberg and W. Kohn, *Phys. Rev.*, 1964, **136**, 864-870.

[5] W. Kohn and L. J. Sham, *Phys. Rev.*, 1965, **140**, 1133-1138.

[6] Y. Zhao and D. G. Truhlar, *Theor. Chem. Account*, 2008, **120**, 215-241.

[7] J. Tomasi, B. Mennucci and R. Cammi, *Chem. Rev.*, 2005, **105**, 2999-3093.